การจำลองระบบเซลล์เชื้อเพลิงชนิดออกไซด์แข็งที่ป้อนเชื้อเพลิงด้วยเอทานอล

นางสาว วาสนา แจ่มศักดิ์

วิทยานิพนธ์นี้เป็นส่วนหนึ่งของการศึกษาตามหลักสูตรปริญญาวิศวกรรมดุษฎีบัณฑิต
สาขาวิชาวิศวกรรมเคมี ภาควิชาวิศวกรรมเคมี
คณะวิศวกรรมศาสตร์ จุฬาลงกรณ์มหาวิทยาลัย
ปีการศึกษา 2550

SIMULATION OF SOLID OXIDE FUEL CELL SYSTEM FUELLED BY ETHANOL

Miss Wasana Jamsak

A Dissertation Submitted in Partial Fulfillment of the Requirements
for the Degree of Doctor of Engineering Program in Chemical Engineering
Department of Chemical Engineering
Faculty of Engineering
Chulalongkorn University
Academic Year 2007

Thesis Title	SIMULATION OF SOLID OXIDE FUEL CELL SYSTEM FUELLED BY ETHANOL
By	Miss Wasana Jamsak
Field of Study	Chemical Engineering
Thesis Advisor	Associate Professor Suttichai Assabumrungrat, Ph.D.
Thesis Co-advisor	Professor Peter L. Douglas, Ph.D.

Accepted by the Faculty of Engineering, Chulalongkorn University in Partial Fulfillment of the Requirements for the Doctoral Degree

.....Dean of the Faculty of Engineering
(Associate Professor Boonsom Lerdhirunwong, Dr. Ing.)

THESIS COMMITTEE

..... Chairman
(Associate Professor Prasert Pavasant, Ph.D.)

..... Thesis Advisor
(Associate Professor Suttichai Assabumrungrat, Ph.D.)

..... Thesis Co-advisor
(Professor Peter L. Douglas, Ph.D.)

..... External Member
(Assistant Professor Worapon Kiatkittipong, D.Eng.)

..... Member
(Associate Professor Kejvalee Pruksathorn, Dr. de L'INPT)

..... Member
(Assistant Professor Amornchai Arpornwichanop, D.Eng.)

..... Member
(Akawat Sirisuk, Ph.D.)

วาสนา แจ่มศักดิ์ : การจำลองระบบเซลล์เชื้อเพลิงชนิดออกไซด์แข็งที่ป้อนเชื้อเพลิงด้วยเอทานอล (SIMULATION OF SOLID OXIDE FUEL CELL SYSTEM FUELLED BY ETHANOL) อ. ที่ปรึกษา : รศ. ดร. สุทธิชัย อัสสะบำรุงรัตน์, อ. ที่ปรึกษาร่วม : Professor Peter L. Douglas, 136 หน้า.

การศึกษาการจำลองระบบเซลล์เชื้อเพลิงชนิดออกไซด์แข็งที่ป้อนเชื้อเพลิงด้วยเอทานอล แบ่งได้เป็น 4 ส่วนหลักคือ การศึกษาสมรรถนะทางทฤษฎีของเซลล์เชื้อเพลิงออกไซด์แข็งที่ป้อนด้วยเอทานอลเมื่อใช้อิเล็กโทรไลต์ที่ต่างกัน (ออกซิเจนไอออน และโปรตอนอิเล็กโทรไลต์) การศึกษาสมรรถนะจริงของเซลล์เชื้อเพลิงออกไซด์แข็งของอิเล็กโทรไลต์ต่างชนิด การศึกษาระบบเซลล์เชื้อเพลิงออกไซด์แข็งที่ติดตั้งหอกลั่นเอทานอล และการออกแบบระบบแลกเปลี่ยนความร้อนสำหรับระบบเซลล์เชื้อเพลิงออกไซด์แข็งที่ติดตั้งหอกลั่นเอทานอล ในการศึกษาสมรรถนะทางทฤษฎีของเซลล์เชื้อเพลิงออกไซด์แข็งเมื่อใช้อิเล็กโทรไลต์ต่างชนิดกัน พบว่าสมรรถนะทางทฤษฎีของเซลล์เชื้อเพลิงที่ใช้อิเล็กโทรไลต์แบบตัวนำโปรตอนดีกว่าค่าที่ได้จากกรณีที่ใช้อิเล็กโทรไลต์แบบตัวนำออกซิเจนไอออน แม้ว่าได้พิจารณาถึงความต้องการน้ำในระบบอิเล็กโทรไลต์แบบออกซิเจนไอออนที่น้อยกว่าแล้วก็ตาม อย่างไรก็ตามสมรรถภาพจริงของเซลล์เชื้อเพลิงเมื่อใช้อิเล็กโทรไลต์แบบตัวนำโปรตอนต่ำกว่ากรณีที่ใช้อิเล็กโทรไลต์แบบตัวนำออกซิเจนไอออนมาก เนื่องจากความสูญเสียทางไฟฟ้าของอิเล็กโทรไลต์แบบตัวนำโปรตอนมีค่าสูงกว่าออกซิเจนไอออนมากถึง 45.6 เท่า เพื่อที่จะให้สมรรถนะของเซลล์เชื้อเพลิงที่ใช้อิเล็กโทรไลต์แบบตัวนำโปรตอนดีเทียบเท่ากับของตัวนำออกซิเจนไอออน ความสูญเสียทางไฟฟ้าที่เกิดจากอิเล็กโทรไลต์ และที่เกิดจากส่วนอื่นของเซลล์ต้องลดลงควบคู่กัน ระบบเซลล์เชื้อเพลิงออกไซด์แข็งที่ติดตั้งด้วยหอกลั่นเอทานอลที่ป้อนด้วยเอทานอลชีวภาพได้ถูกเสนอขึ้นเพื่อปรับปรุงระบบเดิมที่ป้อนด้วยเอทานอลความบริสุทธิ์สูง เพื่อประหยัดพลังงานในการกลั่นแยก ความร้อนที่ได้จากการเผาเชื้อเพลิงส่วนเกินจากเซลล์เชื้อเพลิงถูกนำมาใช้ให้ความร้อนให้กับส่วนต่างๆของระบบ อาทิเช่น เครื่องอุ่นสาร เตาปฏิกรณ์รีฟอร์มิง และเครื่องต้มน้ำของหอกลั่น ผลที่ได้พบว่าระบบเซลล์เชื้อเพลิงที่ติดตั้งหอกลั่นเอทานอลสามารถดำเนินงานโดยปราศจากการพึ่งพาความร้อนจากแหล่งความร้อนภายนอกเมื่อดำเนินการ ณ ค่าความต่างศักย์ดำเนินงานและค่าสัดส่วนการใช้เชื้อเพลิงที่เหมาะสม การพัฒนาระบบเซลล์เชื้อเพลิงออกไซด์ที่ติดตั้งหอกลั่นเอทานอล พบว่าการนำความร้อนที่ระบายออกจากเครื่องควบแน่นของหอกลั่นมาใช้ และการแยกสายอากาศส่วนเกินที่ออกจากเซลล์เชื้อเพลิงบางส่วนกลับมาใช้ใหม่ทำให้ระบบมีประสิทธิภาพสูงสุด และดัชนีค่าใช้จ่ายรวมของระบบต่ำสุด ระบบแลกเปลี่ยนความร้อนที่เหมาะสมคือ สายร้อนที่ออกจากเครื่องเผาไหม้แลกเปลี่ยนความร้อนกับเครื่องแลกเปลี่ยนความร้อนของสายก่อนเข้าแอโนดเครื่องปฏิกรณ์รีฟอร์มิง เครื่องแลกเปลี่ยนความร้อนของอากาศขาเข้า เครื่องแลกเปลี่ยนความร้อนของผลิตภัณฑ์ยอดหอของหอกลั่น และเครื่องต้มน้ำ ตามลำดับ นอกจากนี้การปรับค่าดำเนินงานของระบบเซลล์เชื้อเพลิงสามารถลดค่าดัชนีค่าใช้จ่ายรวมได้

ภาควิชา วิศวกรรมเคมี ลายมือชื่อนิสิต Wasana Jaek

สาขาวิชา วิศวกรรมเคมี ลายมือชื่ออาจารย์ที่ปรึกษา

ปีการศึกษา 2550 ลายมือชื่ออาจารย์ที่ปรึกษาร่วม P.L. Douglas

4671826421 : MAJOR CHEMICAL ENGINEERING
KEY WORD: SOLID OXIDE FUEL CELL (SOFC)/ ETHANOL/ SIMULATION
WASANA JAMSAK : SIMULATION OF SOLID OXIDE FUEL CELL SYSTEM FUELLED BY ETHANOL. THESIS ADVISOR : ASSOCIATE PROFESSOR SUTTICHAI ASSABUMRUNGRAT, Ph.D., THESIS CO-ADVISOR: PROFESSOR PETER L. DOUGLAS, Ph.D., 136 pp.

The research focuses on the simulation of solid oxide fuel cell (SOFC) systems fuelled by ethanol. The study is divided into four parts: theoretical performance analysis of ethanol-fuelled SOFC with different electrolyte, actual performance of ethanol-fuelled SOFC, thermodynamic assessment of SOFC system integrated with bioethanol purification unit and design of thermally integrated bioethanol-fuelled SOFC system with a distillation column. The theoretical performance of SOFC with proton-conducting electrolyte (SOFC-H^+) is found to be superior to that of oxygen ion conducting electrolyte (SOFC-O^{2-}) although the lower requirement of steam input in the case of SOFC-O^{2-} is taken in to account. However, the actual performance of SOFC-H^+ is inferior to that of SOFC-O^{2-} because the resistance is 45.6 times higher than that of SOFC-O^{2-}. In order to develop the performance of SOFC-H^+ to be comparable to that of SOFC-O^{2-}, both electrolyte resistance and other resistances should be simultaneously reduced. A bioethanol-fuelled SOFC system integrated with a distillation column (SOFC-DIS) is proposed to improve the conventional system which was fed by high purity ethanol in order to save distillation energy. The combustion heat from excess fuels is provided to other parts of the system i.e. heaters, a reformer and a reboiler. The SOFC-DIS can operate without demanding heat from an external source when suitable operating voltage and fuel utilizations are selected. To improve the performance of SOFC-DIS, utilization of heat released from a condenser and splitting of some part of cathode outlet stream to be recycled offer the highest efficiency and lowest total cost index. The suitable heat exchanger network for the SOFC-DIS system is that the hot stream from the afterburner is first heat exchanged with the anode-inlet heat exchanger, the reformer, the air heat exchanger, the distillate heat exchanger and a reboiler, respectively. In addition, adjusting SOFC-DIS operating conditions can lower total cost index.

Department ... Chemical Engineering ..... Student's signature Wasana Jamsak
Field of Study Chemical Engineering .... Advisor's signature .....
Academic year ..... 2007 ..... Co-advisor's signature P.L. Douglas

ACKNOWLEDGEMENTS

The author would like to show highly appreciation to Professor Suttichai Assabumrungrat, her advisor for his great guidance in both research study and life attitude throughout her research study and Professor Peter L. Douglas, her co-advisor for his good advice and kind assistance, especially during her stay in Canada. In addition, the author wishes to thank Associate Professor Eric Croiset, Assistant Professor Navadol Laosiripojana, Dr. Rapeepong Suwanwarangkul and Dr. Sumittra Charojrochkul for their collaboration in accomplished papers. She is furthermore grateful to Associate Professor Tharathon Mongkhonsi for expanding her horizon in both academic and non-academic issues and Professor Piyasan Praserthdam for providing her some support and facilities in the lab. Special thank to Associate Professor Prasert Pavasant as the chairman, Associate Professor Kejvalee Pruksathorn, Assistant Professor Worapon Kiatkittipong, Dr. Akawat Sirisuk and Dr. Amornchai Arpornwichanop as the members of the thesis committee.

Many thanks Thailand Research Fund (TRF) for providing her financial supports and great opportunity of working aboard during her Doctoral degree.

She would like to be obliged to Colin Alie, a friend in the same research group during her stay in Canada, for his generosity in giving her some ideas on Aspen Plus techniques and also Thai friends, especially, Anuchart, Rangsima, Tassanee, Monrudee, Sirikanya and Wongphaka for a very good memorial and their caring assistance. Furthermore, gratefully thank members in Center of Excellence on Catalysis and Catalytic Reaction Engineering, Department of Chemical Engineering, Chulalongkorn University who have assisted her over the years of her study.

Finally, the author would like to express great gratitude to her parents and brothers. The author cannot completely achieve a success in her study without the support from her family.

CONTENTS

page

CHAPTERS **page**

CHAPTERS **page**

CHAPTERS **page**

CHAPTERS **page**

LIST OF TABLES

page

LIST OF FIGURES

page

page

page

page

page

page

NOMENCLATURE

A	cell stack area	[m^2]
c	extent of the electrochemical reaction of hydrogen	[mol]
C_{EtoH}	ethanol concentration	[mol %]
C_p	heat capacity	[J kg^{-1} K^{-1}]
E_a	activation energy	[J mol^{-1}]
EMF	electromotive force of a cell	[V]
F	Faraday constant	[C mol^{-1}]
H	enthalpy	[kJ]
i	current density	[A cm^{-2}]
I	current	[A]
K	equilibrium constant of hydrogen oxidation reaction	[$kPa^{-0.5}$]
K_B	equilibrium constant of Boudard's reaction	[kPa^{-1}]
K_{METH}	equilibrium constant of methanation reaction	[kPa^2]
K_{RF}	equilibrium constant of reforming reaction	[kPa^4]
K_{WGS}	equilibrium constant of water gas shift reaction	[-]
LHV_{EtOH}	lower heating value of ethanol	[J mol^{-1}]
n_i	number of moles of component i	[mol]
n_{EtOH}	total ethanol flow rate fed to the distillation column	[mol s^{-1}]
p_i	partial pressure of component i	[kPa]
$p_{r,i}$	relative partial pressure of component i	[-]
P	Pressure	[kPa]
P_{den}	power density	[W cm^{-2}]
q	electrical charge	[A]

Q_{con}	condenser duty	[kW]
$Q_{C,MIN}$	minimum cooling utility	[kW]
Q_D	reboiler duty	[kW]
Q_{ex}	heat from an external heat source	[kW]
$Q_{H,MIN}$	minimum heating utility	[kW]
Q_{MHR}	maximum heat recovery	[kW]
Q_{Net}	net useful heat	[kW]
Q_{PH1}	energy required for Preheater 1	[kW]
Q_{PH2}	energy required for Preheater 2	[kW]
Q_{PH3}	energy required for Preheater 3	[kW]
Q_R	energy involved the combustion of exhausted gases and cooled to the exit temperature	[kW]
Q_{RF}	energy required for a reformer	[kW]
Q_{SOFC}	exothermic heat released from an SOFC stack	[kW]
$Q_{SOFC,Net}$	net exothermic heat from SOFC system	[kW]
Q_u	useful heat	[kW]
r	area specific resistance	[Ω cm^2]
r_{act}	activation polarization area specific resistance	[Ω cm^2]
r_e	Electrolyte area specific resistance	[Ω cm^2]
$r_{H2,cons}$	rate of hydrogen consumed by electrochemical reaction	[mol s^{-1}]
r_o	other area specific resistance	[Ω cm^2]
r_{ohm}	ohmic polarization area specific resistance	[Ω cm^2]
r_{tot}	total area specific resistance	[Ω cm^2]
R	gas constant	[J mol^{-1} K^{-1}]

Sp	split fraction	[-]
T	temperature	[K]
$T_{anode,in}$	anode inlet temperature	[K]
$T_{cath,in}$	cathode inlet temperature	[K]
T_{RF}	reforming temperature	[K]
T_{SOFC}	SOFC Temperature	[K]
ΔT	temperature difference	[K]
ΔT_{min}	minimum temperature difference	[K]
U_f	operating fuel utilization	[%]
$U_{f,i}$	partial fuel utilization	[%]
V	operating voltage	[V]
W_e	electrical power	[kW]
$W_{e,max}$	maximum electrical power	[kW]
x_i	mole fraction of component i	[-]

Subscripts

a	anode
c	cathode

Greek letter

δ	thickness	[cm]
η_{CHP}	CHP efficiency	[%]
η_{elec}	electrical efficiency	[%]
$\eta_{elec,th}$	theoretical electrical efficiency	[%]
$\eta_{ov,elec}$	overall electrical efficiency	[%]

η_{sys}	system efficiency	[%]
φ	potential	[V]
ρ	resistivity	[ohm cm]

CHAPTER I

INTRODUCTION

With increasing economic and environmental concerns, technologies with high system efficiencies and low environmental impact are of great interest. Hydrogen-fuelled fuel cells have emerged as an environmental-friendly technology that releases only steam instead of harmful products from fossil fuel combustion; for example, carbon oxides and nitrogen oxides. In addition, they benefit from high achievable electrical efficiencies compared with conventional processes due to direct energy conversion. Fuel cells are more promising electric generators because they can achieve 45-60% electrical efficiency for a single cycle and 90% for total efficiency when the heat recovery is combined (Badwal & Foger, 1996). For stationary applications, two types of fuel cells (i.e., solid oxide fuel cell (SOFC) and molten carbonate fuel cell (MCFC)) are usually of interest due to their high generated power and wide range of operation. Because an SOFC uses a solid oxide electrolyte, it gains the advantage of easy operation and maintenance, compared to MCFC which normally has problems from corrosion and evaporation of electrolyte.

With high operating temperature (1073-1273 K), fuel types for SOFCs are flexible; for example, hydrogen, methane or natural gas, gasoline, diesel, aviation jet fuel, methanol, ethanol, etc. Currently available fuels are hydrogen, methane from natural gas, diesel and gasoline. However, these fuels are from fossil sources and currently subjected to high price problem and shortage. Therefore, renewable fuels are alternative sources for a green SOFC. Ethanol is an interesting renewable fuel that can be obtained from fermentation of biomass including agricultural materials (e.g. sugar cane) and waste materials from agro-industries. Moreover, it offers advantages of easy storage and handing. However, it was well known that carbon formation is a major problem encountered for SOFC when operated with hydrocarbon-based fuels. Fortunately, this problem can be prevented by introducing an appropriate amount of steam input.

To operate an SOFC, ethanol has to be initially reformed into hydrogen in a reforming section before being fed into the SOFC. Three reactions can be used to reform ethanol; namely, steam reforming reaction, dry reforming reaction and partial oxidation. Among these, steam reforming is chosen in this study due to a common route to produce hydrogen in commercial applications. Theoretically, two types of electrolyte (e.g. proton conducting- and oxygen ion-conducting electrolyte) can be employed in an SOFC operation. The difference between these two electrolytes is the location of steam produced by electrochemical reaction. With an oxygen ion conducting electrolyte, the steam appears at the anode chamber while the steam is produced at the cathode side for a proton conducting electrolyte. Demin et al. (2001, 2002) studied the effect of electrolyte on the performance of SOFCs fuelled by hydrogen and methane; however, the investigations were based on the same inlet steam to ethanol ratio. Assabumrungrat et al. (2004) reported that different electrolytes required different inlet steam to ethanol ratio. The oxygen ion conducting electrolyte required lower steam input than proton conducting electrolyte. Therefore, the benefit of lower steam input in the case of oxygen ion conducting electrolyte should be taken into account. Moreover, the effect of different modes of operations (i.e. plug flow (PF) and well-mixed (WM)) and feeding pattern (i.e. co-current and counter-current), which may affect the requirement of steam input, on SOFC performance were also investigated. In addition, it is well known that a proton conducting electrolyte has high resistivity, implying that SOFC-H^+ should be inferior to SOFC-O^{2-}. Therefore, the current status of SOFC-H^+ and its development should be determined.

An SOFC system operation requires several additional units apart from an SOFC stack, for example, heaters for heating reactants (i.e. mixture of ethanol and steam and air), a reformer and an afterburner for providing heat to other parts of the system. There are many investigations of SOFC systems. The previous systematic studies mostly involved hydrogen-fed and methane-fed SOFC systems; however, investigations of ethanol-fed SOFC plants are still new. Most of ethanol-fuelled SOFC systems use pure ethanol mixed with water to obtain a desired concentration before being fed to the system. This is not efficient from an energy point of view. Some water is needed for ethanol reforming; therefore, concentrating low purity

ethanol concentration to a high purity ethanol is unnecessary. Moreover, distillation energy is wasted. In this study, it is interesting to integrate a distillation column to the SOFC system. Bioethanol is fed as feedstock and purified to yield the desired purity and recovery before feeding to the SOFC system. Previous work has reported that some exothermic heat produced from SOFC system can be used for other parts of the system (Riensche et al., 1998). In our case, the exothermic heat is used for providing heat to heaters, a reformer and a distillation column. Nevertheless, no sequence of thermally-integrated unit operation is investigated. System configurations and design of heat exchanger network are finally investigated.

From the above reasons, this research is, therefore, focused on ethanol-fuelled SOFC systems. The objectives of this study were

1. To study the theoretical performance of an ethanol-fuelled SOFC unit with different types of electrolytes (i.e., a proton- and oxygen ion-conducting electrolytes) when operating under different modes of operation (i.e., well-mixed and plug flow mode) and different feeding patterns (i.e., co-current and counter-counter) by considering the difference in steam requirement of SOFCs,

2. To compare actual performance of the SOFC-H^{+} and the SOFC-O^{2-} by considering losses in SOFC operations,

3. To study the performance of an ethanol-fuelled SOFC system integrated with a distillation column and to investigate the effect of operating parameters on its performance and,

4. To design heat exchanger networks for the ethanol-fuelled SOFC-DIS system.

CHAPTER II

THEORY

This chapter presents a general description of fuel cells including the basic principles, type of fuel cells, the components of fuel cells and its electrical performances. Solid Oxide Fuel Cell (SOFC), SOFCs system, ethanol steam reforming reactions and heat exchanger network are also described.

2.1 Fuel Cell

2.1.1 Basic Principles

A fuel cell is similar to a battery cell (galvanic cell) in terms of generating direct current (DC) electricity from electrochemical reactions. More clearly, fuel cells consist of two electrodes (cathode and anode), one electrolyte sandwiched between electrodes and the path of current connecting the anode and cathode. Fuel is fed to the anode while oxidant is fed to the cathode as presented in Figure 2.1. Fuel (typically hydrogen) and oxidant (typically oxygen) are consumed. The electrochemical reactions take place at the electrodes, the ions and electrons transfer via an electrolyte and current path, respectively. However, the major difference between galvanic cells and fuel cells is that fuel cells are considered as an energy conversion device while galvanic cells are regarded as an energy storage device. Typical fuel cells are continuously fed by fuel/oxidant and operated until fuel/oxidant is no longer supplied to electrodes whereas galvanic cells use solution contained in the cell until the electrode is completely corroded.

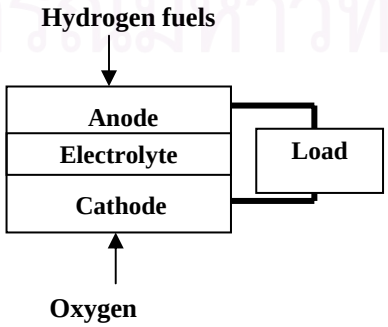

Figure 2.1 Components of a fuel cell and its operation.

2.1.2 Advantages of Fuel Cell

- Higher efficiency than conventional processes
- Low emission of SO_x, NO_x, hydrocarbon, particulates
- Simplicity
- Silent

2.1.3 Cell Components

A fuel cell consists of an electrolyte sandwiched between two electrodes. Current is collected via an interconnector. The required properties for each component can be summarized as follows.

2.1.3.1 Cathode/anode

As shown, the cathode surrounded in the oxidizing atmosphere at high temperature provides pathway of electrons. Therefore, the properties that the cathode should have are presented as follows.

- High electronic conductivity
- Chemical and structural stability during operation and fabrication
- Suitable thermal expansion with other components (electrolyte and interconnector)
- Less reactivity in the vicinity of the electrolyte and interconnector
- Sufficient porosity for gas transport into the cathode

For the anode, the high electronic conductivity is also needed. Because the anode is operated in the reducing atmosphere as presented in the scheme, the required properties are different from that of the cathode. The anode should tolerate a reducing atmosphere. In some cases, the anode is used for catalytic reforming reaction in hydrocarbon-based fuelled system.

2.1.3.2 Electrolyte

The electrolyte provides the pathway of ion produced from electrochemical reaction at the electrodes. The properties of electrolyte are:

- High ion conductivity

- Less electrical conductivity
- Thermal stability during operation
- Dense electrolyte for preventing gas mixing

2.1.3.3 Interconnector

The interconnector is the component which collects current from the SOFC cell; therefore, its required properties are:

- High electronic conductivity
- Chemical and structural stability during operation and fabrication
- Suitable thermal expansion with other components
- Less reactivity with vicinity electrolyte and interconnector

2.1.4 Types of Fuel Cells

Types of fuel cell are classified by electrolyte materials which are significantly related to operating temperature. The information for each type of fuel cell is presented in Table 2.1.

Table 2.1 Mobile ions and operating temperatures for various fuel cells.

Fuel Cell Type	Mobile Ion	Operating Temperature
Alkaline (AFC)	OH^-	323-473 K
Proton exchange membrane (PEM)	H^+	323-373 K
Phosphoric acid (PAFC)	H^+	493 K
Molten carbonate (MCFC)	CO_3^{2-}	923 K
Solid oxide (SOFC)	O^{2-}	773-1273 K

2.1.5 Fuel Cell Applications

Due to different operating temperature and its power demand, their applications can be classified as follows.

2.1.5.1 Portable Application

This type of fuel cell is used as a battery for a notebook or some electronic equipment due to its higher energy density.

2.1.5.2 Vehicle Application

An important requirement for this application is quick start-up; therefore, low operating temperature is required. The fuel cell which is suitable for this propose is PEMFC. However, due to low operating temperature, the active electro-catalyst is necessary and the fuel introduced into the fuel cell must be purified.

2.1.5.3 Stationary Application

High temperature fuel cells (i.e. SOFC and MCFC) are required for this application. Stationary application is generally for a power plant or auxiliary power for industrials or residential purpose.

2.2 Solid Oxide Fuel Cell

2.2.1 Principle of SOFC Operation

Generally, there are two types of electrolytes which are possible for SOFC operation; namely, a proton conducting electrolyte and an oxygen ion conducting electrolyte. Commonly, an oxygen ion conducting electrolyte is employed to SOFC operation, in here called SOFC-O^{2-}. Due to its chemical stability and low resistance, high performance can be obtained. In contrast, a proton conducting electrolyte whose mobile ion is a proton (H^+) has much higher resistance. Therefore, the SOFC with a proton conducting electrolyte (SOFC-H^+) is not widely investigated in a real operation and most of investigations mainly focus on the development in proton conducting materials. Because of the difference in type of mobile ion, the reactions occuring at the electrodes are also different as shown in Figure 2.2.

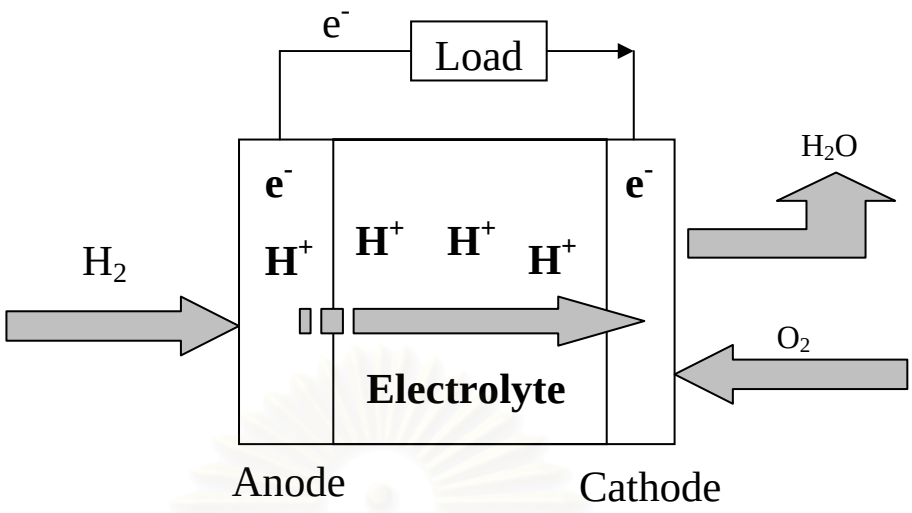

Figure 2.2 Basic principle of SOFC-H^+ operation.

The electrochemical reaction in the SOFC-H^+

Anode : $2H_2 = 4H^+ + 4e^-$ (2.1)

Cathode: $O_2 + 4H^+ + 4e^- = 2H_2O$ (2.2)

Overall : $2H_2 + O_2 = 2H_2O$ (2.3)

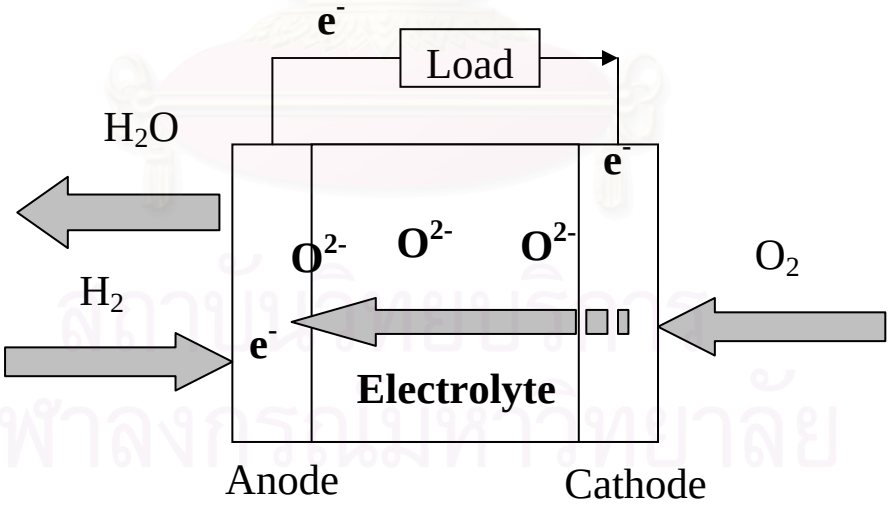

Figure 2.3 Basic principle of SOFC-O^{2-} operation.

The electrochemical reaction in the SOFC-O^{2-}

Anode : $H_2 + O^{2-} = H_2O + 2e^-$ (2.4)

Cathode : $O_2 + 2e^- = O^{2-}$ (2.5)

Overall : $2H_2 + O_2 = 2H_2O$ (2.6)

For the SOFC-O^{2-}, oxygen molecules at the cathode gain electrons from the current circuit and become oxygen ion species passing through the electrolyte. The oxygen ion is then reacted with hydrogen molecules which are fed to the anode. The electrochemical reaction takes place and the steam is generated at the anode. In contrast, in the case of SOFC-H^+, hydrogen molecules at the anode separate into proton ions and electrons. The proton ions then move across the electrolyte and react with oxygen molecules fed to the cathode. The steam is then produced at the cathode. Obviously, the location of the electrochemical steam produced for different types of electrolyte is dissimilar. Briefly, the location of the produced steam is at the anode electrolyte in the case of SOFC-O^{2-}. On the other hand, the steam is located at the cathode for SOFC-H^+.

2.2.2 Characteristics of SOFCs

2.2.2.1 Electromotive Force

Electromotive force (EMF) is the maximum possible voltage that can be achieved when are operating at a specific condition. Due to different concentration of components between the anode and the cathode, this causes different potential at the anode and cathode and results in EMF of the cell. EMF drives electrons from one electrode to another and generates current.

2.2.2.2 Losses

Though the EMF is the theoretical maximum possible voltage, the actual voltage of SOFC is always less than the theoretical value due to presence of losses. Losses can be divided into four types.

a) Activation Loss

Activation loss is the loss which occurs from electrochemical reaction at the electrodes. Some energy is required as an activation energy for electrochemical reaction, e.g. adsorption of reactant on the electrode surface and desorption of product

out of the surface. Normally, activation loss dominates at low current density and the characteristics curve also exhibit non-linear. However, at the high operating temperature like SOFC temperature, the rate of this step is very fast, resulting in small value of activation losses. The linear characteristics curve can be observed.

b) Ohmic Loss

Ohmic loss is a major loss in the SOFC stack when compared to other losses. Ohmic loss results from the resistance of flow of electrons through the electrodes and an interconnectoror and the resistance of flow of ion passing through an electrolyte.

c) Fuel Crossover or Internal Current Loss

Normally, an electrolyte should transport only ions through the cell and no fuel cross over the electrolyte. However, fuel crossing through an electrolyte or electrons leaking to an electrolyte is possible. Generally, fuel crossover loss is very small.

d) Concentration Loss

Concentration loss is caused by the large reduction in concentration of fuel or oxidant when operating SOFC at high current density or high fuel utilization. The difference between the concentration of gas in the bulk and the concentration of gas on the electrode surface causes this type of loss. At lower fuel utilization and current density, concentration loss is very small.

2.3 An SOFC System and its Subsystems

2.3.1 System Components

For SOFC system, two types of system can operated, that is, a gas turbine solid oxide fuel cell system (SOFC-GT) and a combined heat and power solid oxide fuel cell system (SOFC-CHP). For SOFC-GT, the additional power is achieved from combustion energy of unreacted fuels from a fuel cell using for driving a gas turbine. The purpose of SOFC-GT system is to be a power plant as it can produce power in the range of megawatt. In contrast, SOFC-CHP recovers heat from the combustion energy and provides heat to other equipments in the SOFC system. The excess heat left after heat exchanging in the system is used for hot water or air conditioning production. The generated power is in the range of 1-200 kilowatt. No additional

electricity is produced for the type of system. SOFC-CHP system is generally applied for auxiliary power for industrial plant and residential purpose. In this study, the SOFC-CHP is only investigated. To produce electricity for real utilization, some additional process equipments are required. The processes in addition to the SOFC, which is the most significant process for electric generation, are called 'subsystems'. Simply, the SOFC system can be classified into four main sections: fuel processing, electric generation, heat recovery and electric power conditioning.

2.3.1.1 Fuel Processing Section

The fuel processing section's function is to prepare incoming reactants before feeding to SOFC. Mainly, the hydrocarbon fuels are reformed into synthesis gas in order to avoid carbon formation in the SOFC stack. The major equipment in fuel processing section as listed below.

- A distillation column is used for purifying ethanol to reach the preferable purity before being fed to an SOFC unit.
- A blower is used for transporting reactants (fuels and oxidants) into equipments.
- A vaporizer generates steam and ethanol vapour before coming into a reformer.
- A reformer converts hydrocarbon fuels into the hydrogen fuel for the SOFC unit.

Although desulphurization processes are common in petroleum fuel processing processes, there are not needed for the ethanol-fuelled SOFC system because ethanol does not come from petroleum products which contain large amounts of sulphur in crude oils. In contrast, ethanol is derived from the fermentation of agricultural products.

2.3.1.2 Electric Generation

The main unit operation is an SOFC stack. The synthesis gas from the external reformer and the heated air are fed to the anode and cathode, respectively. The SOFC produces DC power via electrochemical reaction.

2.3.1.3 Heat Recovery Section

The heat recovery system consists of heat exchangers and an afterburner used for burning unreacted fuel from the anode chamber with depleted air from the cathode chamber. The heat obtained from the afterburner is used to provide energy to other equipment. Moreover, the anode off-gas can also be used for preheating streams. The configurations for heat recovery system are numerous and discussed in the literature review section.

2.3.1.4 Electric Power Conditioning

For additional electricity generating process, a gas turbine is used for generating the additional electricity for the main process. Moreover, the electric power conditioning consists of a direct current-alternating current (DC-AC) inverter which is used for converting DC into AC for actual utilization. However, no additional turbines or DC-AC inverter are considered in this study.

2.4 Ethanol Steam Reforming Reaction

2.4.1 Reactions

For ethanol steam reforming reaction, Eq. (2.7), two reactions generally take place coupling with steam reforming reaction. One is the water gas shift reaction, Eq. (2.8) and the other is the methanation reaction, Eq. (2.9) as shown in the following scheme.

$$C_2H_5OH + H_2O \rightarrow 4H_2 + 2CO \quad (2.7)$$

$$H_2O + CO = CO_2 + H_2 \quad (2.8)$$

$$3H_2 + CO = CH_4 + H_2O \quad (2.9)$$

It is known that steam reforming is a highly endothermic and slow reaction. The water gas shift reaction is fast and it can reach equilibrium quickly (Nagata et al., 2001). Lastly, methanation is an exothermic reaction; however, above 1000 K, methanation hardly takes place.

Generally, hydrocarbon fuels, in this study ethanol, are reformed into hydrogen and carbon oxides (CO, CO_2). These carbon oxides can lead to carbon formation which is a major problem for SOFC performance by decreasing active surface of electrode and causing cell component crack due to the difference in thermal expansion. Carbon formation takes place from the following reactions:

$$2CO = CO_2 + C \quad (2.10)$$

$$CH_4 = 2H_2 + C \quad (2.11)$$

$$CO + H_2 = H_2O + C \quad (2.12)$$

For carbon formation, the most constrained reactions is Boudard's reaction, Eq (2.10). This is because Boudard's reaction yields the lowest Gibb's reaction which implies that the reaction is more likely to take place compared to other reactions. To notify if carbon forms in one certain condition, the activity of carbon formation is then calculated as shown in Eq (2.13).

$$\alpha_c = \frac{K_c P_{CO}^2}{P_{CO2}} \quad (2.13)$$

Carbon is formed when carbon activity is greater or equal to 1 (Garcia & Laborde et al, 1996).

2.4.2 Types of Reforming Operation for SOFC

There are various fuels which can be fed to the SOFC; for example, hydrogen, methane, methanol, ethanol, gasoline or even biomass. However, hydrocarbon fuels need to be reformed into hydrogen before being fed to the SOFC in order to prevent coking inside SOFC. There are three modes of reforming operation for the SOFC: i.e. External Reforming (ER), Indirect Internal Reforming (IIR) and Direct Internal Reforming (DIR). Each type of operation will be discussed as follows.

(a)

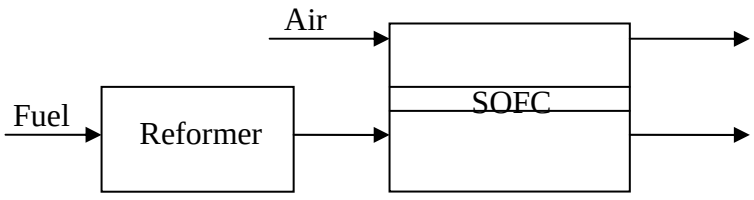

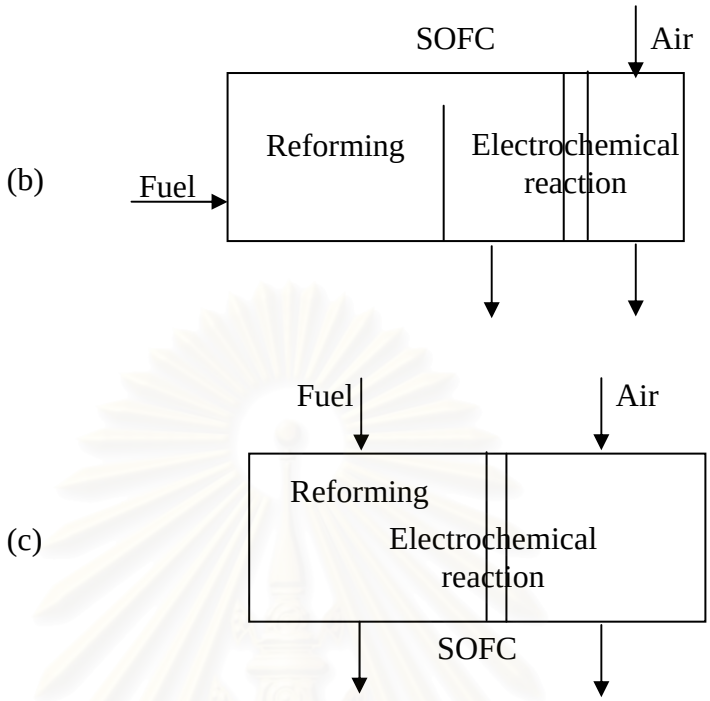

Figure 2.4 Type of reforming reaction for SOFC operation: (a) ER, (b) IIR and (c) DIR.

As illustrated in Figure 2.4, the differences in types of reforming are the location of reforming section. It should be noted that electrochemical reactions are exothermic and reforming reaction is endothermic. It is beneficial to use exothermic heat from the SOFC section to the endothermic area, the reforming section. As shown in Figure. 2.4(a), ER shows that the reforming section and the SOFC section (in other words, electrochemical section) are completely separated. Therefore, no electrochemical steam and heat from the SOFC section involves the reforming section. For IIR in Figure 2.4(b), it can be seen that the reforming section is attached next to the SOFC section, but the reforming reaction still separates from the SOFC section. In this case, IIR benefits the exothermic heat from the SOFC section to the reforming section. However, no electrochemical steam involves the reforming section. For DIR, it can be seen in Figure 2.4(c) that the reforming section and electrochemical section are in the same location. Therefore, both electrochemical steam and exothermic heat directly influence the reforming section.

2.5 Heat Exchanger Network (HEN)

2.5.1 Composite Curves

The hot composite and cold composite curves are constructed on the temperature and enthalpy axes. As depicted in Figure 2.5, temperature is plotted on Y axis and enthalpy on X axis. The inverse of the slope of the curve is heat capacity. Commonly, the temperature of the hot composite is hotter than that of the cold composite curve for all points. The enthalpy region that the hot composite curve overlaps the cold composite curve indicates the amount of heat that can be recovered (Q_{MER}). The region of the cold stream beyond the hot stream is an amount of hot utility required (Q_{HMin}). On the other hand, the part of the hot composite stream beyond the cold stream is an amount of cold utility required (Q_{CMin}).

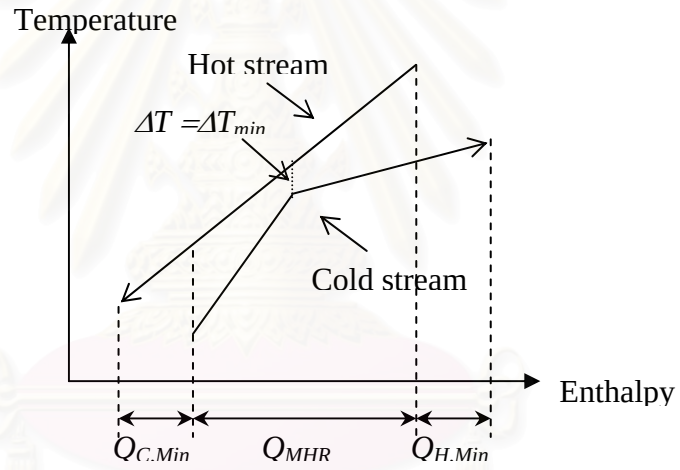

Figure 2.5 Composite curves for pinch problem.

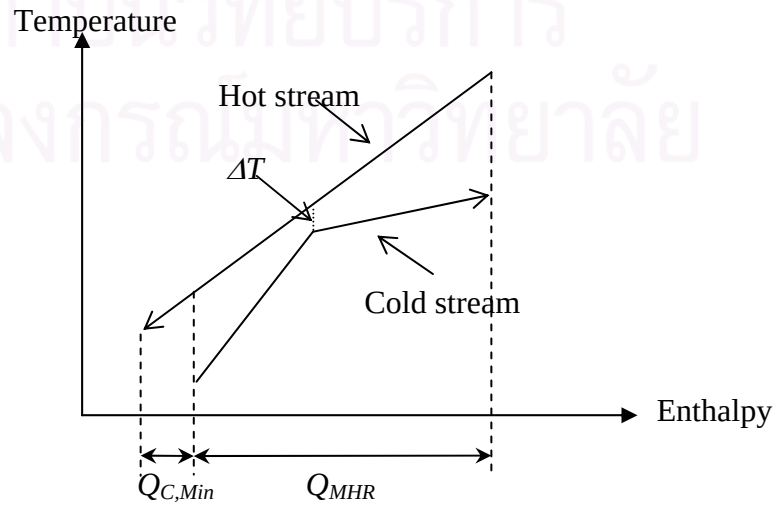

Figure 2.6 Composite curves for threshold problem.

Generally, two types of composite curve can be found: the so-called pinch case and threshold case. For pinch case, the cold composite curve is moved horizontally toward the hot composite curve until it reaches the minimum temperature difference (ΔT_{min}). In contrast, for threshold case, the cold composite curve moves toward the hot composite curve until either Q_{HMin} or Q_{CMin} reaches 0. The narrowest gap between hot and cold composite curve for the threshold case is ΔT which is generally higher than ΔT_{min}. Examples of composite curves for pinch case and threshold case are illustrated as shown in Figure 2.5 and 2.6, respectively. In Figure 2.6, the Q_{HMin} has been eliminated and only Q_{CMin} remains.

2.5.2 Heat Exchanger Network Design

To design heat exchanger network to reach the maximum energy recovery (MER), the cold composite curve is moved horizontally toward the hot composite curve. As mentioned earlier, two different types of composite curves (i.e. pinch case and threshold case) can be detected. The heat exchanger network design for pinch case and threshold case are described as follows.

2.5.2.1 Pinch Case Design

For pinch case, the cold composite curve is horizontally moved to the hot composite curve till two composite curves are close to ΔT_{min}. The amount of cold utility required for MER case is the minimum of cold utility so-called $Q_{C,min}$. On the other hand, the amount of hot utility required for MER design is the minimum hot utility and so-called $Q_{H,min}$. Rules of MER design, which offers minimum utilities, comply with the following concepts.

- No use of cold utility above pinch
- No use of hot utility below pinch
- No heat transfer across the pinch

As mentioned earlier, in order to obtain MER design, no heat transfer across the pinch point. Hence, the design of heat exchanger network is separated into two

parts: above pinch and below pinch. To avoid temperature crossover, the MER design for both below pinch and above pinch should start at the pinch point. The detail of designing for each part is described as follows.

a) HEN Design above Pinch

As shown in Figure 2.5, the composite curves above pinch are narrowed to the pinch point. The slope of the hot streams near the pinch point should be higher than that of the cold streams so that the temperature does not cross over. As mentioned earlier, the inverse of the slope of the hot or cold stream is the heat capacity of that stream. In other words, the heat capacity of the hot stream should be lower than that of the cold stream as shown in Eq. (2.14) if we are going to match them in a heat exchanger network.

$$C_{P,H} < C_{P,C} \tag{2.14}$$

b) HEN Design below Pinch

For below pinch, the hot streams near the pinch point with higher heat capacity should match with the cold streams which have lower heat capacity as shown in Eq (2.15).

$$C_{P,C} < C_{P,H} \tag{2.15}$$

c) Heat Exchanger Loop and Utility Path

Loop is a circle of heat shifted around the heat exchanger network. Figure 2.7 illustrates the matching streams for one heat exchanger network. The circle specifying E, H and C inside represents heat exchanger, heater and cooler, respectively. From Figure 2.7, there is one loop inside the network i.e., E2-E4-E4-E2.

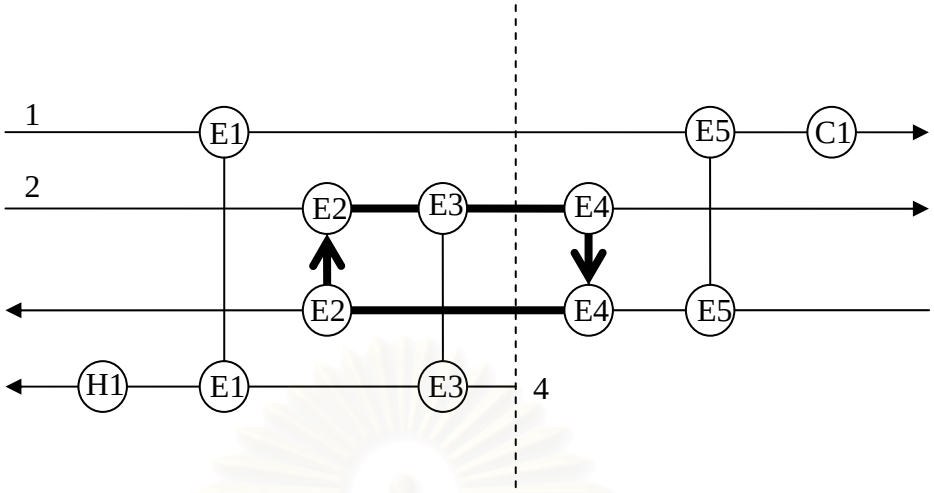

Figure 2.7 Loop in a heat exchanger network.

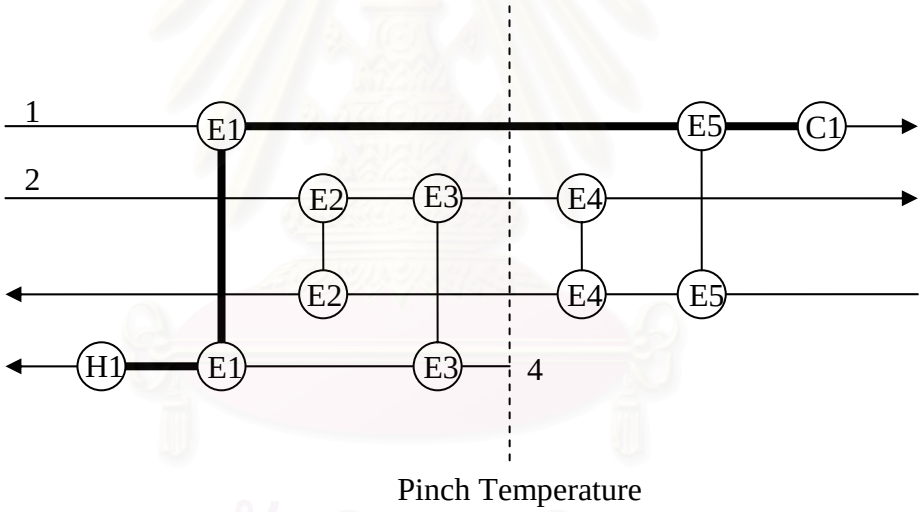

Figure 2.8 Utility path in heat exchanger network.

Utility path is a connection line between a heater and a cooler via heat exchangers. As depicted in Figure 2.8, H1-E1-C1 is considered as a utility path of the heat exchanger network. The network performance with the existence of heat exchanger loop and utility path should be further considered after obtaining the MER design.

2.5.2.2 Threshold Case

The design of the threshold problem is similar to that of pinch problem. However, the narrowest gap in the composite curve is called ‘pseudo-pinch’ point. The heat exchanger network design follows the concept of MER design for the pinch problem but depends on where the location of pseudo-pinch is. Three possible location of pseudo-pinch are presented as follows. Figures 2.9, 2.10 and 2.11 illustrate the location of pseudo-pinch in the middle, at the hot end and at the cold end of composite curve, respectively. For the mid pseudo-pinched case, the composite curve is most restricted in the middle of the composite curve. The design of composite curves is, therefore, divided into ‘above pseudo-pinch’ and ‘below pseudo-pinch’. Both ‘above pseudo-pinch’ and ‘below pseudo-pinch’ follow the same rules as presented in the pinch problem.

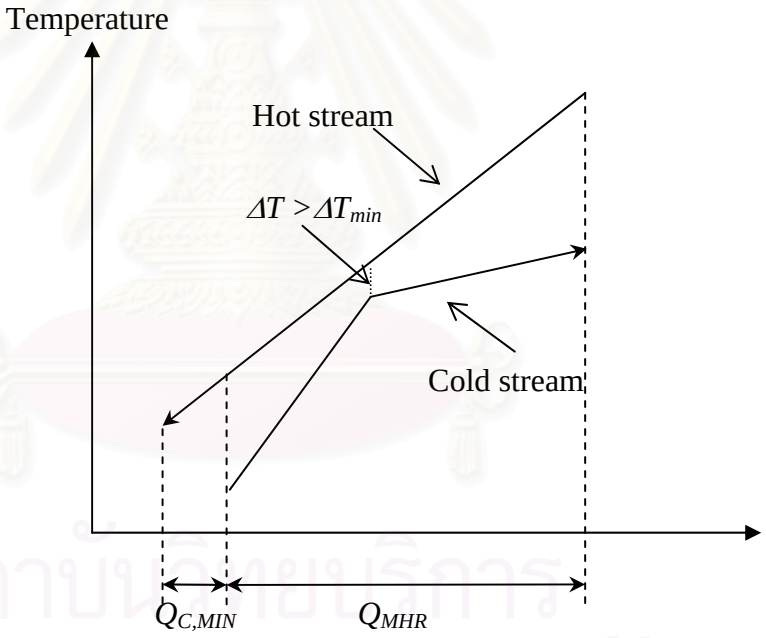

Figure 2.9 Pseudo-pinch point in the middle of composite curves.

For pseudo-pinch at the hot end in Figure 2.10, the pseudo-pinch point, or most restricted point, take places at the hot end. The heat exchanger design follows the below pinch design as presented in the pinch problem.

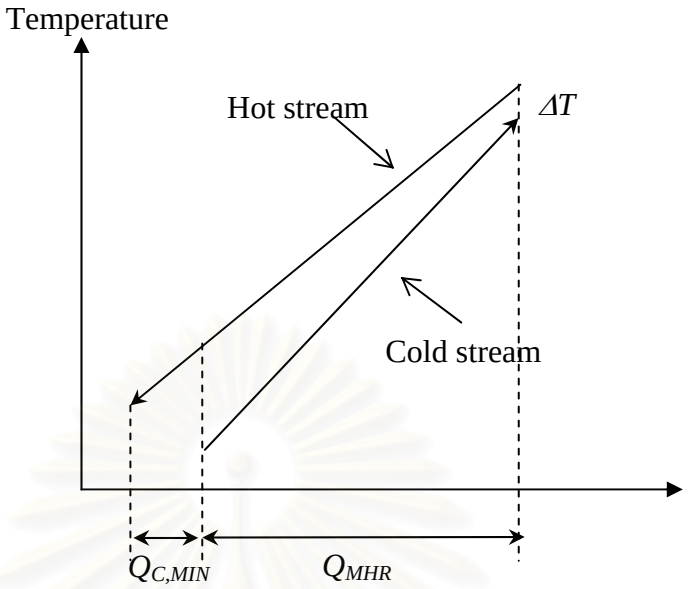

Figure 2.10 Psuedo-pinch point at the hot end.

For the case of pseudo-pinch at the cold end as shown in Figure 2.11, the location of pseudo-pinch is at the cold end. The design of heat exchanger will follow the rule for designing the above pinch as described in the pinch problem section.

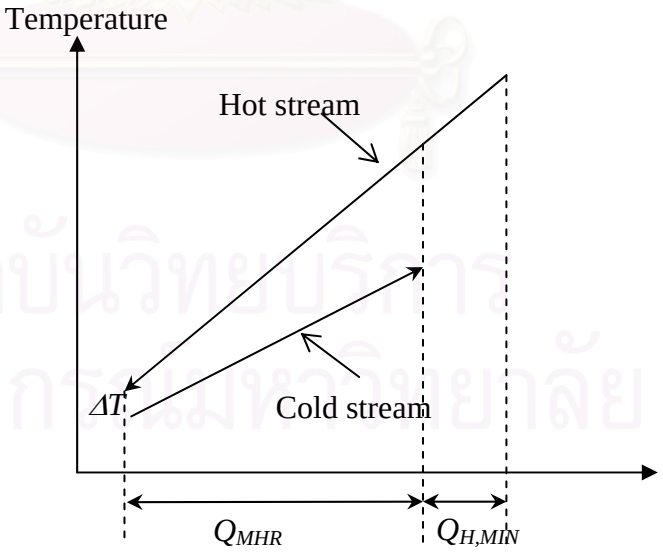

Figure 2.11 Psuedo-pinch at cold end.

CHAPTER III

LITERATURE REVIEW

In this chapter, the literature involving SOFCs is reviewed. The chapter is divided into three topics: 1) Ethanol fuels with high temperature fuel cells, 2) SOFC model and 3) SOFC system. In the beginning, previous work on ethanol fuels used for high temperature fuel cells (i.e. MCFC and SOFC) is reviewed. Next, the developed SOFC models for mass balance, energy balance and electrochemistry are summarized. Lastly, the reviews of SOFC system describing types of simulator used for SOFC system and its system configurations are presented.

3.1 Ethanol Fuels with High Temperature Fuel Cells

Due to wide interest on its renewability and environmental friendliness, ethanol is becoming an alternative fuel for SOFCs. There are several theoretical studies about ethanol reforming with high temperature fuel cells. Maggio et al. (1996) studied indirect internal reforming molten carbonated fuel cell (IIR-MCFC) fed with different fuels (i.e. methane, methanol and ethanol). The results revealed that ethanol provided higher electrical and overall efficiencies than did methane and any other fuels in the IIR-MCFC. Three issues (i.e. electrical, thermal and chemical energy) were analyzed for the performance of fuel cells. Electrical energy was defined as the produced electric power while thermal energy was defined as energy involving in heating-up reactants and heat of reactions in the reformer and the electrochemical section. Last of all, chemical energy was defined as combustion heat from unreacted fuels coming from an anode. The results showed that ethanol provided the highest voltage and electrical energy among other fuels. Its thermal energy was close to equilibrium compared with methanol-fed system; however, it was not as good as that of the methane-fed case which performs perfect thermal equilibrium.

Freni et al. (1996) studied direct internal reforming MCFC (DIR-MCFC) fed by ethanol. The operating parameters such as temperature and current density on the MCFC performance were investigated. It was found that the higher temperature, the higher EMF was obtained due to higher hydrogen production and lower ohmic loss.

However, the limitation of high temperature operation is mainly arisen from the material fabrication for MCFCs. The effect of fuel utilization on electrical efficiency was also examined. It was found that there was optimal fuel utilization around 70%. This value is applicable for practical operation due to the smaller size of the SOFC stack. The performance of ethanol-fed MCFC was also compared with that of the methane-fed MCFC at the same operating parameters. The results found that ethanol yielded higher EMF (1099.9 mV) and higher electrical efficiency (34.2%) than that of methane-fed system (1073.6 mV and 31.9%), respectively.

For an ethanol-fed SOFC, Tsiakaras et al. (2001) examined the performance of an external reforming solid oxide fuel cell (ER-SOFC) fed by products from various ethanol processings; i.e. steam reforming, CO_2 reforming and partial oxidation (POX). The SOFC was operated in the region of no carbon formation. The results revealed that the products from ethanol steam reforming reaction yielded the maximum SOFC efficiency at T < 950K and at high operating temperature (T >1100K). This high temperature is suitable for an SOFC operation. Douvartzides et al. (2002) studied the influence of fuel options on SOFC performance. Methane, methanol, ethanol and gasoline were used as fuels for the SOFC. It was reported that the minimum steam required for preventing carbon formation for different fuels can be ordered in the sequence: methane < ethanol < methanol < gasoline. However, at high temperatures (>1200 K), the minimum steam requirement for the methane-fed system was the same as that of the ethanol-fed system. The maximum efficiency was obtained close to the boundary of carbon formation for all fuels. The maximum efficiency for the methane was the highest (96%) while ethanol and methanol yielded approximately 94% and 91%, respectively. Douvartzides et al. (2004) continued their study and compared the performance of ethanol-fuelled- and methane-fuelled SOFC power plants by using the exergy analysis. The results reported that the SOFC fed by methane resulted in a higher efficiency than that fed by ethanol.

3.2 SOFC Model

For SOFC modelling, three equations are generally involved, i.e. mass balance equation, energy balance equation and electrochemical model. The equations can be simply divided into two classes: 1) zero dimension or thermodynamic-based equations and 2) transport-based equations. For the transport equations, it can be classified by dimension (i.e. one-, two- and three dimension). The decision for selecting a suitable

dimension depends on the objective of the research. Generally, one dimension is used for examining the simple profile along the stack. Two dimensions are used for investigating the profile on the surface of SOFC cell stack. Lastly, three dimensions focus on the entire stack. In this study, only one dimension is presented as below.

3.2.1 Mass Balance Equations

3.2.1.1 Thermodynamics-based Equations

As mentioned earlier, there are two solution approaches: zero dimension or thermodynamic-based approach and transport-based approach. For the first approach, there are many papers reported in the literature. Two groups are commonly classified for the thermodynamics-based approach: minimization of Gibbs free energy and stoichiometric equilibrium-based equation.

Garcia and Laborde (1991) studied ethanol steam reforming reaction with the consideration of carbon formation by using non-stoichiometric formulation or the minimization of Gibbs free energy in calculations. Six components (i.e. ethanol, H_2O, CO_2, CO, CH_4 and H_2) were assumed to be found in the system. The equations were solved using a computational program based on the ZSPOW subroutine in the IMSL library. The components were then analyzed by considering the possibility of carbon formation in Eq. (2.13). The investigation was carried out under the following conditions: 1-9 atm, 400-800 K, and various water/feed ratios from 0 to 10. The best hydrogen production was obtained at temperature higher than 650 K, atmospheric pressure and the excess water in the feed. Vasudeva et al. (1996) modified Garcia and Laborde's work by considering nine components in the system. The additional components were ethylene, acetaldehyde and solid carbon. It was assumed that the carbon was simultaneously formed with gaseous components. The minimization of Gibbs free energy method was also used. The non-linear equations were solved using a mathematical solver based on sequential quadratic programming. The results of this study indicated that small traces of ethylene and acetaldehyde were observed. Freni et al. (1996) also used this method for a direct internal reforming and indirect internal reforming molten carbonate fuel cell (IIR-MCFC). The results were first described in the previous section. Matelli et al. (2004) used STANJAN Chemical Equilibrium Solver for calculating equilibrium composition in the reformer section. The solver was based on minimization of Gibbs free energy. The performance of MCFC and SOFC system were then calculated and compared in this study. The

practical efficiency of SOFC was higher than that of MCFC; however, SOFC emitted CO_2 lower than MCFC. It was concluded that SOFC was more efficient than MCFC. The stoichiometric formulation was also used for calculating gaseous components in the ethanol reforming system operated with fuel cells.

3.2.1.2 Transport-based Equations

Another approach is the mass transport equations which are based on the kinetic rate of reaction. The composition profile is generally based on the distance along the channel. Some researchers, (Aguiar et al, 2004; Hernandez-Pecheco et al, 2005), used mass transport equations to obtain the profile of components.

3.2.1.3 Combination of Thermodynamics-based and Transport-based Equations

Nagata et al. (2001) used the combination between thermodynamic and transport approach in calculating reforming components. As mentioned in the theory section, reforming is a slow reaction whereas water gas shift reaction is a rapid reaction which reaches equilibrium rapidly. Therefore, a mass transport equation is employed in a reforming reaction while a thermodynamic equation was used in water gas shift reaction. Numerical method is used for solving the components. Assabumrungrat et al. (2004) used another method in calculations for DIR-SOFC. Normally, the profile obtained from the transport-based equation is dependent on the distance along the stack. However, this combination approach shows the profile dependent on fuel utilization. It was assumed that all reactions of Eqs. (4.1)-(4.3) were in equilibrium and the hydrogen fuel was gradually consumed along the SOFC cell. The obtained profile was based on fuel utilization and the average components for one operating fuel utilization can be achieved by the numerical integration along the profile. Bove et al. (2005) applied an analytical model for the SOFC. The mass balance for each component and voltage in the SOFC were derived in the term of fuel utilization. The results showed the difference between the simulated voltage and the experimental values. It was shown that the polarization is similar; however, EMF was slightly different.

3.2.2 Energy Balance Equations

Two approaches for energy balance of SOFC stack were presented in here, that is, zero and one dimensional approaches. In general, the zero-dimension energy

balance was used for the study of an overall system. The equations follow the first law of thermodynamics which involves enthalpy change in the controlled system. Some works (Matelli et al, 2004; Omosun et al., 2004) are based on the zero-dimension equations. However, some researchers (Nagata et al., 2001; Aguiar et al., 2004) used the one dimensional approach and focused on the temperature profile along the stack. For the one dimension approach, it usually considered the conduction in the bulk gas and the heat transfer from the adjacent solid cell in calculations. The calculation from the latter method is complicated because the temperature of solid part of cells is also involved.

3.2.3 Electrochemical Model

3.2.3.1 Models for Losses in SOFC Stack

a) Activation Loss

For the electrochemical model, there are many expressions proposed for polarization in SOFCs. For activation polarization, three types of models are generally used; for example, Butler-Volmer equation, Tafel equation and semi-correlation. For semi-correlation, three expressions are commonly used; that is, Achenbach's, Hendriksen's and Karoliussen's correlations. The comparison of these activation polarization models was investigated by Hernandez-Pacheco et al. (2004). It was illustrated that Butler-Volmer equation gave the most accurate polarization when compared with the other two methods which give approximately 5% error. For the semi-correlations, three semi-correlations gave very close values but the values were much smaller when compared with those of Butler-Volmer method at high temperature (more than 1273 K). At low temperature (less than 1073 K), the polarizations from those semi-correlations were unrealistic. However, it was suggested that semi-correlations yielded realistic value between 1173 and 1273 K. In summary, Butler-Volmer was suggested to predict the activation loss.

b) Ohmic Loss

Hernandez-Pacheco et al. (2004) also compared the correlations for predicting the resistivity of YSZ electrolyte, the commercial electrolyte for SOFC. There are many types of expressions and parameters for predicting the resistivity of YSZ electrolyte. It was proven that at 873-1073 K, all those expressions gave similar values. However, there was a small discrepancy at temperatures higher than 1173 K.

c) Concentration loss

For concentration polarization, three models are normally used; that is, the Dusty gas model, Stefan-Maxwell and Fick's law. It was suggested that the Dusty gas model was the most appropriate equation for calculating concentration polarization due to the inclusion of Knudsen effect (Suwanwarangkul et al., 2003).

3.2.3.2 SOFC Performance

The models are developed for investigating various types of SOFC systems. There are various types of state (i.e. steady or time dependent), dimensional (one, two or three dimensional), design (i.e. tubular, planar or integrated planar), flow patterns (i.e. co-, counter- or cross flow), mode of reforming (i.e. ER, IIR or DIR) and types of electrolyte (i.e., proton- and oxygen ion- conducting electrolyte). However, in this study, only the steady state was examined. A history of SOFC modelling is outlined below.

a) Types of Electrolytes

The performance of SOFC with different types of electrolyte (i.e. proton- and oxygen ion-conducting electrolyte) was first reviewed. The developed the model for comparing the performance of SOFC with a proton conducting electrolyte and that of an oxygen ion conducting electrolyte in a hydrogen-fed (Demin et al., 2001) and in methane-fed system (Demin et al., 2002). The calculation was based on the same inlet steam to ethanol ratio. It was revealed that the efficiency of SOFC-H^+ was theoretically 15% higher than that of SOFC-O^{2-} at the same conditions for both hydrogen- and methane-fed systems. Demin et al. (2002) continued investigating the performance of SOFC with a co-ionic electrolyte, which is a mixed proton and oxygen ion conducting electrolyte. The proton transfer number was set at 0.5 which means the equality of mobility of proton and oxygen ion. The EMF distribution of the SOFC with different types of electrolytes (pure oxygen ion-, pure proton- and co ionic-conducting electrolyte) was compared. The operation was studied at the maximum power and at relative power of 0.7. The result was found that the higher proton conduction yielded the higher efficiency. The EMF distribution of SOFC-O^{2-} was more irregular than that of SOFC-H^+. This corresponded to the non uniform profile of temperature within the SOFC stack. The uniform EMF of SOFC with a co-

ionic electrolyte was observed when operated at full power. However, it was found that the calculated current density due to oxygen ion mobility was negative. It was implied that electrons flow counter-currently and, therefore, it was useless to operate at this condition. When the SOFC with a co-ionic electrolyte was operated at relative power of 0.7, the uniform profile and positive current was detected. Moreover, the efficiency of co-ionic conducting electrolytes was found to be close to that of proton conducting electrolyte when operated at this condition.

Assabumrungrat et al. (2004) developed the model for predicting the minimum steam to ethanol ratio required for preventing carbon formation for different types of electrolyte (i.e. proton and oxygen ion conducting electrolyte) in a direct internal reforming SOFC (DIR-SOFC). The effect of temperature and an extent of hydrogen consumption on the minimum inlet steam to ethanol ratio were also investigated. It was found that an SOFC with an oxygen ion conducting electrolyte (SOFC-O^{2-}) required less steam than that with proton conducting electrolyte (SOFC-H^{+}) due to the benefit of electrochemical steam produced at the anode in the case of SOFC-O^{2-}. Moreover, the effect of extent of electrochemical reaction for different electrolytes was examined. For the SOFC-H^{+}, the greater the extent of electrochemical reaction, the more steam required. In contrast, the SOFC-O^{2-} required less steam when the extent of electrochemical reaction increased. This is because the benefit of electrochemical steam produced at the anode. The results also showed that the minimum steam input was decreased when increasing temperature for both electrolytes.

b) Effect of Operating Conditions on SOFC Performance

Nagata et al. (2001) studied the methane-fed tubular SOFC with internal reforming. The assumption used for this study was one dimensional for mass and temperature distribution along the gas flow direction. Grading catalyst along the channel is used as an alternative solution for non-uniform temperature distribution. The influence of operating parameters (e.g. fuel recirculation, fuel inlet temperature, air recirculation and air inlet temperature) was also examined. The results reported that the graded catalysts could help flatten temperature distribution. The internal reforming rate required less air flow rate and results in lower temperature of effluent. Consequently, the achieved voltage and efficiency were less. An increase in fuel inlet

temperature improved electrical efficiency. However, efficiency decreased when oxidant/fuel recirculation was increased. Colpan et al. (2007) investigated the effect of anode recirculation ratio and fuel utilization on SOFC performances in DIR-SOFC system fed by synthesis gas. The results indicated that anode recirculation ratio did not have a significant effect on power output, electrical efficiency at low current density; however, it strongly affected SOFC performances at high current density. Similar to Nagata's work, the higher recirculation, the lower power output and electrical efficiency were yielded. In contrast, fuel utilization strongly influenced both power output and electrical efficiency. At higher fuel utilization (85%), the lower power output was obtained but yielded higher electrical efficiency.

The effect of flow direction on SOFC performance was also investigated. Larrain et al. (2004) developed the SOFC model for a general configuration. The study was based on hydrogen-fed planar SOFC with the different feeding configurations (i.e. central feed and counter flow). The results found that the cell potentials obtained from the two different flows were the same. Nevertheless, the maximum temperature for two cases in the solid was different. The temperature of the solid for the case of counter flow showed is higher than that of the central flow. Aguiar et al. (2004) examined the anode-supported direct internal reforming SOFC at an intermediate temperature. The results showed that the SOFC operated under counter current flow showed the same results that the steep temperature gradient along the cell and asymmetry current distribution.

The effect of fuel composition introduced to the SOFC stack was examined. Costamagna et al. (2004) developed model of 20 cell stack for an integrated planar solid oxide stack (IP-SOFC). Different fuel concentrations; for example, 1) high hydrogen content, 2) low hydrogen with high CO content and 3) low hydrogen with low CO content) were investigated. The results showed that high hydrogen containing fuel with high CO content showed higher voltage than other cases because the shifting reaction occurring inside the SOFC cell leaded to higher production of hydrogen. Hernandez-Pacheco (2005) studied the influence of different syngas composition on SOFC performance. The results found the similar results to Costamagna's work that high concentration of hydrogen is preferable because of higher performance. Moreover, it was reported that high steam to fuel ratio can suppress coke formation.

The temperature distribution along the SOFC stack was also investigated. It was found that methane was rapidly consumed via steam reforming reaction at the entrance of the channel while the electrochemical reaction took place beyond the entrance and resulted in lower temperature at the entrance and higher temperature at the end of channel. The current density increased along the channel; however, it dropped sharply at the end of channel because of high concentration and activation polarization.

The effect of steam to fuel ratio on SOFC performance was investigated. Generally, it found that increasing steam to fuel ratio decreases efficiency of the SOFC. The maximum efficiency was found at the boundary of carbon formation for all types of fuels such as methane, ethanol, methanol and gasoline. Also, the minimum steam to fuel ratio decreased with increasing temperature (Douvartzides et al., 2003). Assabumrungrat et al. (2004) studied the effect of steam (e.g. inlet steam to fuel ratio and electrochemical steam produced by fuel utilization) on the minimum steam to fuel ratio and gas components in DIR-SOFC with different types of electrolyte. The results found that hydrogen increased with increasing steam ratio while CO initially increased and dropped at higher steam ratio for an oxygen ion conducting electrolyte. The effect of temperature on the minimum steam to fuel ratio showed the similar results to Douvartzides' work. However, the effect of hydrogen consumption by electrochemical reaction on the minimum steam input was different for different types of electrolyte. It was found that at higher hydrogen consumption, the lower minimum steam input was required for SOFC-O^{2-} while the higher minimum steam input was required for SOFC-H^{+}.

3.3 Solid Oxide Fuel Cell System

Although the investigation in SOFC stack is extensive, the rest of system is also important. SOFC systems are widely investigated by many researchers. Two approaches are used in system analysis; namely, 1) modelling all process equipment and simulating by using a mathematic solver (Chan et al, 2002; Omosun et al., 2004; Matelli et al, 2004) and 2) simulating the entire system by using a process simulator (Dick and Martin, 1998; Riensche et al., 1998; Herle et al., 2001; Zhang et al., 2005).

3.3.1 Types of Simulation

3.3.1.1 Mathematical Solver-based System

For the former approach, a mathematical solver is used for calculating energy, mass balance for all process equipments. There are few studies based on this method. Chan et al. (2002) used Visual Basic program for mass, energy and exergy analysis in hydrogen- and methane-fed SOFC system. The system consists of pre-heaters, a fuel cell and an afterburner. In methane-fed system, there were a pre-reformer and a vaporizer included in the flowsheet. In this work, a stream from an afterburner was used to preheat reactants (i.e. fuels and water). Both exergy and energy were employed for performance analysis. The results were found that the electrical efficiency of methane-fed system was higher than that of hydrogen for both energy-based and exergy-based analysis. Omosun et al. (2004) used gPROMS to simulate a biomass-fuelled SOFC system. For biomass-fuelled SOFC system, a gasifier converted biomass into gaseous component and then fed to a clean-up process which eliminates particles and tar from gas stream. The clean gas steam was then fed to the fuel cell stack. There were some differences in process between hot and cold processes. For example, a fluidized gasifier operating at higher temperature was used for the hot process while the cold process used a fixed bed. Furthermore, a wet precipitator and a bag filter were employed in the cold process whereas only ceramic filter was used in the hot process. The study compared two different biomass processing: cold process and hot process. The results showed that the hot process yielded higher efficiency than the cold process; however, cost of equipment was higher. The hot process gained the benefit of high temperature effluent from the system.

3.3.1.2 A process Simulator-based System

For the latter approach which uses a process simulator to simulate the SOFC system, it offers some advantages rather than the former approach due to extensive available thermodynamic data and unit operation models in a simulator. However, there is no SOFC stack module provided in simulators. Therefore, an SOFC stack has to be developed by computer languages and then linked with the simulator. Generally, a simulator is written as a series of subroutine for each unit operation. Each subroutine is written in computer languages; for example, FORTRAN™ and C++. The required language depends on simulators used. Dicks and Martin (1998)

employed in-house code created by ER/BG Company and then integrated it with SpeedUp (Aspentech) for studying a 5 kW natural gas-fed system. However, this study investigated the dynamic process which is not a scope in our study. The results suggested that control tools were needed for maintaining power output, fuel utilization and stack temperature.

Riensche et al. (1998) used Pro/II simulator with FORTRAN subroutine for a 200 kW natural gas-fuelled system. The system consists of a pre-reformer, an air pre-heater, a boiler for vaporizing water, a fuel cell, an after burner and heat recovery units. A FORTRAN subroutine was developed for an SOFC stack. The other unit operations in the system (i.e. a boiler, an afterburner, heat recovery units) were simulated by Pro/II. The influence of operating parameters (e.g. reforming rate, air temperature increase in a stack, cell voltage and fuel utilization) on plant efficiency and effective cost was examined. Herle et al. (2001) employed VALI^{TM} interfaced with MATLAB for biogas-fuelled system. In this study, MATLAB^{TM} was used to vary operating conditions (i.e. inlet fuel composition, CO_2 content, air excess and reformer/stack temperature). The system consists of a mixer, a reformer, an anode zone and a post combustor. The reactions involving the system were partial oxidation and steam reforming. The influence of air ratio, CO_2 content, steam content, air excess and stack temperature on electrical efficiency were investigated and discussed in this study. Fontell et al. (2004) used an in-house code linked with a general heat and mass balance program (GHEMB) in 250 kW natural gas-fed SOFC for combined heat and power (CHP) application. The system incorporates a sulphur removal unit, a pre-reformer, heat exchangers, a fuel cell, an afterburner, power electronics and control unit. The operating conditions were optimized for each unit. The 55-85% system efficiency was obtained. Economic analysis was performed; it was found that a stack, system control and power electronic were the major cost in the system. Zhang et al. (2005) created an SOFC unit integrated with AspenPlus^{TM}. The minimum requirement for linking of a subroutine was considered. The general equipments for SOFC system were used; for example, a reformer, a fuel cell including an anode and a cathode, a heat exchanger, an after burner. An equilibrium reactor module *gGibb* and a separator module *Sep* were used for the anode and the cathode, respectively. No user-subroutine was created for an SOFC stack. The electrochemical model used in this study was semi-correlation which was related to the difference in pressure, temperature, current density, fuel and air compositions. The influences of fuel

utilization, current density, power output and steam to carbon ratio on SOFC system were investigated.

3.3.2 SOFC-CHP System Configuration and Heat Integration

As mentioned earlier, only SOFC-CHP system was focused on this study. Riensche et al. (1998) simulated a 200 kW natural gas-fuelled SOFC system. The system consists of a pre-reformer, an air pre-heater, a boiler for vaporizing water, a fuel cell, an afterburner and a heat recovery unit. The steam produced by a boiler was mixed with fresh natural gas and then reformed into synthesis gas. The syngas was fed to anode of the SOFC. Fresh air was fed to the cathode. Unreacted fuel was burnt in an afterburner and the hot effluent gas was used for providing heat to the pre-reformer, the air heater and the boiler, respectively. The heat left after the hot flue gas heat exchanged with those unit operations was then recovered by cooling water. The influence of operating parameters (i.e. reforming rate, air temperature increase in a stack, cell voltage and fuel utilization) on plant efficiency and effective cost was investigated. The results showed that to reduce cost a complete internal reformer, low air inlet, a large increase in air stack temperature, 65% fuel utilization and the reduction of internal resistance in an SOFC stack are required. Riensche's work was extended to study the integration of cathode and anode gas recycling and the location of heat recovery unit. It was recommended that a cathode gas recycling with a jet pump and anode gas recycling should be implemented to the system. The location of heat recovery unit should be located after the boiler due to lower cost of heat exchangers (Riensche et al., 1998).

Dicks et al. (1998) studied a 5 kW natural gas-fed system. The system configuration is rather complicated. It was composed of a desulphuriser, a pre-reformer, pre-heaters, a fuel cell and a combustor. Anode effluents were divided into two streams. The first stream was re-circulated for pre-heating outlet stream from a pre-reformer and being mixed with the outlet from the desulphuriser. The other was fed to the combustor. The cathode effluent was first fed to preheat the air inlet and was then burnt with unreacted fuels in the combustor. Controlling system, for maintaining fuel utilization, stack temperature and unstable power output was required. In addition, a novel combustor, sealing for an anode recirculation fan and high temperature – low cost heat exchangers were also important issues for SOFC system.

Fontell et al. (2004) studied natural gas-fed system integrated with a desulphurization unit. The anode effluent provided heat to the anode incoming stream and then was split into two streams. One was burnt with the air effluent from the cathode in the afterburner. The other was re-circulated and mixed with the inlet stream before fed to the pre-reformer. The exhaust gas from the afterburner preheated both water stream and the sulfur-free stream. Omosun et al. (2004) studied biomass-fueled SOFC system and compared between hot and cold process. The overall system consists of three subsystems (e.g. gasification, cleanup and fuel cell subsystem). The difference between hot and cold process was addressed at gasification and clean up system. For the cold process, the co-current fixed bed reactor for cracking biomass into gases and a set of a cyclone, a filter and a wet electrostatic precipitator for eliminating tar, particulates and alkali compounds were used. In contrast to the cold process, the hot process uses a fluidized catalytic bed for gasifying biomass and no wet electrostatic precipitator is required due to low level of tar. The heat exchanger networks of fuel cell section for these systems are different. For the cold process, the anode and cathode effluent preheated the incoming anode and cathode stream, respectively, before burnt in the afterburner. On the contrary, there is no use of anode effluent to heat the incoming anode stream for the hot process. Only cathode effluent was used. In summary, the heat management of hot process gave the superior electrical and overall efficiency to that of the cold process. However, the cost of hot process is higher than that of the cold process due to the fluidized bed gasifier and the hot ceramic filter.

Zhang et al. (2005) studied SOFC system fed by desulphurized natural gas stream. The two split of anode outlet stream was the same as Fontell's work but not used for preheating the incoming anode stream. The pre-reformer was operated under adiabatic condition. The exhaust gas from the afterburner was used to heat the air inlet stream only. The effects of overall fuel utilization, current density, power output and steam to carbon ratio on the electrical performance were investigated. Braun et al. (2006) studied an anode supported SOFC with micro CHP for residential applications. The effect of types of fuels (hydrogen/methane), mode of methane reforming (internal/external reforming), fuel processing with anode recirculation, oxidant processing with cathode recirculation and the combination of recycle and internal reforming on the system performance were investigated and compared. The results showed that the methane-fuelled system with cathode and anode recirculation with

internal reforming yielded the highest efficiency among other designs. System electrical efficiency and CHP efficiency are 40% (HHV) and 79% (HHV), respectively. Interestingly, it was found in this work that when operating methane-fuelled SOFC without anode and cathode recirculation. The location of boiler used for producing steam for steam reforming has to be immediately downstream of the external reformer. The hot flue gas is then heat exchanged with an air preheater and waste heat hot water heater, respectively. This selection of the location of the boiler can prevent the pinch temperature occurred. For the case that SOFC operating under internal reforming without recirculation, it is also reported that if the methane conversion in the external reformer increases (or decreasing internal reforming) higher than 60%, this results in less thermal energy and insufficiency for heat exchanging. It was suggested the boiler has to be located at the higher temperature gas source. However, for the case which operates under internal reforming mode with anode and cathode recirculation, the boiler can be located between an air preheater and waste heat recovery hot water heater. Obviously, the sequence in heat exchanger network for SOFC-D system is very crucial for the SOFC system.

Few investigations on ethanol-fed system were published. Generally, ethanol-fueled SOFC system consists of a vaporizer, preheaters, a reformer, an SOFC stack and an afterburner. Douvartzides et al. (2003) used exergy analysis and optimization strategy to investigate the system. Pure ethanol is heated and then mixed with steam before entering the reformer. The synthesis gas from the reformer is then introduced to the SOFC stack. The excess air and unreacted fuels from stack was burnt in the afterburner. The combustion heat is supplied to the vaporizer and the reformer to sustain the reaction. Finally, the hot flue gas was heat exchanged with an ethanol/water mixture and incoming air, respectively. The exergy loss of SOFC was minimized by matching the appropriate reforming temperature and air preheating temperature. With the same system configuration, Douvartzides et al. (2004) compared the performance of SOFC system fuelled by methane or ethanol by using exergy analysis. The result found that the efficiency of methane-fed system is higher than that of ethanol-fed one. Arteaga et al. (2008) studied bioethanol-fed SOFC system. The pseudo-homogenous model for ethanol steam reforming reaction was used to investigate the external reforming reactor. The rate constants and exponent numbers of ethanol reforming are derived from experimental data by using optimization method to minimize the difference of selectivity, conversion and yield

between the calculation and experimental data. The SOFC model is based on methane reforming, water gas shift and hydrogen oxidation. The bioethanol-fed SOFC plant was simulated and composed of a mixer, a vaporizer, an ethanol/water mixture heater, a compressor, a reformer, a fuel cell stack and a furnace. The effects of steam to ethanol ratio and SOFC temperature on heat consumption in all process steps were investigated. It was reported that the heating consumption for vaporizing the H_2O/EtOH mixture increases with increasing the steam to EtOH ratio. Moreover, it was found that the H_2 production initially increases but decreases when H_2O:EtOH ratio is higher than 8. For the effect of reforming temperature, the higher reforming temperature increases the fuel cell efficiency and also decreases energy used for heating up the synthesis gas from reforming temperature to SOFC temperature. However, the higher energy consumption for heating up the mixture from room temperature to reforming stage and for the external reformer is needed. Also, the H_2 selectivity increases with increasing temperature. At higher temperature the water gas shift reaction becomes reversed and results in higher amount of CO.

CHAPTER IV

MODELLING

This chapter presents mathematical models developed for use in this study. The models include mass balances, energy balances and electrochemical reactions. The flowchart of calculation is also presented in this chapter.

4.1 Mass Balance Equations

4.1.1 Types of Electrolytes

As mentioned earlier, there are two types of electrolyte, i.e., oxygen ion-conducting- and proton conducting electrolyte. The reactions inside the SOFC stack are, therefore, different. The main difference for different types of electrolyte is the location of electrochemical steam produced as shown in Figure 4.1. For proton conducting electrolyte, the electrochemical steam is produced at the cathode chamber. On a contrary, the steam is produced at the anode chamber for the oxygen ion conducting electrolyte. Due to the difference in location of electrochemical steam generated, mass balance for different types of electrolyte is also dissimilar.

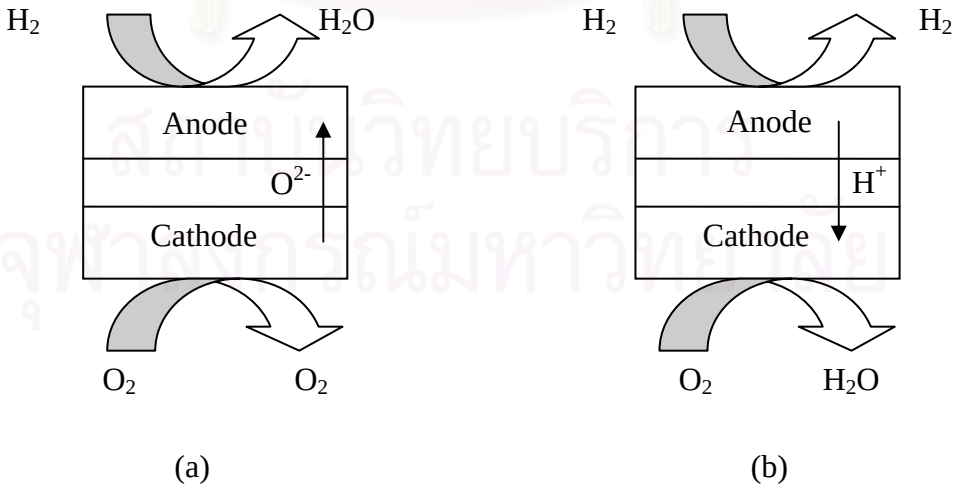

Figure 4.1 Electrochemical reactions for different types of electrolyte: a) Oxygen-ion conducting electrolyte, b) Proton conducting electrolyte.

As described in Chapter II (Theory), three reactions are considered in this section, i.e., ethanol reforming, water gas shift and methanation. Due to different location of electrochemical steam, the models for two electrolytes are, therefore, different as shown in Eqs. (4.1) – (4.12). Briefly, most of components for two different electrolytes are the same except for moles of water. It should be bear in mind that the mole of produced electrochemical steam equals to the mole of hydrogen consumption '*c*'. The moles of oxygen consumed by electrochemical reaction equals to half of hydrogen consumption. For anode's component, the moles of water are added by electrochemical steam in the case of SOFC-O^{2-} as shown in Eq. (4.6) whereas no mole of electrochemical steam is added for SOFC-H^{+} as shown in Eq. (4.7). For cathode's component, electrochemical steam is added in moles of water for SOFC-H^{+} as presented in Eq. (4.12) while the moles of water are the same for SOFC-O^{2-} as shown in Eq. (4.11). It should be noted that for the cathode chamber, O_2 is only involved the electrochemical reaction. N_2 is assumed to be inert.

For anode's components

$$n_{EtOH} = n_{EtOH,in} - x \tag{4.1}$$

$$n_{CH_4} = z \tag{4.2}$$

$$n_{CO} = 2x - y - z \tag{4.3}$$

$$n_{CO_2} = y \tag{4.4}$$

$$n_{H_2} = 4x + y - 3z - c \tag{4.5}$$

$$n_{H_2O} = n_{H_2O,in} + c - y + z \quad \text{(for oxygen ion conducting electrolyte)} \tag{4.6}$$

$$n_{H_2O} = n_{H_2O,in} - y + z \quad \text{(for proton conducting electrolyte)} \tag{4.7}$$

$$n_{tot} = \sum_{i-1}^{6} n_i \tag{4.8}$$

For cathode's components

$$n_{O_2,c} = n_{O_2,in} - 0.5c \tag{4.9}$$

$$n_{N_2,C} = n_{N_2,in} \tag{4.10}$$

$$n_{H_2O,C} = n_{H_2O,in} \quad \text{(for oxygen ion conducting electrolyte)} \tag{4.11}$$

$$n_{H_2O,C} = n_{H_2O,in} + c \quad \text{(for proton conducting electrolyte)} \tag{4.12}$$

where $n_{EtOH,in}$ $n_{H_2O,in}$ $n_{O_2,in}$ $n_{N_2,in}$ represent moles of ethanol inlet, steam inlet, oxygen inlet and nitrogen inlet, respectively, *c* mole of hydrogen consumed by electrochemical reaction, *x* an extent of ethanol reforming reaction, *y* an extent of water gas shift reaction, *z* an extent of methanation.

4.1.2 Types of Reforming

4.1.2.1. SOFC-DIR Operation

As mentioned earlier, SOFC has several types of reforming operation (i.e. External Reforming (ER), Indirect Internal Reforming (IIR) and Direct Internal Reforming (DIR)). In Chapter V and VI, the SOFC-DIR is employed in the study. For the case of ethanol-fed SOFC-DIR system, three reactions take place inside the anode chamber, i.e., ethanol reforming, water gas shift reaction and methanation. All reactions were assumed in equilibrium (Freni et al., 1996).

$$C_2H_5OH + H_2O = 4H_2 + 2CO \quad (4.13)$$

$$H_2O + CO = CO_2 + H_2 \quad (4.14)$$

$$3H_2 + CO = CH_4 + H_2O \quad (4.15)$$

Mass balance for each component in the SOFC can be calculated as shown below.

For anode's components

$$n_{EtOH} = n_{EtOH,in} - x \quad (4.16)$$

$$n_{CH_4} = z \quad (4.17)$$

$$n_{CO} = 2x - y - z \quad (4.18)$$

$$n_{CO_2} = y \quad (4.19)$$

$$n_{H_2} = 4x + y - 3z - c \quad (4.20)$$

$$n_{H_2O} = n_{H_2O,in} + c - y + z \text{ (for oxygen ion conducting electrolyte)} \quad (4.21)$$

$$n_{H_2O} = n_{H_2O,in} - y + z \text{ (for proton conducting electrolyte)} \quad (4.22)$$

$$n_{tot} = \sum_{i-1}^{6} n_i \tag{4.23}$$

$$P_i = \frac{n_i}{n_{tot}} P \tag{4.24}$$

$$K_{RF} = \frac{P_{H_2}{}^4 P_{CO}{}^2}{P_{EtOH} P_{H_2O}} \tag{4.25}$$

$$K_{WGS} = \frac{P_{CO_2} P_{H_2}}{P_{CO} P_{H_2O}} \tag{4.26}$$

$$K_{Meth} = \frac{P_{CH_4}\ P_{H_2O}}{P_{CO} P_{H_2}^3} \tag{4.27}$$

For cathode's components

$$n_{O_2,c} = n_{O_2,in} - 0.5c \tag{4.28}$$

$$n_{N_2,C} = n_{N_2,in} \tag{4.29}$$

$$n_{H_2O,C} = n_{H_2O,in} + c \qquad \text{(for proton conducting electrolyte)} \tag{4.30}$$

where $n_{EtOH,in}$ $n_{H_2O,in}$ $n_{O_2,in}$ $n_{N_2,in}$ represent moles of ethanol inlet, steam inlet, oxygen inlet and nitrogen inlet, respectively, c mole of hydrogen consumed by electrochemical reaction, x an extent of ethanol reforming reaction, y an extent of water gas shift reaction, z an extent of methanation. K_{RF} , K_{WGS} and K_{Meth} are equilibrium constants for ethanol reforming, water gas shift and methanation, respectively. Subscript 'a' and 'c' represent anode and cathode, respectively. The moles of anode's component can be numerically solved by equilibrium constants of Eqs. (4.16) – (4.27). Newton's method was used for solving the corresponding extents of reactions (x, y and z).

4.1.2.2 SOFC-ER Operation

In Chapter VII, SOFC-ER is performed in the study. The reactions taking place inside the reformer are the same as that of DIR operation. Ethanol reforming, water gas shift and methanation are considered. However, as described in Chapter II (Theory), the electrochemical reaction does not involve the reforming section. No hydrogen consumption from electrochemical reaction shifts the equilibrium reactions.

Therefore, in calculation, *c* (mole of hydrogen consumed by electrochemical reaction) is set equal to zero. The mass balance equation for an external reformer is presented in the following equations.

For an external reformer:

$$n_{EtOH,RF} = n_{EtOH,in} - x \tag{4.31}$$

$$n_{CH_4,RF} = z \tag{4.32}$$

$$n_{CO,RF} = 2x - y - z \tag{4.33}$$

$$n_{CO_2,RF} = y \tag{4.34}$$

$$n_{H_2,RF} = 4x + y - 3z \tag{4.35}$$

$$n_{H_2O,RF} = n_{H_2O,in} - y + z \tag{4.36}$$

$$n_{tot} = \sum_{i-1}^{6} n_i \tag{4.37}$$

$$P_i = \frac{n_i}{n_{tot}} P \tag{4.38}$$

$$K_{RF} = \frac{P_{H_2}{}^4 P_{CO}{}^2}{P_{EtOH} P_{H_2O}} \tag{4.39}$$

$$K_{WGS} = \frac{P_{CO_2} P_{H_2}}{P_{CO} P_{H_2O}} \tag{4.40}$$

$$K_{Meth} = \frac{P_{CH_4}\ P_{H_2O}}{P_{CO} P_{H_2}^3} \tag{4.41}$$

For SOFC stack in the case of SOFC-ER, because ethanol is completely reformed and methanation hardly takes place at high temperature, these two reactions are neglected. Only water gas shift and electrochemical reaction are considered inside the SOFC stack. The mass balance equations inside the SOFC stack for SOFC-ER are shown in the following equations.

For an SOFC stack:

$$n_{CO,SOFC} = n_{CO,RF} - x_1 \tag{4.42}$$

$$n_{CO_2,SOFC} = n_{CO_2,RF} + x_1 \tag{4.43}$$

$$n_{H_2,SOFC} = n_{H_2,RF} + x_1 - c \tag{4.44}$$

$$n_{H_2O,SOFC} = n_{H_2O,RF} - x_1 + c \tag{4.45}$$

$$n_{tot} = \sum_{i-1}^{6} n_i \tag{4.46}$$

$$P_i = \frac{n_i}{n_{tot}} P \tag{4.47}$$

$$K_{WGS} = \frac{P_{CO_2} P_{H_2}}{P_{CO} P_{H_2O}} \tag{4.48}$$

where n_i represents mole of component *i*, *c* mole of hydrogen consumed by electrochemical reaction, and x_1 an extent of water gas shift reaction inside the SOFC stack. Subscript 'SOFC' and 'RF' represent location at the SOFC stack and at the external reformer, respectively. The moles of component can be numerically solved by equilibrium constants of Eqs. (4.42) – (4.48). Newton's method was used for solving the corresponding extent of reactions, x_1.

4.1.3 Modes of Operation

Two modes of operation (i.e., well-mixed and plug flow) were examined in this research study. For well-mixed, there is no composition gradient inside the SOFC cell stack. The outlet composition equals that of inside in the stack as shown in Figure 4.2. However, for plug flow operation, the composition gradient was observed along the cell stack. Hydrogen in anode is gradually consumed by electrochemical reaction. Figure 4.3 shows the schematic diagram of plug flow operation. The example of SOFC-O^{2-} is shown in the schematic diagram below. One should bear in mind that the mole of hydrogen consumed by electrochemical reaction is represented by '*c*'. The gradient of moles inside the cell also influences EMF distribution along the cell for the plug flow SOFC-O^{2-}. The details of EMF calculation for each mode of operation will be described in electrochemical model section.

4.1.3.1 Well-Mixed

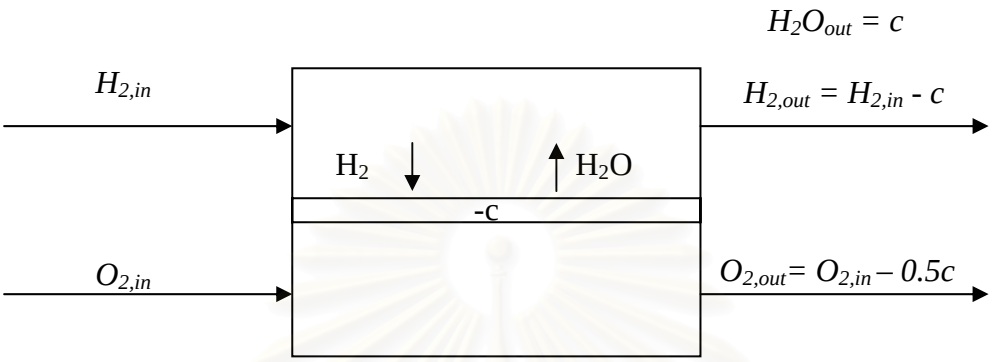

Figure 4.2 Schematic diagram of well-mixed SOFC-O^{2-}.

4.1.3.2 Plug Flow

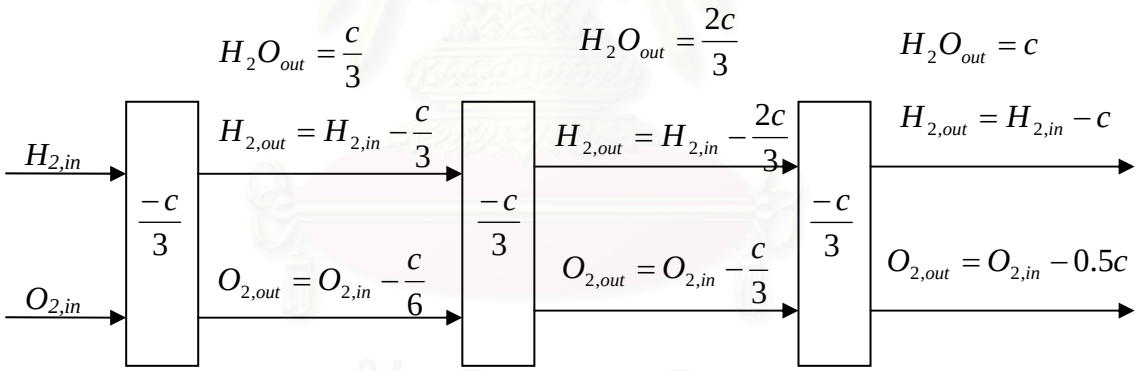

Figure 4.3 Schematic diagram of plug flow SOFC-O^{2-}.

4.1.4 Feeding Patterns

In this study, two feeding patterns were investigated in Chapter V, i.e., co-current and counter current. Type of feeding pattern strongly affects the composition inside the cell stack for plug flow operation With respect to the direction of the anode flow, the composition inside the cathode chamber for different feeding patterns as shown in Figures 4.4 and 4.5.

4.1.4.1 Co-Current

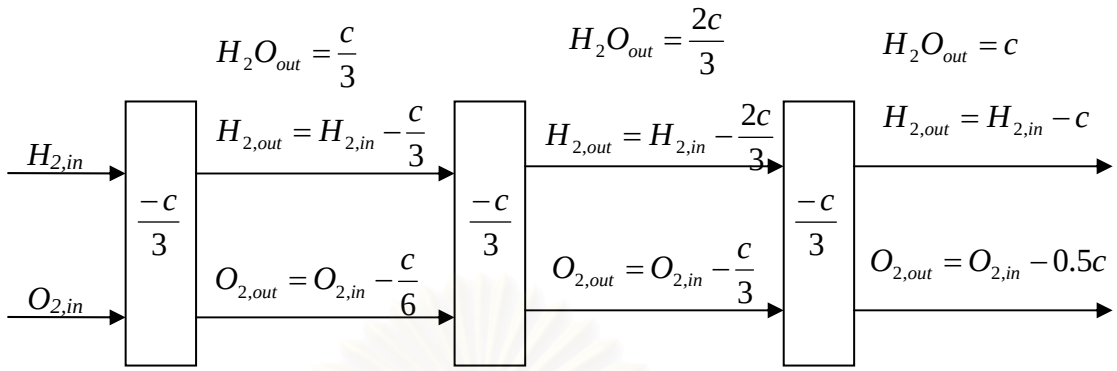

Figure 4.4 Schematic diagram of co-current plug flow SOFC-O^{2-}.

4.1.4.2 Counter-Current

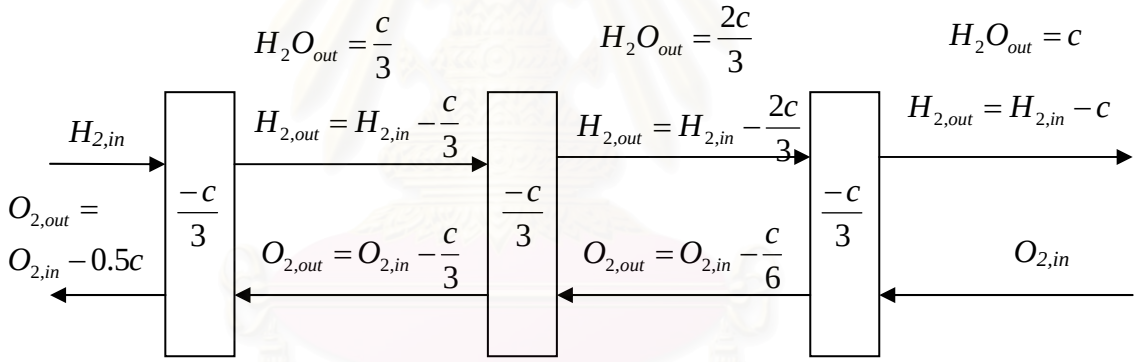

Figure 4.5 Schematic diagram of counter current SOFC-O^{2-}.

4.1.5 Carbon Formation

When hydrocarbon fuel, in this study ethanol, is used as a reactant, some carbon can be formed inside a reactor or an SOFC stack. Carbon formation is commonly known that it could decrease both the activity of catalysts and performance of SOFC. The following three reactions are the most probable reactions which lead to carbon formation in the reaction system.

$$2CO = CO_2 + C \qquad (4.49)$$

$CH_4 = 2H_2 + C$ (4.50)

$CO + H_2 = H_2O + C$ (4.51)

Generally, Boudard's reaction, Eq. (4.49), has the lowest Gibb's reaction compared to other reactions. Therefore, Boudard's reaction is usually the reaction assumed most responsible for carbon formation. In practice, however, the SOFC operates under a carbon-free condition. To check whether carbon elements form in the system, the activity of carbon in Boudard's reaction is calculated by using Eq. (4.49). Carbon activities are more than one indicates that carbon forms in the system (Garcia and Laborde, 1991).

$$\alpha = \frac{K_B P_{CO}^2}{P_{CO_2}} \quad (4.52)$$

4.2 Energy Balance Equations

Heat involved in the SOFC system can be divided into two main groups: non-reactive case and reactive case. For non-reactive case, it consists of heaters and coolers unit whose starting temperature (T_1) is elevated to the operating temperature (T_2). The heating/cooling energy can be calculated by the following equation.

$$Q_k = \int_{T1}^{T2} Cp(T)\,dT \quad (4.53)$$

For reactive case, reactions take place inside the unit operation. For an isothermal operation, the heat involving reaction can be calculated by heat of reaction as shown in the following.

$$Q_k = (\sum \nu_i H_i)_{product} - (\sum \nu_i H_i)_{reactants} \quad (4.54)$$

where H_i and ν_i represent enthalpy of component *i* and stoichiometric number of component *i* for one reaction, respectively. Q_k represents heat involved unit operation *k*.

For energy balance around the SOFC stack, the calculation is special due to the power (W_e) generated from the control volume. The energy equation can be calculated by enthalpy change and power around the SOFC stack as presented in Eq. (4.55).

$$0 = H_{fuel,in} + H_{air,in} - H_{fuel,out} - H_{air,out} - W_e \quad (4.55)$$

4.3 Electrochemical Model

In this section, equations used for calculating SOFC performances (e.g. EMF, losses, voltage, power density, power, electrical efficiency) are presented as follows.

4.3.1 Electromotive Force

4.3.1.1 Type of electrolyte

EMF significantly depends on types of electrolyte. For SOFC-O^{2-}, EMF is calculated from the difference in partial pressure of oxygen at the cathode and anode as shown in Eq. (4.56). On the contrary, the EMF for SOFC-H^+ is obtained from the difference of partial pressure of hydrogen at the anode and the cathode as presented in Eq. (4.58).

a) SOFC-O^{2-}: $$EMF = \frac{RT}{4F}\ln\frac{p_{O_2,c}}{p_{O_2,a}} = -\frac{\Delta G}{2F} - \frac{RT}{2F}\ln\frac{P_{H_2O,a}}{P_{H_2,a}P_{O_2,c}^{0.5}} \quad (4.56)$$

where $p_{O_2,a}$ is partial pressure of oxygen at anode chamber which can be calculated by the following equation.

$$p_{O_2,a} = \left(\frac{P_{H_2O,a}}{K_{H_2O}P_{H_2,a}}\right)^2 \quad (4.57)$$

b) SOFC-H^+: $$EMF = \frac{RT}{2F}\ln\frac{p_{H_2,a}}{p_{H_2,c}} = -\frac{\Delta G}{2F} - \frac{RT}{2F}\ln\frac{P_{H_2O,c}}{P_{H_2,a}P_{O_2,c}^{0.5}} \quad (4.58)$$

$$p_{H_2,C} = \frac{P_{H_2O,c}}{K_{H_2O}P_{O_2,C}^{0.5}} \quad (4.59)$$

4.3.1.2 Mode of Operation

As shown the difference in mass balance section, the EMF is also different. For well-mixed, because there is one composition inside the SOFC cell stack which equals to that of outlet composition, one EMF is obtained as shown in Figure. 4.6.

a) Well-Mixed

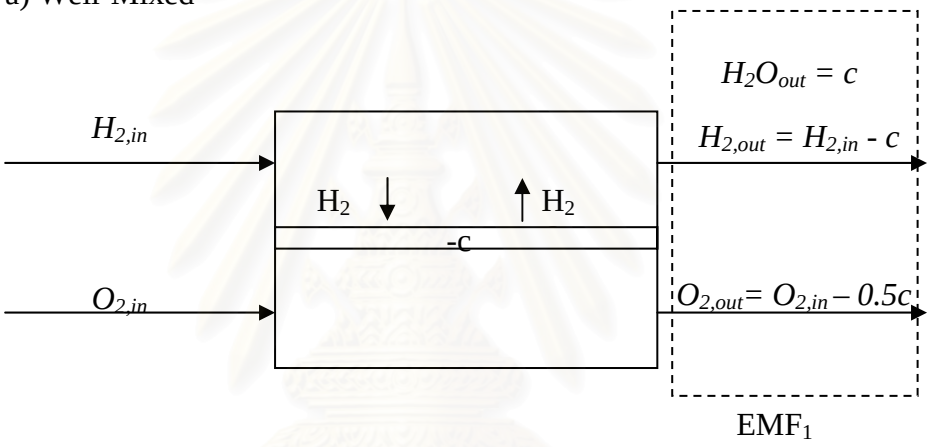

Figure 4.6 Schematic diagram of EMF for well-mixed SOFC.

b) Plug Flow

As described in mass balance section, there is a composition profile along the cell stack for plug flow operation. This results in a distribution of EMF as shown in Figure 4.7. EMF_0 though EMF_n represents value of individual EMF in each section along the stack. One should bear in mind that the example divides a cell stack into four sections for simple explanation. The average EMF can be calculated by numerical integration respective to fuel utilization along the stack.

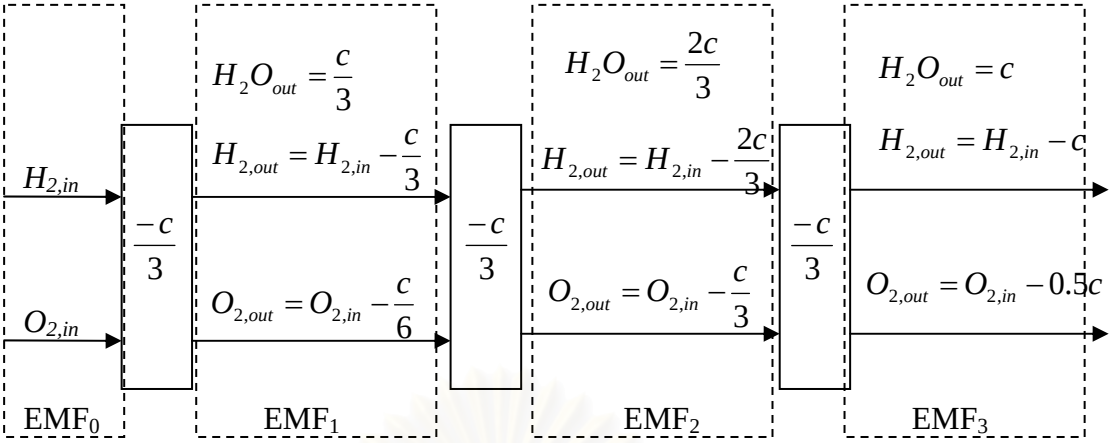

Figure 4.7 Schematic diagram of EMF for plug flow SOFC.

4.3.1.3 Feeding Pattern

a) Co-current

EMF calculation for co-current SOFC-O^{2-} was discussed in the plug flow mode, the previous section. For counter-current SOFC-O^{2-}, with respect to the direction of anode flow, the composition in the cathode chamber is different from that of co-current flow as illustrated in Figure 4.9. This results in difference in individual EMF (EMF_i) and average EMF.

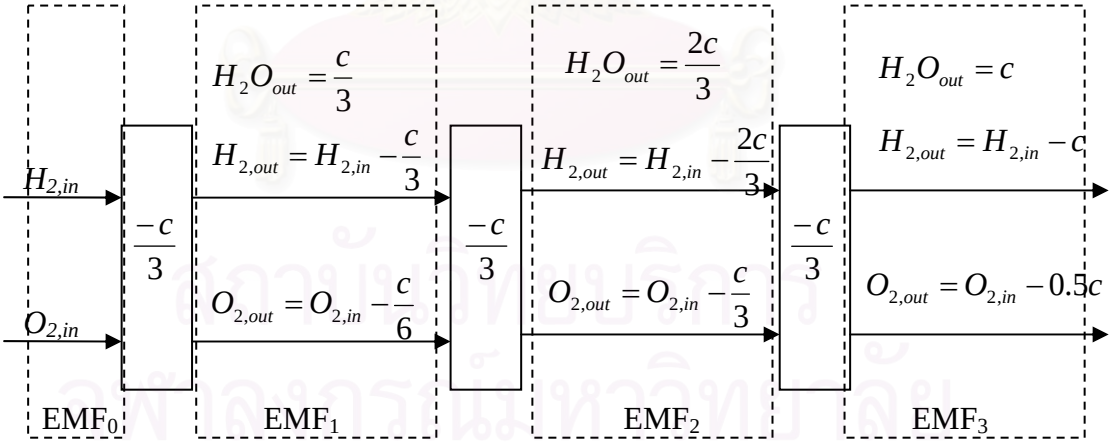

Figure 4.8 Schematic diagram of EMF for co-current plug flow SOFC.

b) Counter-current

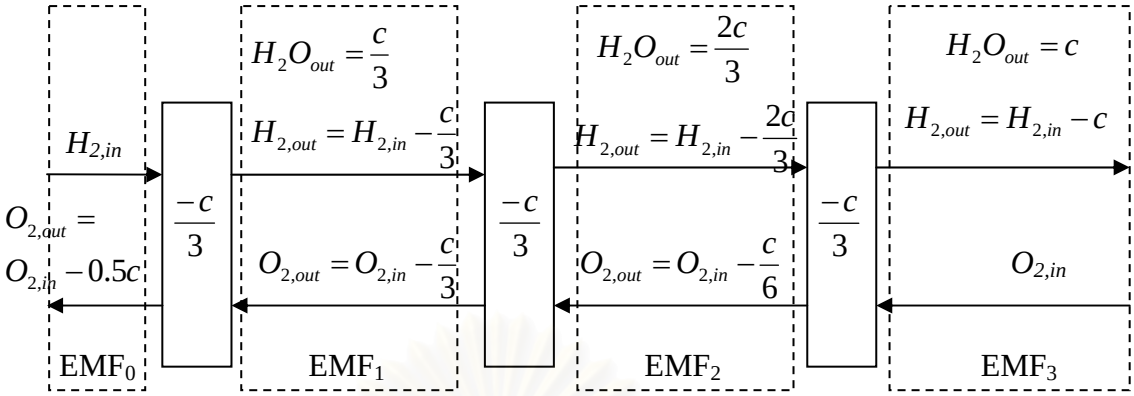

Figure 4.9 Schematic diagram of EMF for counter-current plug flow SOFC.

4.3.2 Losses

Two losses are considered in this study: ohmic loss and activation loss. For activation loss, Achenbach's correlation was used. Achenbach's correlations at an anode and a cathode are presented in Eqs. (4.60) and (4.61), respectively.

Activation loss:

$$r_{act,c} = \left[\frac{4F}{RT} k (p_{O_2,c})^m \exp\left(-\frac{E_{a,c}}{RT} \right) \right]^{-1} \tag{4.60}$$

$$r_{act,a} = \left[\frac{2F}{RT} k (p_{H_2,a})^m \exp\left(-\frac{E_{a,a}}{RT} \right) \right]^{-1} \tag{4.61}$$

Ohmic loss:

$$r_{ohm,j} = \rho_j \delta_j \tag{4.62}$$

$$\rho_j = \alpha_j \exp(\frac{\beta_j}{T}) \tag{4.63}$$

where R the gas constant, T the SOFC temperature, F the Faraday's constant, r_{act} the activation resistance, $E_{a,a}$ and $E_{a,c}$ the activation energies at anode and cathode, respectively, $p_{O_2,c}$ and $p_{H_2,a}$ the mole fractions of oxygen in the cathode chamber and hydrogen in the anode chamber, respectively, r_{ohm} the ohmic resistance, ρ_j the

resistivity of material j, α_j and β_j the constants specific to material j. All parameters used for calculating the ohmic and activation losses in Eqs. (4.60) – (4.63) are listed in Tables 4.1 and 4.2.

Table 4.1 Parameters for activation loss (Achenbach, 1994)

$r_{act}(\Omega\ cm^2)$	$k(\times 10^{-13}\ A\,cm^2)$	$E_a(kJ\ mol^{-1}K^{-1})$	m (-)
$r_{act,c}$	14.9	160	0.25
$r_{act,a}$	0.213	110	0.25

Table 4.2 Parameters of ohmic loss in SOFC cell components (Chan et al., 2002)

Materials	Parameters		Thickness (μm)
	α ($\Omega\ cm$)	β (K)	
Anode (40% Ni/YSZ cermet)	2.98×10^{-5}	-1392	150
Cathode (Sr-doped $LaMnO_3$: LSM)	8.11×10^{-5}	600	2000
Electrolyte (Y_2O_3 doped ZrO_2: YSZ)	2.94×10^{-5}	10350	40
Interconnector (Mg doped $LaCrO_3$)	1.256×10^{-3}	4690	100

However, it should be noted that the losses of SOFC-H^+ are not as developed as those of the SOFC-O^{2-}. The resistances of the components in the SOFC-H^+ cell are not available in the open literature. For SOFC-H^+, resistances are divided into two groups: 1) ohmic loss from electrolyte (r_e) and 2) the other resistance (r_o) which consists of activation loss and ohmic loss from electrodes and an interconnector as shown in Eqs. (4.64)-(4.65). The other resistance is derived from the deviation of the total resistance and the electrolyte resistance. The values of the total resistance are

obtained from the literature (Salar et al., 2001) while the electrolyte resistance is reported in Iwahara's work (1996).

$$r_{tot} = r_e + r_o \tag{4.64}$$

$$r_o = r_{act} + r_{ohm,electrode} + r_{ohm,\text{int}erconnect} \tag{4.65}$$

4.3.3 SOFC Performance

For SOFC performances, power density, power, current density and efficiencies are presented in this section. The operation voltage and power density can be calculated as shown in the following equations.

4.3.3.1 Voltage and Power density

$$V = EMF - i(r_{ohm} + r_{act}) \tag{4.66}$$

$$P_{den} = iV \tag{4.67}$$

$$I = r_{H_2,cons} * 2F \tag{4.68}$$

$$r_{H_2,cons} = r_{H_2in,equivalent} * U_f \tag{4.69}$$

$$r_{H_2in,equivalent} = 6 * r_{EtOH,d} \tag{4.70}$$

$$A = \frac{I}{i} \tag{4.71}$$

where *EMF* is the electromotive force, *V* the operating voltage, *i* the current density, *I* the overall current, *R* the gas constant, *T* the SOFC temperature, *F* the Faraday's constant, r_{act} the activation resistance, r_{ohm} the ohmic resistance, $r_{H2,cons}$ the molar flow rate of hydrogen consumed in the electrochemical reaction, $r_{H2in,equivalent}$ the maximum hydrogen molar flow rate coming into the anode chamber (6 times of ethanol flow rate), U_f the fuel utilization factor, $r_{EtOH,d}$ the ethanol flow rate in the distillate fed into the SOFC system, *A* the total active area of SOFC stack, W_e the electrical power and P_{den} the power density.

The simulated electrochemical model was compared with experimental work in pure H_2 system (Hagiwara et al., 1999). The fuel inlet consists of 98.64% H_2 and

1.36% H_2O at 1173 K and air stream at 873 K were fed to anode and cathode, respectively. The SOFC operates at 85% U_f. The results in Figure 4.10 show that the simulation is in good agreement with the experimental data.

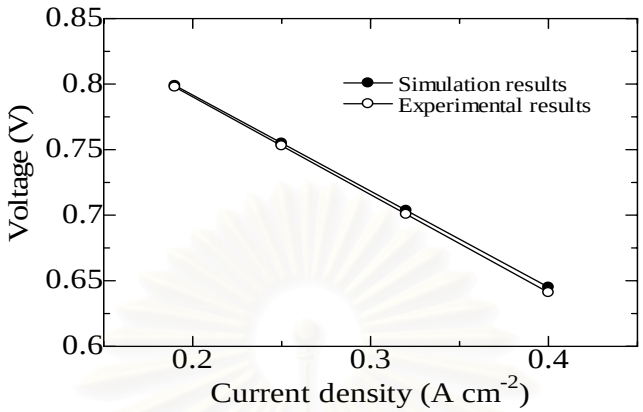

Figure 4.10 Verification of the SOFC model

4.3.3.2 Electrical Power

For electrical power, two definitions are expressed here: the maximum electrical power ($W_{e,\max}$) and the actual electrical power (W_e). Clearly, $W_{e,\max}$ represents the maximum electrical power when losses are not considered. $W_{e,\max}$ is defined by the multiplicity of electrical charge passing through the SOFC and average EMF as shown in Eq. (4.72). For W_e, the losses are considered and the actual voltage is calculated. W_e is defined by the multiplicity of current and operation voltage as shown in Eq. (4.73).

$$W_{e,\max} = qE \tag{4.72}$$

$$W_e = IV \tag{4.73}$$

4.3.3.3 Efficiencies

Three types of electrical efficiency are shown in here, the theoretical electrical efficiency, the actual electrical efficiency and the overall electrical efficiency. In details, the theoretical electrical efficiency in Eq. (4.74) represents the maximum electrical power compared to the energy input by incoming ethanol. Chapter V used this type of efficiency definition. The actual electrical efficiency in Eq. (4.75)

representing the obtained actual power compared to energy input from incoming ethanol is chosen to be representative of electrical efficiency in Chapter VI. Lastly, the overall electrical efficiency shown in Eq. (4.76) defined as the ratio of obtained actual power over energy input to the system is used in Chapters VII and VIII. In this case, energy input includes energy input from combustion heat of incoming ethanol and heat from an external heat source. All equations for all types of electrical efficiencies are presented as follows.

$$\eta_{elec,th} = \frac{qE}{n_{EtOH} * LHV_{EtOH}} \tag{4.74}$$

$$\eta_{elec} = \frac{W_e}{n_{EtOH} * LHV_{EtOH}} \tag{4.75}$$

$$\eta_{ov,elec} = \frac{W_e}{(n_{EtOH} * LHV_{EtOH}) + Q_{ex}} \tag{4.76}$$

For system efficiency, as mentioned earlier, the type of SOFC system in this study is SOFC with Combined Heat and Power (SOFC-CHP) system. Overall, both electrical power and useful heat (Q_u) are produced from SOFC-CHP. System efficiency or CHP efficiency can be calculated by the following equation. Noticeably, the numerator is summation of obtained power and useful heat (Q_u). The denominator is energy input from both incoming ethanol and an external heat (Q_{ex}).

$$\eta_{sys} = \frac{W_e + Q_u}{(n_{EtOH} * LHV_{EtOH}) + Q_{ex}} \tag{4.77}$$

where

$$Q_{Net} = Q_{SOFC,Net} - Q_D \tag{4.78}$$

$$Q_{SOFC,Net} = Q_{SOFC} + Q_R - Q_{PH1} - Q_{PH2} - Q_{PH3} - Q_{RF} \tag{4.79}$$

It should be noted that in Chapter VII, Q_u and Q_{ex} can be determined by Q_{Net}. From Eq. (4.78), Q_{Net} is calculated from $Q_{SOFC,Net}$ subtracted from distillation energy (Q_D) where $Q_{SOFC,Net}$ is exothermic heat left after providing exothermic heat from irreversibility of SOFC stack (Q_{SOFC}) which can be calculated from energy balance around SOFC stack and the exothermic heat from cooling hot effluent gas from the

afterburner (Q_R) to preheaters (Q_{PHi}) and the reformer (Q_{RF}). In addition, Q_{Net} can be positive, zero or negative. For positive Q_{Net}, the system does not need external heat from outside and there is some exothermic heat left from the system. This means that Q_{ex} equals zero but Q_u is positive. For zero Q_{Net}, the overall exothermic heat is just sufficient to the endothermic heat from all unit operations. In this case, Q_u and Q_{ex} equal zero. Finally, for negative Q_{Net}, the exothermic heat is not sufficient for the demanding heat. Therefore, some heat from an external heat source is required. In this case, Q_{ex} is positive and Q_u is zero.

4.4 Simulation of SOFC System

4.4.1 Simulation of SOFC System using MATLAB™

The flowchart of the program used in Chapters V to VII is shown in Figure 4.11. The mathematical models were programmed using MATLAB™. The desired values of H_2O:EtOH ratio, air excess, final fuel utilization ($U_{f,final}$) and voltage are initially input into the program. The calculation begins at the entrance of the anode chamber where the individual fuel utilization, $U_{f,i}$, is equal to zero. The mass balance of each component is first calculated. Then the electrochemical calculation performs and yields EMF and activation loss. The value of $U_{f,i}$ is then checked whether it reaches the $U_{f,final}$ or not. If $U_{f,i}$ is still lower than $U_{f,final}$, the mass balance is then re-calculated with a new $U_{f,i}$. and the corresponding activation loss are then calculated. The iteration runs until $U_{f,i}$ is equal to $U_{f,final}$ which means that SOFC operate untill it meets the desired value of $U_{f,final}$. The performances of SOFC are then achieved by electrochemical model. Finally, energy balance and heat involving each unit operation are calculated.

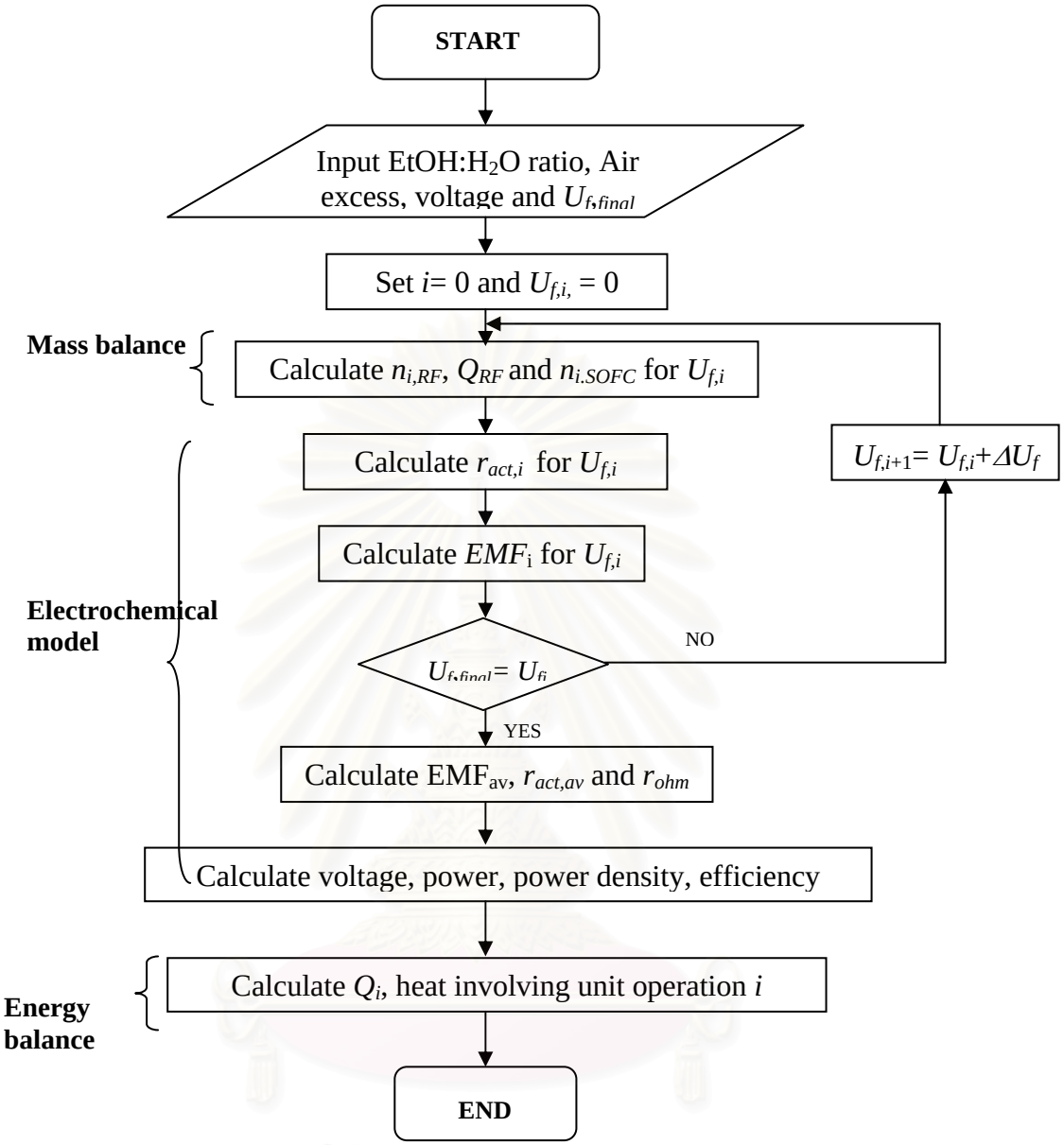

Figure 4.11 Flowchart of numerical method for calculating SOFC performance**.**

4.4.2 Simulation of SOFC System using Aspen Plus™ Simulator

In Chapter VIII, the SOFC-DIS system is investigated by using Aspen Plus™. Figure 4.11 shows the simplified process diagram of SOFC-DIS system. It consists of a distillation column, heaters, an external reformer, an SOFC stack and an afterburner connected consecutively**.** All the SOFC-DIS system is simulated by using Aspen Plus™ version 2006. The details of modelling for each component in the system are described as follows.

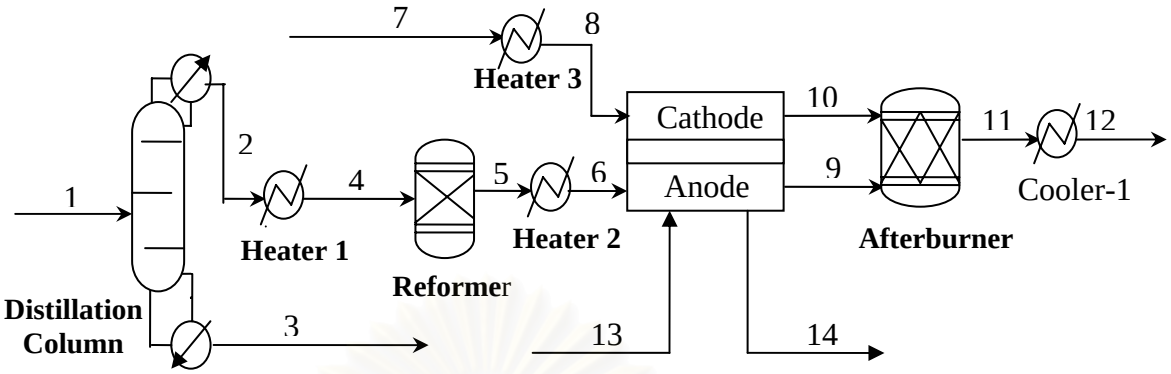

Figure 4.12 Schematic diagram of SOFC-DIS system.

4.4.2.1 Distillation Column

The distillation column is modelled by using a *RadFrac* module. A partial condenser and a kettle reboiler are used in this study. Four stages are sufficient to purify bioethanol until it reaches the 41 mol% and 99% recovery. It should be noted that 41 mol% is the maximum ethanol concentration that can be fed to the external reformer without carbon formation as reported in Assabumrungrat et al.'s work (2004). Unifac is used as a thermodynamic equation for the distillation column. Generally, Unifac is suitable for polar components system at atmospheric pressure. A built-in design spec by adjusting distillate rate and reflux ratio is used for obtaining the desired ethanol concentration and recovery.

4.4.2.2 Ethanol Reformer

An *RGibbs* reactor is used for simulating an external reformer. Previous experimental results confirmed that a gas mixture at thermodynamic equilibrium contains only six components with noticeable concentration: i.e. carbon monoxide, carbon dioxide, hydrogen, steam, methane and ethanol (Garcia and Laborde, 1991) Therefore, all these six components are modelled in the reactor.

4.4.2.3 SOFC Stack

The SOFC stack is simulated by using a user subroutine named *USRUSR*. Inside the subroutine, it contains mass balance equation, energy equations and electrochemical performance equations. For the mass balance, synthesis gas which

contains CO, CO_2, H_2, CH_4 and H_2O is fed to the SOFC stack. Only water gas shift reaction and electrochemical reactions take place inside the SOFC stack as shown in the following equations.

$$CO + H_2O = H_2 + CO_2 \quad (4.80)$$

$$H_2 + ½\ O_2 \rightarrow H_2O \quad (4.81)$$

It should be bear in mind that water gas shift reaction is fast equilibrium reaction. Moreover, ethanol reforming is not considered in the stack due to complete ethanol reforming in the external reformer. Also, methanation hardly takes place at high temperature. Therefore, both reactions can be neglected in calculations. The components inside the SOFC stack were calculated based on thermodynamic calculations assuming that components inside the stack are at their equilibrium compositions using Eq. (4.42)-(4.48). The details of energy balance equation and performance calculations are presented in the previous section. All equations were written in FORTRAN. The inlet and outlet temperature of the streams was set and the required amount of air was finally obtained.

4.4.2.4 Afterburner

For an afterburner, the stoichiometric reactor is used. All unreacted products from a SOFC stack (i.e. CH_4, CO, and H_2) are reacted with the unreacted O_2 as shown in Eqs. (4.82) – (4.84). The complete combustion is assumed. It should be noted that ethanol is not present in the afterburner due to complete ethanol reforming at high reforming temperature (Assabumrungrat et al, 2004). In this study, N_2 is assumed an inert and no NO_X is produced.

$$CH_4 + 2O_2 \rightarrow CO_2 + 2H_2O \quad (4.82)$$

$$CO + ½\ O_2 \rightarrow CO_2 \quad (4.83)$$

$$H_2 + ½\ O_2 \rightarrow H_2O \quad (4.84)$$

4.4.2.5 Process Simulation

As mentioned earlier, the SOFC-DIS system consists of a distillation column, an external reformer, heaters, an SOFC stack and an afterburner as shown in Figure 4.12. Bioethanol typically contains 1-7 mol% of ethanol (Roger et al., 1980; Buchholz

et al. 1987; Shell et al., 2004; Alzate et al., 2006). In this study, 5 mol% of ethanol used as a representative was introduced to the distillation column at atmospheric pressure and temperature and purified to reach the desired concentration and recovery of ethanol. Thereafter, the concentrated ethanol is fed to the *Heater 1* prior to entering the external reformer in order to reform ethanol to H_2. Synthesis gas from the external reformer is heated by *Heater 2* and then fed to the anode side of the SOFC. A fresh air stream is heated by *Heater 3* and then fed to the cathode. The exhaust gas from the SOFC stack containing unreacted fuels and depleted air enter the afterburner where all fuel is combusted. The post-combustion stream is heat recovered by cooling down to 403 K before emitted to the surrounding.

For thermodynamic option set, Peng Robinson was used for the rest of the system except for the distillation column. In addition, it is suitable for non-polar light component system. *Design spec 1* was used to adjust incoming bioethanol flow rate (stream no. 1) in order to reach the target fuel utilization. It should be noted that 2448 SOFC tubes with the active surface area of 834 cm^2 for each tube were used for simulations. Inside *Design spec 1*, the stack area was set and the current was then calculated by the stack area multiplied by the current density derived from the SOFC subroutine. The moles of hydrogen consumption via electrochemical reaction can be calculated by the known current as shown in Eq. (4.68). Fuel utilization is finally obtained from moles of hydrogen consumption divided by the maximum hydrogen produced from ethanol inlet as shown in Eq. (4.69). The bioethanol flow rate (stream no. 1) keeps varying until the right match of current density and current meet the target fuel utilization. The amount of cooling air can be calculated by energy balance equation inside the subroutine. The calculator simulation option was performed after SOFC and used to set the amount of air inlet (stream no. 7) equal to the calculated air stream from the SOFC stack. The target fuel utilization and voltage was input through material stream number 13. The calculation of mass balance, energy balance and performances performs inside the user-subroutine by using the data of the anode stream (stream no. 6), the cathode stream (stream no. 8) and target input (stream no. 13). The calculated mass, enthalpy and other physical properties (i.e. density, molecular weight) of anode and cathode stream was sent through material stream number 9 and 10, respectively. The value of calculated performances (e.g. power density, power and current density) was transferred through the material stream number 14.

CHAPTER V

THEORETICAL PERFORMANCE ANALYSIS OF ETHANOL-FUELLED SOLID OXIDE FUEL CELLS WITH DIFFERENT ELECTROLYTES

In this chapter, theoretical performances of ethanol-fed SOFC with different types of electrolyte (i.e. proton- and oxygen ion-conducting electrolyte) were investigated. The study begins with the profile of components' partial pressure in SOFC stack and their performances for different types of electrolyte at the same inlet steam to ethanol ratio. Later, the effect of steam presence in an SOFC stack on electrical performances was also considered. All parameters which affect steam presence were studied; for example, mode of operation (i.e. well-mixed and plug flow), feeding pattern (i.e. co current and counter current) and operating conditions (i.e. inlet steam to ethanol ratio and fuel utilization). The performances of SOFC with different types of electrolyte at their best conditions were lastly compared and discussed.

5.1 Introduction

There are a number of studies published dealing with the use of ethanol for fuel cells. Ethanol was found to provide higher electrical, overall efficiency, power density and operating voltage than methane in DIR-MCFC (Freni et al., 1996), in IIR-MCFC (Maggio et al.,1998). As mentioned earlier in the theory section, there are two types of electrolyte: proton conducting electrolyte and oxygen ion conducting electrolyte. Although two types of electrolytes are possible for SOFC operations, an oxygen ion conducting electrolyte is more commonly used than a proton conducting electrolyte. Until now, there are very few studies related to the use of the proton conducting electrolytes the open literature (Demin et al., 2001; Salar et al., 2001; Demin et al., 2002; Shimada et al., 2004). Demin et al. (2002) reported an interesting result that an SOFC with a proton conducting electrolyte (SOFC-H^+) provides higher efficiency than an SOFC with an oxygen ion conducting electrolyte (SOFC-O^{2-}) for

the system fed with methane. The comparison study was based on the same steam: methane feed ratio for both SOFC-O^{2-} and SOFC-H^{+}. However, it was reported in previous work that the steam requirement of SOFC-O^{2-} is lower than that of the SOFC-H^{+} because water produced from the electrochemical reaction of hydrogen appears in the anode chamber (Assabumrungrat et al., 2004). Therefore, it is unclear whether the SOFC-H^{+} still shows better performance than the SOFC-O^{2-} when the benefit from the lower steam requirement in SOFC-O^{2-} is taken into account.

In this study, the performance of ethanol-fuelled SOFCs with two different electrolytes is investigated by considering the benefit of lower steam requirement in SOFC-O^{2-}. All operating parameters which affect the steam requirement are also examined. Different modes of operation (i.e., plug flow (PF) and well-mixed (WM)) and different feeding patterns for the plug flow mode (i.e. co-current and counter-current) were investigated. In addition, the SOFC channel behaves like plug flow operation because hydrogen fuels are gradually consumed along the SOFC channel. For well-mixed operation, the SOFC can operate under this mode by recycling until the concentration inside the SOFC channel is equally the same. Well-mixed mode is beneficial for SOFC-O^{2-} because the concentration of steam is highest and probably affects the required inlet steam: EtOH ratio and SOFC performances. Also, two feeding patterns of the PF mode (i.e., co-current (Co) and counter-current (CC)) were considered due to the different characteristics of concentration inside the SOFC channel as shown in Chapter IV. The efficiencies of SOFC-O^{2-} and SOFC-H^{+} were compared, taking into account the benefit from the lower steam requirement for SOFC-O^{2-}. This is important in determining whether future SOFCs should be based on which type of the electrolyte.

5.2 Results and Discussion

5.2.1 Characteristics of SOFCs with Different Types of Electrolyte

5.2.1.1 Anode Components' Partial Pressure

Figure 5.1 (a) and (b) shows the anode components' partial pressure at different fuel utilizations (U_f) for proton conducting SOFC (SOFC-H^{+}) and oxygen ion conducting SOFC (SOFC-O^{2-}), respectively. The inlet H_2O:EtOH ratio is at the stoichiometic value of 3 and the temperature is 1200 K. It should be noted that, for the

WM mode, the partial pressure in the cell is equal to the value at the exit U_f due to the well-mixed condition. In contrast, in the PF mode, the composition change along the cell is represented by the partial pressure profiles from U_f of zero (the entrance of the SOFC stack) to the target U_f (the exit of the SOFC stack).

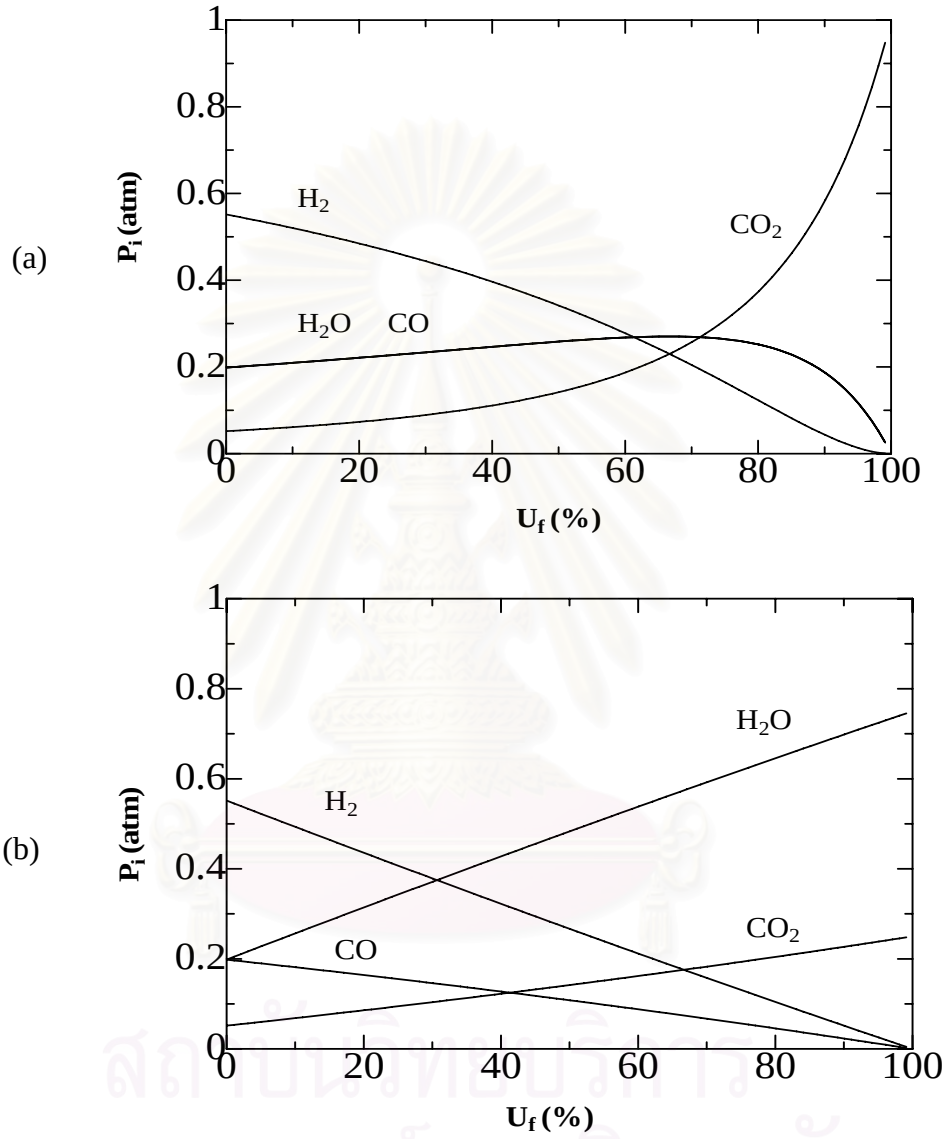

Figure 5.1 Anode components' partial pressure at different fuel utilization for SOFCs with different types of electrolytes: (a) SOFC-H^+, (b) SOFC-O^{2-} (inlet H_2O:EtOH = 3, T = 1200 K, P = 101.3 kPa, 400% excess air).

The type of electrolyte has a significant effect on the anode partial pressure as shown in Figures 5.1 (a) and (b), respectively. From Figure 5.1, it is obvious that the partial pressure of steam for the SOFC-H^+ and SOFC-O^{2-} are considerably different

due to the different location of steam generation as described in the preceding section. In the SOFC-H^+ case, the partial pressure of steam initially increases with increasing U_f and the results are contradictory to the general idea that no steam is produced in the anode channel. This is because the total moles in the anode chamber decreases as hydrogen is consumed and result in higher partial pressure of steam. At high fuel utilizations, the partial pressure of steam drops significantly because the hydrogen consumption from the electrochemical reaction shifts the water gas shift reaction and results in higher carbon dioxide production as shown in Figure 5.1 (a). In contrast, for the SOFC-O^{2-} case as presented in Figure 5.1 (b), the partial pressure of steam increases dramatically over the entire anode chamber due to the major effect of electrochemical steam production at the anode side. Moreover, it can be noticed that the partial pressure of hydrogen in the SOFC-H^+ case is higher than that in the SOFC-O^{2-} case because there is no dilution effect of the electrochemical steam at the anode side in the SOFC-H^+ case. It should be noted that there is a negligible amount of ethanol and methane observed from the calculations due to the complete reforming reaction and insignificant methanation at this operating temperature.

The effect of two feeding patterns (i.e. co-current SOFC-PF: SOFC-(PF-Co) and counter current SOFC-PF: SOFC-(PF-CC)) was considered for the PF mode. No difference in the profile of anode components' partial pressure with different feeding patterns for both SOFC-H^+ and SOFC-O^{2-} was observed because it was assumed in our calculations that all anode components are in equilibrium which relates to the fuel utilization (U_f) along the anode chamber. Therefore, at the same operating fuel utilization the profiles of anode components in both feeding patterns are similar. In other words, the feeding patterns have no effect on the profile of anode components' partial pressure for both electrolytes.

5.2.1.2 Cathode Components' Partial Pressure

The influence of mode of operation, feeding pattern and type of electrolyte on the cathode components' partial pressure at various fuel utilizations are shown in Figure 5.2. The results show that the partial pressure of oxygen in the SOFC-H^+ case is always lower than that in the SOFC-O^{2-} case due to the presence of the electrochemical steam at the cathode for the SOFC-H^+. However, the differences are not significant due to high value of excess air (400%) used in calculations. It should

be noted that 300-600% excess air is commonly used in SOFC operations for good heat management in SOFC cell stacks (Bedringas et al., 1997)

(a)

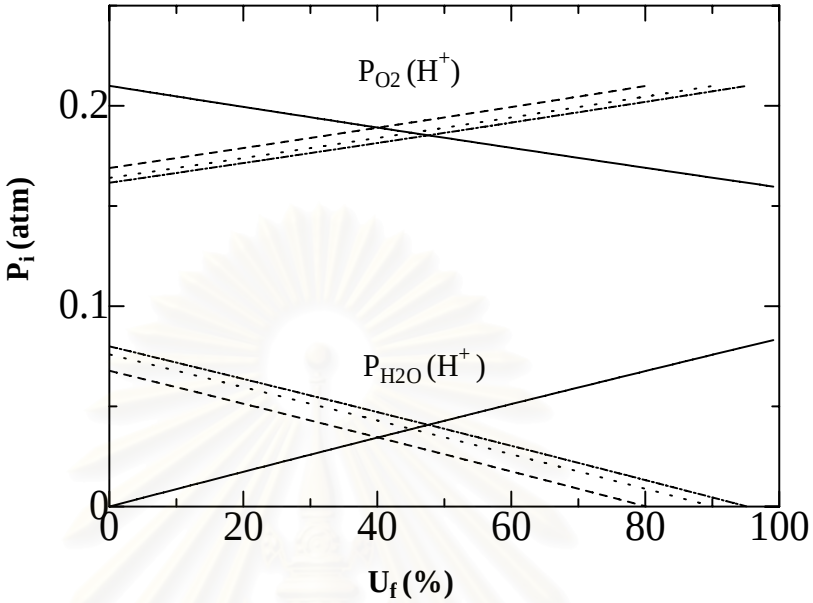

(b)

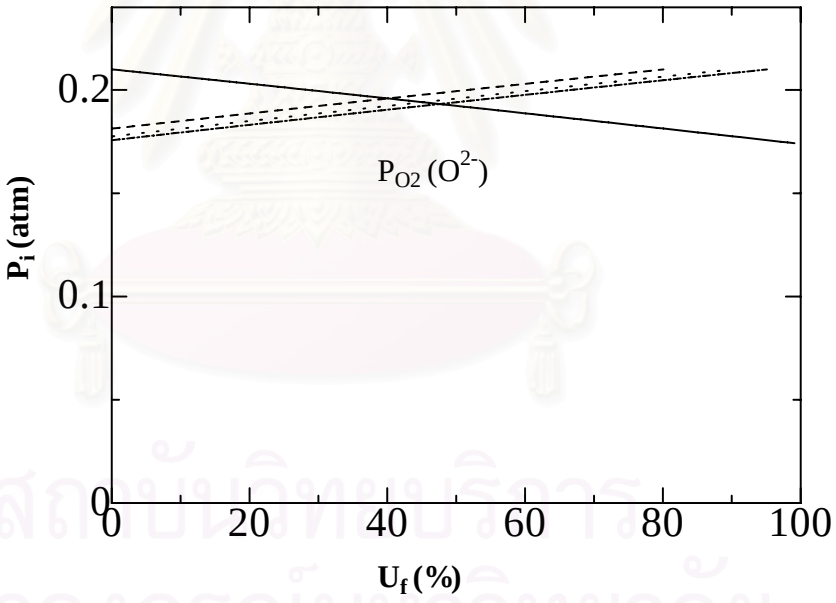

Figure 5.2 Cathode components' partial pressure at different fuel utilization for SOFCs with different types of electrolytes for co-current (solid line) and counter-current at 80%U_f (dashed line), 90%U_f (dotted line), 95%U_f (dashed dotted line): (a) SOFC-H^+, (b) SOFC-O^{2-} (inlet H_2O:EtOH = 3, T = 1200 K, P = 101.3 kPa, 400% excess air).

The mode of operation and feeding pattern show a slight impact on the partial pressure of oxygen in the cathode for both SOFC-H^+ and SOFC-O^{2-}. For the SOFC (PF-Co) cases, air is fed co-currently with the fuel. The partial pressure of oxygen decreases whereas the partial pressure of steam increases (for the SOFC-H^+ case) with increasing fuel utilization. The partial pressure profiles within the cell of the SOFC (PF-Co) cases are represented by the partial pressures between the fuel utilization at zero (the entrance of fuel channel) and the exit U_f (the exit of fuel channel); whereas, those of the SOFC (WM) correspond to the value at the exit fuel utilization. In contrast, for the SOFC (PF-CC), air is introduced to the cathode entrance located at the exit of the anode stream and, therefore, the partial pressure profile is different from those of the SOFC (PF-Co) among different fuel utilizations. The partial pressure of oxygen in the cathode is 0.21 atm at the entrance to the cathode side and decreases along the cathode chamber until the cathode exit located at the entrance of the anode feed.

5.2.1.3 EMF Distribution

From the obtained partial pressure profiles, the EMF at different fuel utilization along the cell can be calculated using Eqs. (4.56) for SOFC-O^{2-} and (4.58) for SOFC-H^+. The EMF distribution of SOFC at different SOFC cases is presented in Figure 5.3. From Figure 5.3, it is shown that the EMF distributions in all SOFC-H^+ cases are higher than those in all SOFC-O^{2-} cases. This can be explained by considering the partial pressure of components involved in the Nerstian term of Eqs. (4.56) and (4.58). The partial pressure of hydrogen in the anode for the SOFC-H^+ case is higher than that for the SOFC-O^{2-} case due to no dilution effect of the electrochemical steam at the anode side in the SOFC-H^+ case. Moreover, the partial pressure of steam in the cathode side for the SOFC-H^+ case is much lower than that in the anode side for the SOFC-O^{2-} case (see Figures 5.1 and 5.2), the Nerstian term of the SOFC-O^{2-} case shows a more negative value than that in the SOFC-H^+case, and consequently, the SOFC-H^+ cell gives a higher EMF than does the SOFC-O^{2-}cell. It should be noted that the partial pressures of oxygen in the cathode for both SOFCs are not taken into account in the Nerstian term comparison due to the use of excess air in the operation. The result confirms that the SOFC-H^+ cell has a higher performance than the SOFC-O^{2-} cell when the steam: fuel feed ratio is the same as reported earlier in other system (Demin et al., 2002).

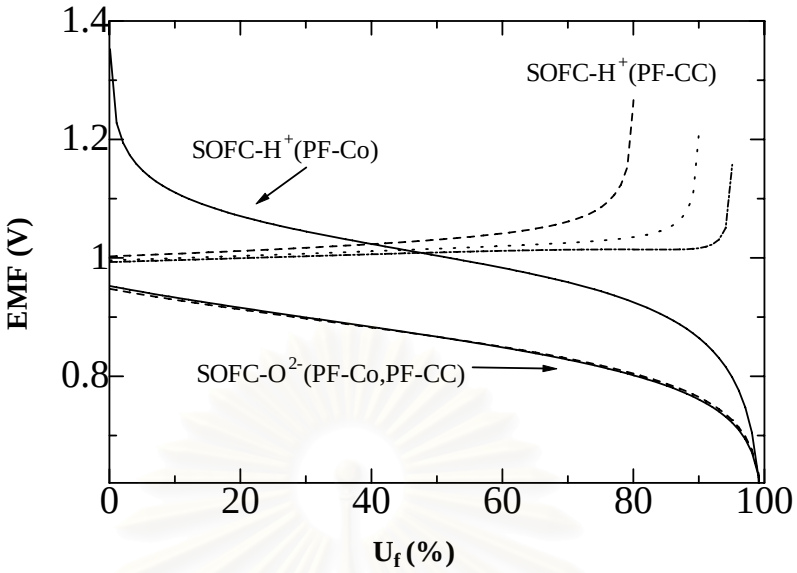

Figure 5.3 EMF distribution along the SOFC-O^{2-} and SOFC-H^{+} operated under PF and WM modes for co-current (solid line) and counter-current at 80%U_f (dashed line), 90%U_f (dotted line), 95%U_f (dashed dotted line): (inlet H_2O:EtOH = 3, T = 1200 K, P = 101.3 kPa, 400% excess air).

From Figure 5.3, it is noticed that the feeding pattern has a significant impact on the EMF distribution in the SOFC-H^{+} cell whereas only a slight effect is observed in the SOFC-O^{2-} cell. For the SOFC-H^{+} case, the value of EMF is strongly dependent on both the partial pressures of oxygen and steam in the cathode as shown in Eq (4.58). The components' partial pressures in the anode are not considered as they are similar for both feeding patterns as mentioned earlier. The feeding pattern significantly impacts the partial pressure profile of steam in the cathode as shown in Figure 5.2 (a) and, therefore, the EMF distribution is different for different feeding patterns. For the SOFC-O^{2-} case, the value of the EMF depends on the partial pressure of oxygen in the cathode and partial pressure of hydrogen and water in the anode as shown in Eq. (4.56). However, the partial pressure of components in the anode is the same for different feeding pattern. Therefore, the EMF depends on only the partial pressure of oxygen in the cathode. The results show that the EMF is not significantly dependent on the feeding pattern due to the high excess air. The partial pressure

profile of oxygen in the cathode for both feeding patterns is nearly identical. Consequently, the EMF of SOFC-O^{2-} for both feeding patterns is almost the same.

5.2.1.4 Average EMF and Efficiency

The average value of the EMF for the SOFC (PF) can be obtained by the numerical calculation of the EMF distribution, while the EMF of SOFC (WM) can be achieved directly from the value at the corresponding fuel utilization. The obtained average EMF can be used in calculating efficiency as defined in Eq. (4.74). Figures 5.4 (a) and (b) show the comparative results of average EMF and efficiency of SOFCs for various fuel utilizations, respectively. At 80% operating fuel utilization, the SOFC-H^+ (WM) and the SOFC-O^{2-}(WM) yield EMF of 0.92 and 0.80 V, respectively, whereas the average values of the EMF are 1.03 and 0.89 V for the SOFC-H^+ (PF) and the SOFC-O^{2-} (PF), respectively. It was found that the feeding pattern has no significant effect on the average EMF for both electrolytes although the EMF distributions are different. The average EMF of SOFCs at a inlet H_2O:EtOH ratio of 3 and 80% fuel utilization can be ordered as follows SOFC-H^+(PF-Co) ≈ SOFC-H^+(PF-CC) > SOFC-H^+(WM) > SOFC-O^{2-}(PF-Co) ≈ SOFC-O^{2-}(PF-CC) > SOFC-O^{2-}(WM). Clearly, the SOFC-H^+ provides greater EMF than the SOFC-O^{2-} for both PF and WM modes.

(a)

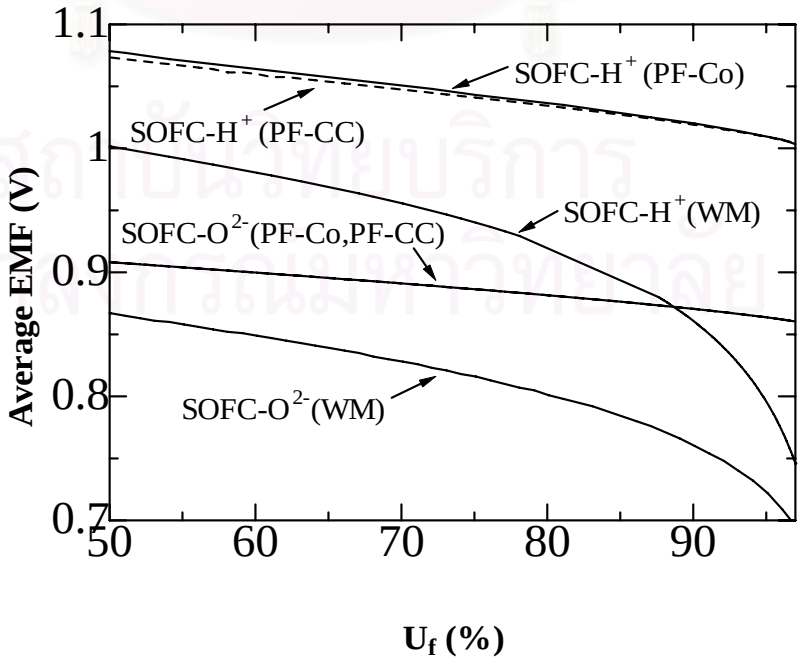

(b)

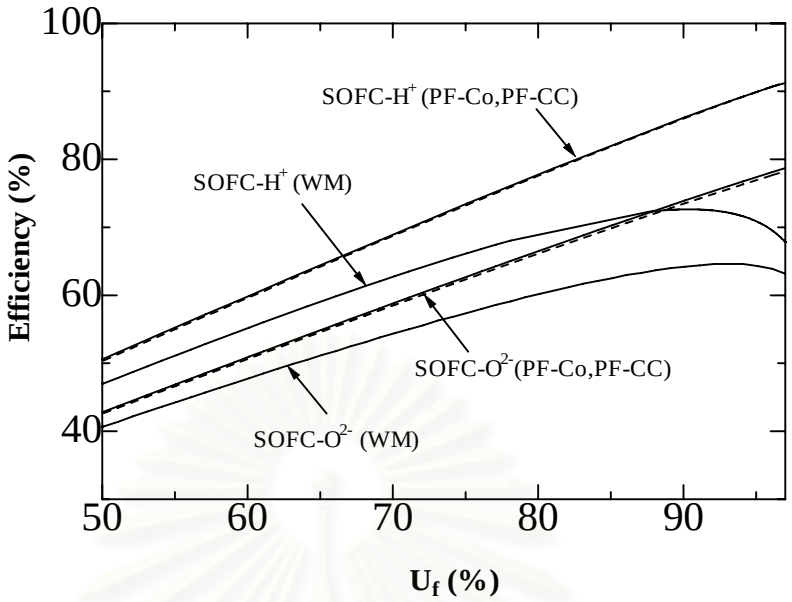

Figure 5.4 Performances of SOFC-O^{2-} and SOFC-H^+ operated under PF and WM modes: (a) Average EMF, (b) Efficiency (inlet H_2O:EtOH = 3, *T* = 1200 K, *P* = 101.3 kPa, 400% excess air).

Furthermore, it can be noticed that the WM mode results in a lower EMF than the PF mode for both electrolytes because the partial pressure of hydrogen in the WM mode is kept at its lowest value along the cell. Figure 5.4 (b) represents the SOFC efficiency at different cases. It was found that the efficiency increases in sequence SOFC-H^+(PF) > SOFC-H^+(WM) > SOFC-O^{2-}(PF) > SOFC-O^{2-}(WM); however, at high fuel utilization, the SOFC-O^{2-}(PF) case shows higher efficiency than the SOFC-H^+(WM) case. It is obvious that under the same operation mode, the SOFC-H^+ cell is superior to the SOFC-O^{2-}cell. This is in good agreement with the previous work (Demin et al., 2002) which was reported that the SOFC-H^+ case gives the maximum efficiency 15% higher than that of the SOFC-O^{2-} case in the range of inlet H_2O:CH_4 ratio of 2.0-3.0. Furthermore, it can be noticed that the feeding pattern has no influence on the efficiency of SOFCs for both types of electrolyte.

5.2.2 Effect of Inlet H_2O:EtOH Ratio on SOFC Performances at Different Values of Fuel Utilization

Figures 5.5 and 5.6 show the influence of the inlet H_2O:EtOH ratio on the average EMF and efficiency of SOFCs at different fuel utilizations. The inlet H_2O:EtOH ratio is considered only in the range where carbon formation is thermodynamically infeasible. The minimum ratio for the SOFC-O^{2-} (WM) and SOFC-O^{2-}(PF) cells is almost 0 and 1, respectively. However, the minimum ratio is higher for the SOFC-H^+ cell particularly at high fuel utilization for both modes of operation. The SOFC-O^{2-}(WM) cell can be operated without steam input because steam produced from the electrochemical reaction of hydrogen can compensate some of required steam inlet. It should be noted that some steam is still needed in the feed during the start-up period before the cell can be self-sustaining. For both SOFC-O^{2-} (PF) and SOFC-O^{2-} (WM) cases, the EMF and efficiency decrease with increasing inlet H_2O:EtOH ratio. Therefore, their highest values are at the limit of carbon formation for each value of the fuel utilization. This indicates that the introduction of steam into the cell decreases the EMF and efficiency due to hydrogen dilution. In the SOFC-H^+(WM) and SOFC-H^+(PF) cases, the minimum inlet H_2O:EtOH ratios are 1.9 and 3.2 at 80% and 90% fuel utilization, respectively. The greater fuel utilization requires greater steam input. This is consistent with the previous work (Assabumrungrat et al., 2004). From Figures 5.5 and 5.6, it is found that there is an optimum steam input in the SOFC-H^+ for both modes of operation at each fuel utilization. The introduction of steam initially increases the EMF and efficiency but has the negative effect at higher values. An appropriate inlet H_2O:EtOH ratio should be selected because steam is essential for the hydrogen production from the ethanol steam reforming but, on the other hand, it also acts as a diluent in the system. All optimum points found for each value of fuel utilization are beyond the limit of carbon formation. Furthermore, it is confirmed that there is no influence of feeding patterns on the EMF and efficiency for all ranges of the inlet H_2O:EtOH ratio.

(a)

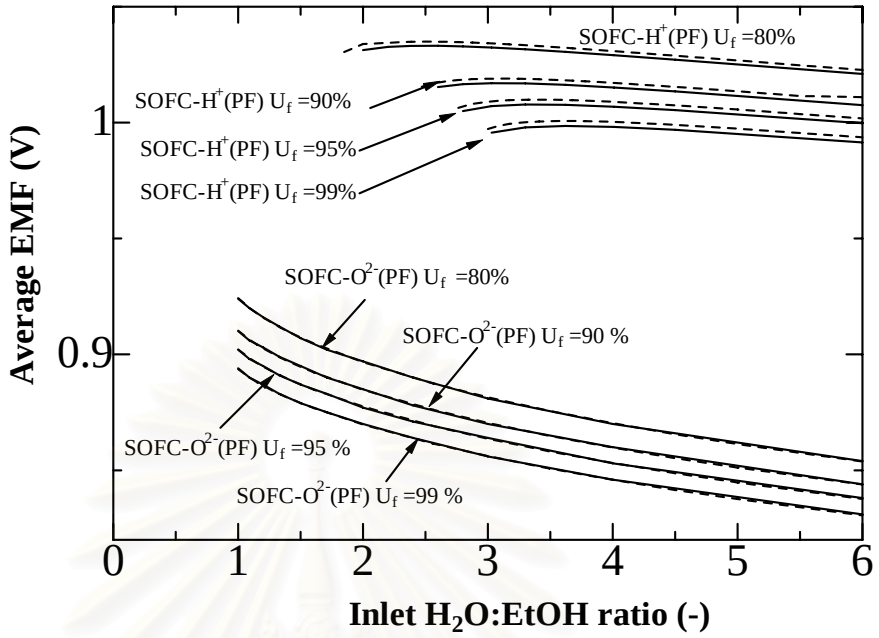

(b)

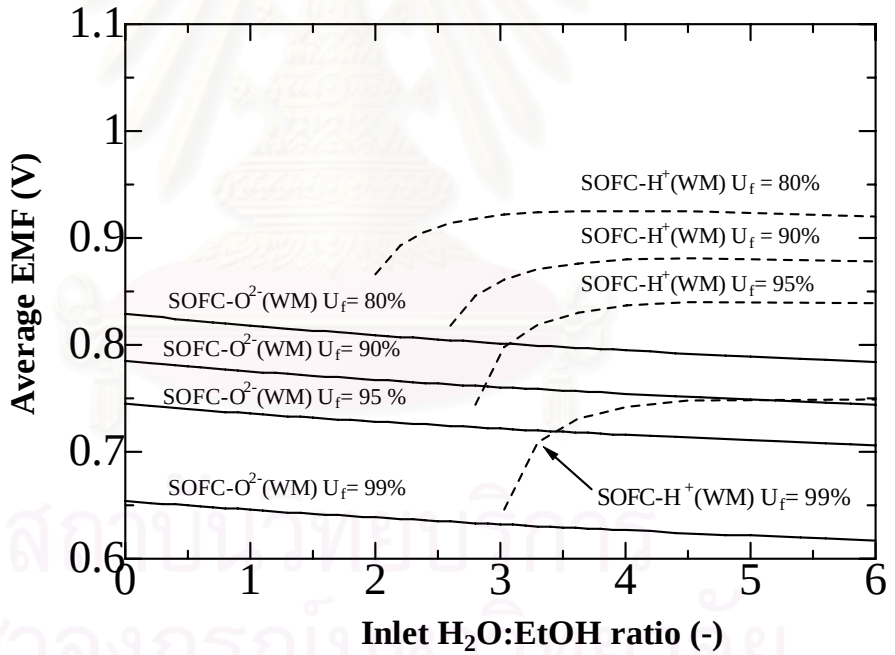

Figure 5.5 Influence of inlet H_2O:EtOH ratio on SOFCs average EMF at different values of fuel utilization: (a) PF mode, (b) WM mode (T = 1200 K, P = 101.3 kPa, 400% excess air).

(a)

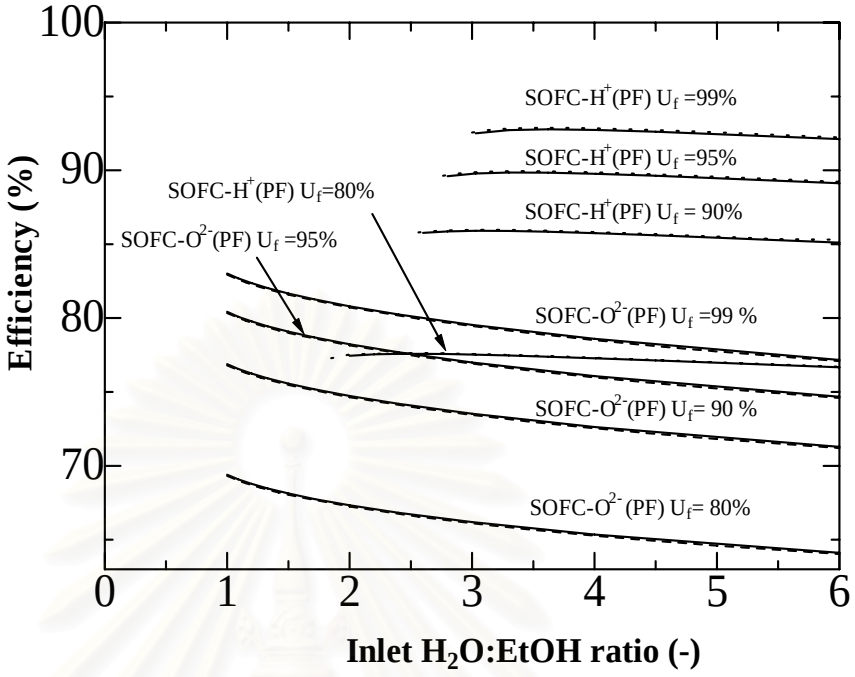

(b)

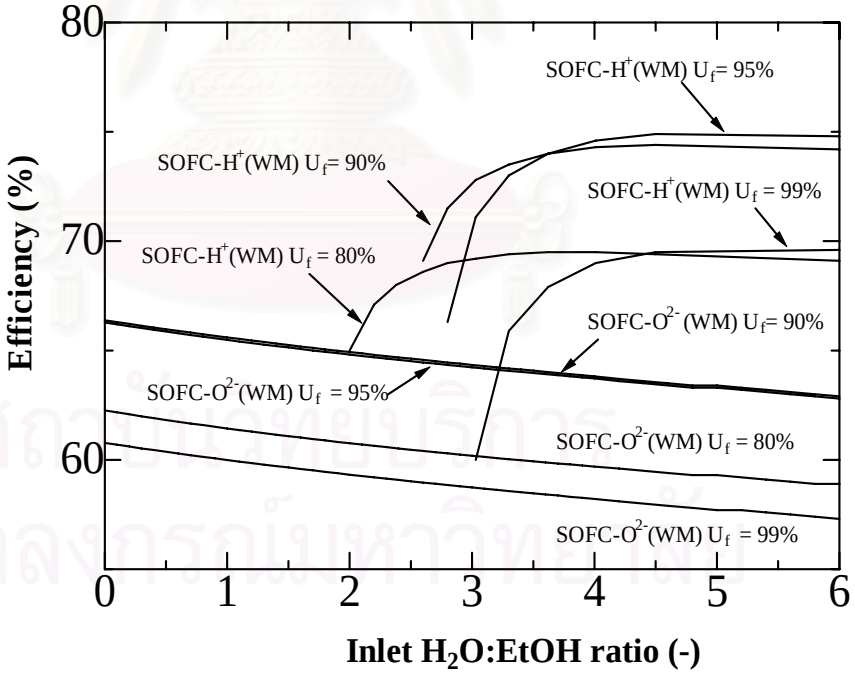

Figure 5.6 Influence of inlet H_2O:EtOH ratios on SOFCs efficiency at different values of fuel utilization: (a) PF mode ; (b) WM mode (T = 1200 K, P = 101.3 kPa).

5.2.3 Maximum Efficiency of SOFC-O^{2-} and SOFC-H^{+} at Different Operating Temperatures

By performing the calculations at various values of inlet H_2O:EtOH ratio and fuel utilization, it is possible to determine the maximum efficiency and the corresponding conditions for both SOFC-O^{2-} and SOFC-H^{+} cells at each temperature level as shown in Figures 5.7. From figures, it is obvious that the maximum SOFC efficiency follows the sequence of SOFC-H^{+}(PF) > SOFC-O^{2-}(PF) > SOFC-H^{+}(WM) > SOFC-O^{2-}(WM) for all temperatures (1000-1200 K). The maximum efficiency for all cases decreases with increasing temperature. This is consistent with the decrease in the EMF due to Gibb's free energy.

(a)

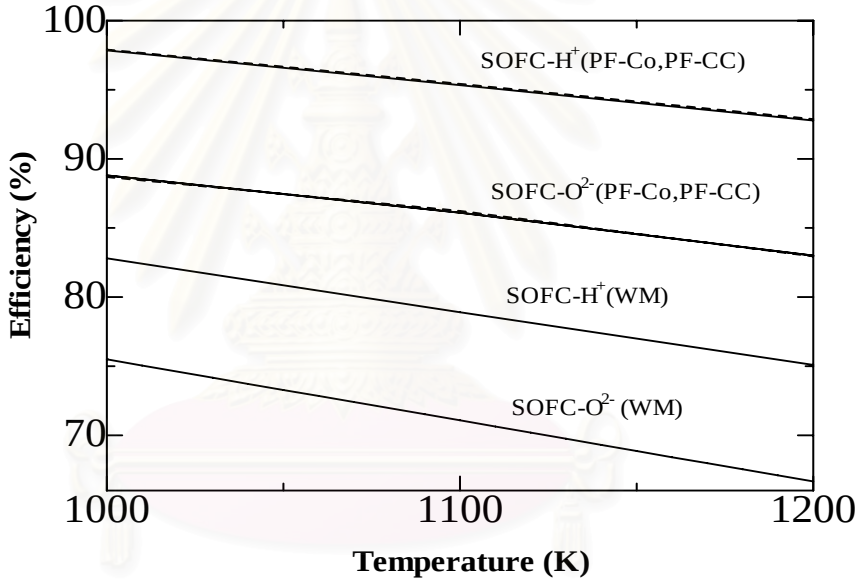

(b)

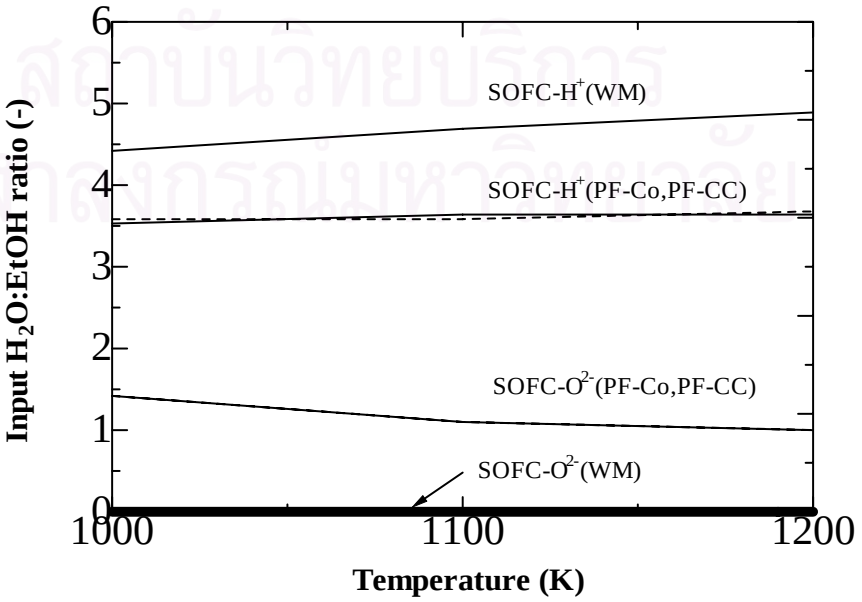

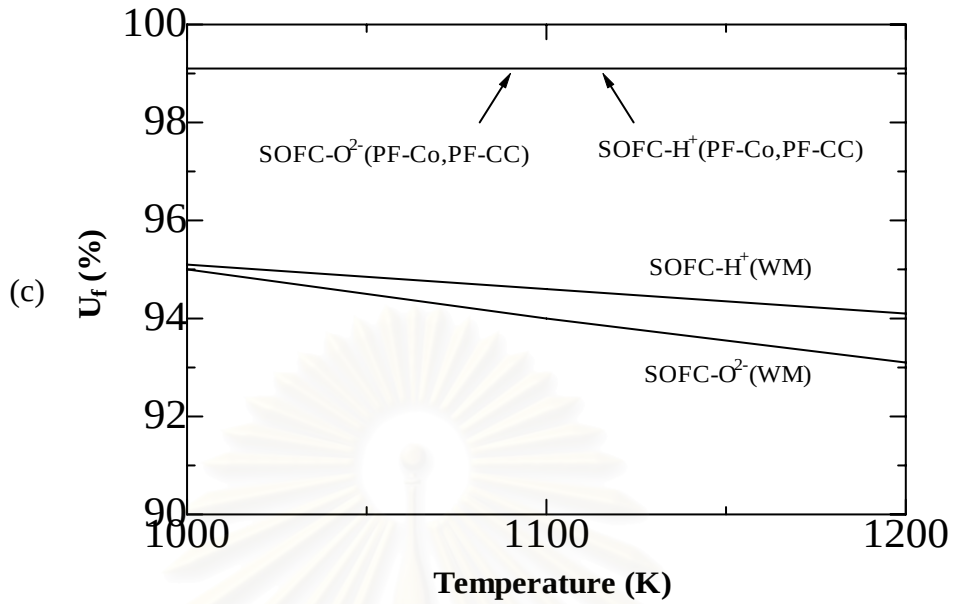

Figure 5.7 Influence of temperature on SOFC-H+ and SOFC-O2-: a) Maximum efficiency b) Corresponding inlet H_2O:EtOH ratio and c) Corresponding U_f (P = 101.3 kPa, 400% excess air).

The corresponding inlet H_2O:EtOH ratio is always approximately zero for the SOFC-O^{2-}(WM). For the SOFC-O^{2-}(PF), the corresponding ratio is about 1.4 and 1 at 1000 K and 1200 K, respectively. In the case of the proton conducting electrolyte, the SOFC-H^+(PF) requires a lower inlet H_2O:EtOH ratio than the SOFC-H^+(WM). For the SOFC-H^+(PF), the corresponding inlet H_2O:EtOH ratio is about 3.5 at 1000 K and increases with increasing temperature. While that for the SOFC-H^+(WM), is about 4.4 at 1000 K and also increases when operating temperature increases. This is probably because the water gas shift reaction is exothermic and therefore more steam is required to move the reaction to the right to produce hydrogen. The corresponding fuel utilization at the maximum efficiency of the SOFC (PF) for both electrolytes is almost constant at approximately 99% but it slightly decreases for the SOFC (WM) in both electrolytes when the temperature increases from 1000 to 1200 K.

From the above studies, it was found that although the benefit of lower steam requirement in the SOFC-O^2 is taken into account in the calculations, the SOFC-H^+ cell still shows higher efficiency than the SOFC-O^{2-} cell. This implies that the

development of SOFCs should be directed to the use of a proton conducting electrolyte.

5.3 Conclusion

Thermodynamic analysis of ethanol-fueled SOFCs using proton and oxygen ion conducting electrolytes in different modes of operation (i.e., plug flow and well-mixed) and feeding patterns (co-current and counter-current) has been presented in this chapter. At stoichiometric inlet H_2O:EtOH ratios, the SOFC-H^+(PF) provides the highest EMF and efficiency among various electrolytes and modes of operation. In order to compare the performances of SOFCs with different electrolytes, the benefit of reduced inlet steam requirement for the oxygen ion conducting electrolyte is taken into account. It was demonstrated that the use of proton conducting electrolytes is more attractive than the use of oxygen ion conducting electrolytes. The SOFC-H^+(PF) gives the highest efficiency. Moreover, it was found that there is no influence of the feeding patterns on the average EMF and efficiency although the EMF distribution along the cell is different.

Although the proton conducting electrolyte seems to be the most appropriate one for use in a solid oxide fuel cell from the theoretical calculations, it has a higher resistance than that of oxygen ion conducting electrolyte. If the ohmic loss of the electrolyte is considered, proton conducting electrolyte might perform worse than oxygen ion conducting electrolyte. More details of the electrolyte selection including all resistances (i.e., ohmic loss and activation loss) will be further investigated in the Chapter VI.

CHAPTER VI

ACTUAL PERFORMANCE OF ETHANOL-FUELLED SOLID OXIDE FUEL CELLS: PROTON AND OXYGEN ION CONDUCTORS

In this chapter, actual performances of ethanol-fuelled solid oxide fuel cells with different types of electrolyte (i.e. proton- and oxygen ion-conducting electrolytes) are investigated. Losses in SOFC operation (i.e. activation loss and ohmic loss) are considered. The actual performances of SOFC with different electrolytes and its development are lastly compared and discussed.

6.1 Introduction

As mentioned earlier, there are two types of electrolyte for SOFC operation. Most SOFC studies have employed oxygen-ion conducting electrolytes. Some studies focus on the development of material properties of proton-conducting ceramic electrolytes for high temperature applications (Shimada et al., 2004; Schober et al., 1997; Iwahara, 1996; Schneller et al., 2003). To date, there are very few studies using proton-conducting electrolyte in an SOFC operation (Salar et al., 2001; Browning et al., 2002). The performance of SOFCs with proton-conducting electrolytes (SOFC-H^+) in Yb doped $SrCeO_3$ (SCY) electrolyte with platinum electrodes system (Pt |SCY| Pt) were investigated in different atmospheres.

From Chapter V, it was shown that theoretical performance of the SOFC-H^+ provides higher efficiency than the SOFC with oxygen-ion conducting electrolytes (SOFC-O^{2-}) when the benefit of lower steam requirement of SOFC-O^{2-} was considered. However, the calculations neglected the presence of losses encountered in a real SOFC operation. Therefore, the aim of this chapter is to compare the actual performance of SOFCs with different electrolytes while the benefit of lower steam input is taken into account. Although it is well known that current proton-conducting electrolytes have high resistivity and thus the performance of SOFC-H^+ should be inferior to SOFC-O^{2-}, it is still necessary to determine the status of the SOFC-H^+ technology compared to that of SOFC-O^{2-}. The information from this chapter is

important in determining property targets (i.e. resistivity, electrolyte thickness and other resistance) for SOFC-H^+ in order to yield comparable performance as that of the SOFC-O^{2-}.

6.2 Results and Discussion

6.2.1 Characteristics of Actual Performance of SOFCs with Different Electrolytes

Figure 6.1 shows the characteristics of SOFC performance at different fuel utilizations for both SOFC-O^{2-} and SOFC-H^+. The calculations were based on a feed with an H_2O:EtOH ratio of 3 and temperature of 1200 K.

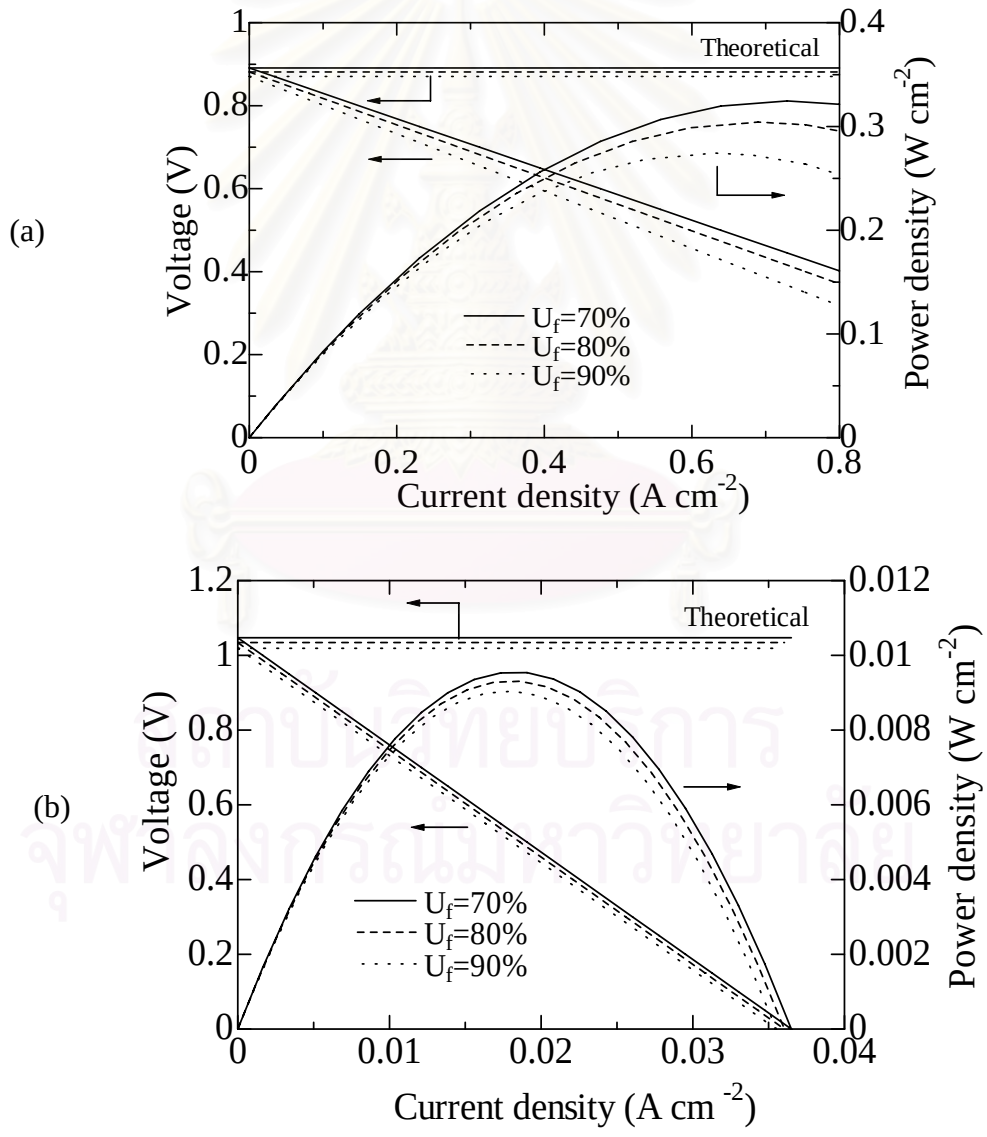

Figure 6.1 Performance of SOFCs for various fuel utilizations: (a) SOFC-O^{2-} and (b) SOFC-H^+ (Inlet H_2O:EtOH ratio=3, *T*=1200 K, *P*=101.3 kPa, 400% excess air).

The cell voltage decreases as the current density increases due to increasing losses. The power density initially increases with increasing the current density and drops at the higher values. For each value of fuel utilization, there is an optimum current density that maximizes the power density. The maximum power density decreases with increasing fuel utilization due to the effect of fuel depletion downstream. The observed values of the maximum power density of the SOFC-O^{2-} are within the range of the best value of 0.4 W cm^{-2} reported in the literature with an ethanol-fed system (Fuel Cells Bulletin 8, 2005, pp 8). Figure 6.1 also shows that the value of the current density at the maximum power density is insensitive to the fuel utilization factor (at least in the range 70-90%) in the case of SOFC-H^{+}. The insensitivity of power density to fuel utilization in the case of SOFC-H^{+} is due to the very large ohmic resistance. The ohmic loss in the SOFC-H^{+} overshadows all other losses. Since it is independent of the fuel utilization, there is almost no difference in cell voltage for the different fuel utilizations, as seen in Figure 6.1(b). As a consequence, the obtained maximum power density is insensitive to fuel utilization. For the SOFC-O^{2-}, the corresponding current density at the maximum power density decreases as the fuel utilization factor increases.

Performance comparisons between the two different electrolytes show that the SOFC-H^{+} results in an EMF of around 1.01 V whereas it is approximately 0.89 V for the SOFC-O^{2-}. It is clear that the performance of SOFC-H^{+} is theoretically superior to that of SOFC-O^{2-}, which is in good agreement with previous reports on SOFCs run with H_2 and CH_4 feeds (Demin and Tsiakaras, 2001; Demin et al., 2002) and ethanol feed (Tsiakaras and Demin, 2001). The difference in the EMF between the SOFCs with different types of electrolytes is mainly due to the location of the steam generated by the electrochemical reaction. However, for an actual operation, losses strongly affect the performances of the SOFCs. It is clearly seen from Figure 6.1 that the SOFC-H^{+} does not perform well as the SOFC-O^{2-}. The voltage in the SOFC-H^{+} decreases significantly faster than that of the SOFC-O^{2-} as the current density increases, and the resulting maximum power density for the SOFC-H^{+} is approximately 34 times lower than that of the SOFC-O^{2-}.

Another important indicator representing SOFC performance is the electrical efficiency defined in Eq. (4.75). The values of the electrical efficiencies at various

current densities and fuel utilizations are illustrated in Figure 6.2. When operating at the constant fuel utilization, the efficiency decreases with the increasing current density. The SOFC-H^+ can be operated over a much smaller range of current density than the SOFC-O^{2-} due to its higher losses. The maximum or theoretical efficiency is obtained when the current density approaches zero. At this condition, the SOFC-H^+ provides higher efficiency than the SOFC-O^{2-} although it is not a practical operating condition as the power density is very low and, therefore, a large cell area would be required. When the fuel utilization increases, the efficiency increases although the opposite trend may be observed at high current densities which yield low efficiency. It should be noted that the selection of suitable operating fuel utilization and current density is important as they influence the electrical efficiency and the power density which are among the key parameters to evaluate SOFC performance.

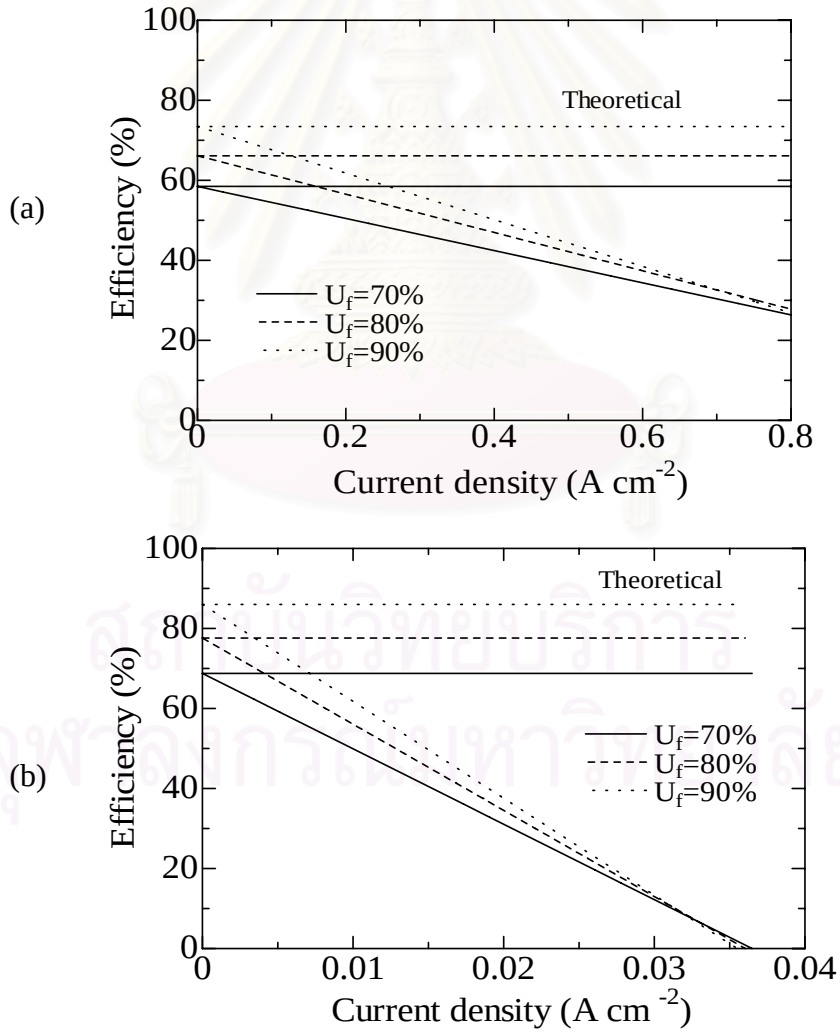

Figure 6.2 Efficiency of SOFCs for various fuel utilizations: (a) SOFC-O^{2-} and (b) SOFC-H^+ (Inlet H_2O:EtOH ratio=3, T=1200 K, P=101.3 kPa, 400% excess air).

6.2.2 Influence of H_2O:EtOH Ratio on SOFC Performances with Different Electrolytes

The feed composition is another important parameter to be considered. From the results shown in Chapter V, it was found that the SOFCs with different electrolytes required different inlet H_2O: fuel ratios to obtain their maximum EMFs. The effect of inlet H_2O:EtOH ratio on the voltage and power density is shown in Figures 6.3 and 6.4, respectively. In the calculations, the fuel utilization was kept at 80% which is a typical operating condition used in the literature (Hernandez-Pacheco et al., 2004; Hernandez-Pacheco et al., 2005). The inlet H_2O:EtOH ratio starts from its boundary of carbon formation which can be determined by following the procedure illustrated in the previous work (Assabumrungrat et al., 2004; Assabumrungrat et al., 2005; Sangtongkitcharoen et al., 2005)

(a)

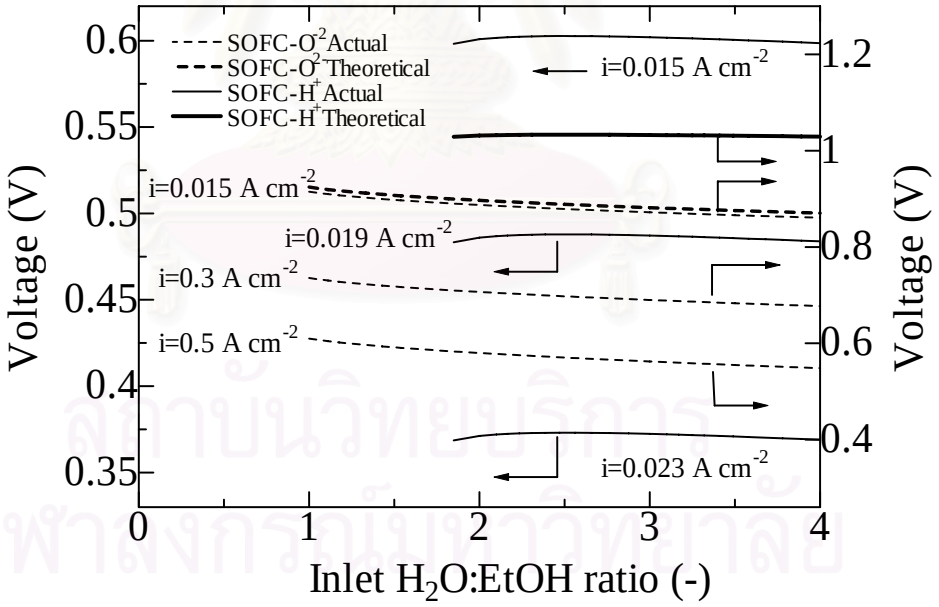

(b)

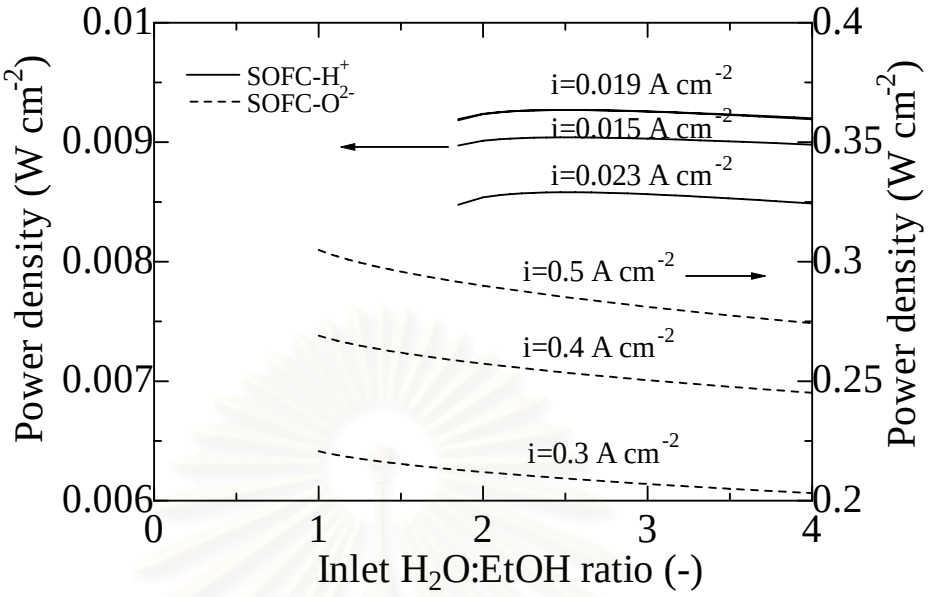

Figure 6.3 Influence of inlet H_2O:EtOH ratio on (a) voltage and (b) power density at various current densities (T=1200 K, P=101.3 kPa, U_f = 80%, 400% excess air).

From Figure 6.3, it was found that the SOFC-O^{2-} yields the maximum voltage and power density at the boundary of carbon formation whereas those of the SOFC-H^+ are found at a ratio beyond the boundary of carbon formation. In order to compare the performance of the SOFCs with different types of electrolytes, the best performance of each SOFC should be considered. The current density, H_2O:EtOH ratio and fuel utilization were varied to determine values which yield the highest power density for each type of SOFC.

6.2.3 Maximum Power Density and its Corresponding Operating Parameters for Different Electrolytes

Figure 6.4 shows the maximum power density and the corresponding current density and inlet H_2O:EtOH ratio at different fuel utilizations. As expected, the maximum power density and the corresponding current density decrease with an increase in fuel utilization due to the effect of fuel depletion.

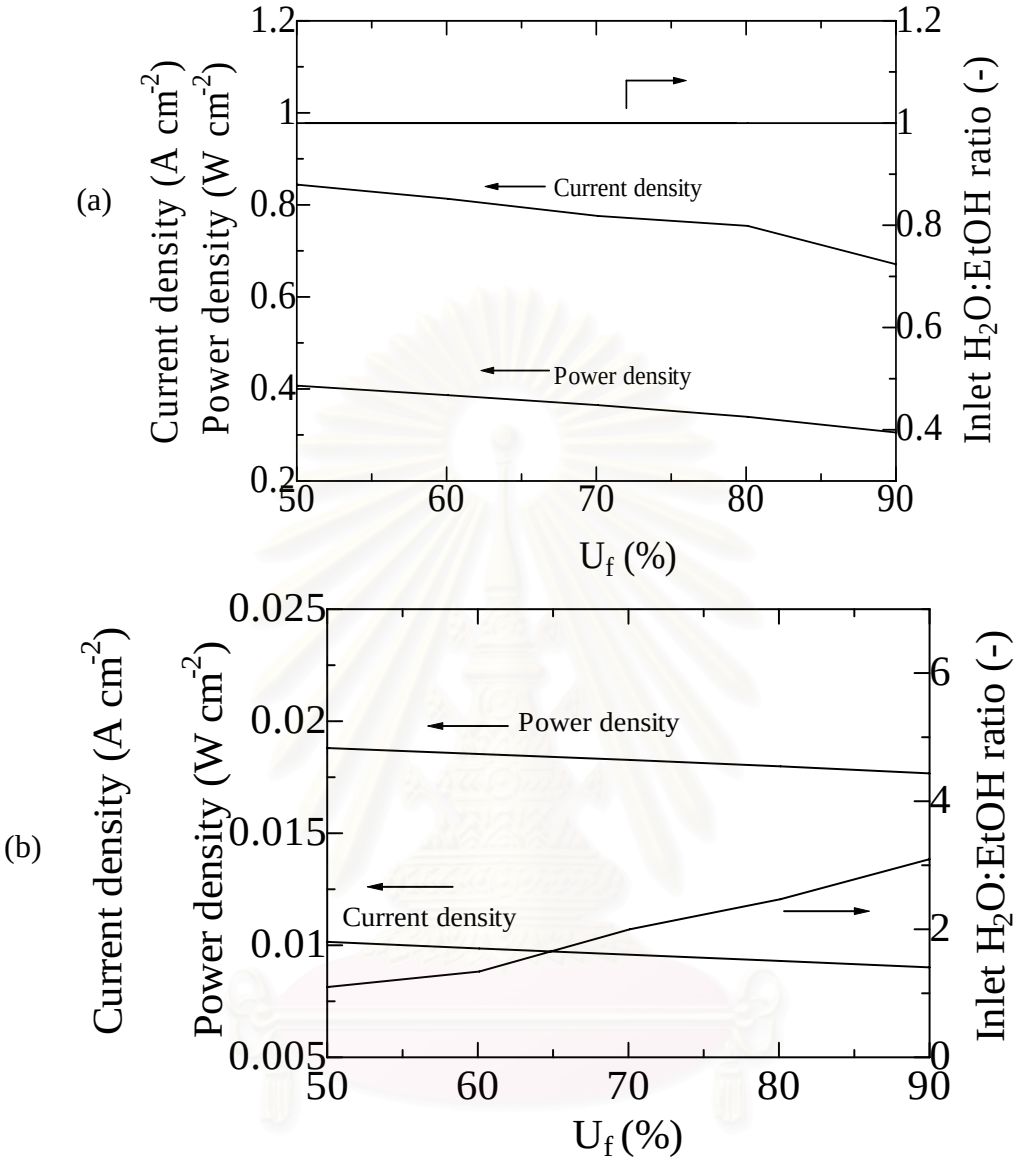

Figure 6.4 Maximum power density of SOFCs and their corresponding conditions (inlet H_2O:EtOH ratio, current density) at various fuel utilizations: (a) SOFC-O^{2-} and (b) SOFC-H^{+}.

Considering the corresponding values of the inlet H_2O:EtOH ratio, it can be noticed that for the SOFC-O^{2-} the values are independent of fuel utilization whereas it increases with increasing fuel utilization for the SOFC-H^{+}. The results can be explained by considering the influence of fuel utilization on the boundary of carbon formation. For the SOFC-O^{2-} case, the optimum H_2O:EtOH ratio is at the boundary of carbon formation. The fuel utilization does not affect the boundary of carbon

formation because the critical condition for carbon formation occurs at the feed inlet which corresponds to the fuel utilization of zero. The possibility for carbon formation becomes less severe when more hydrogen is consumed, in other words higher fuel utilization, yielding water which helps suppress carbon formation. However, for the SOFC-H^+ case, at high fuel utilization, more hydrogen disappears without benefiting from the steam generated from the electrochemical reaction in the anode gas mixture, leading to higher possibility for carbon formation. Therefore, higher inlet H_2O:EtOH ratios are required to thermodynamically suppress carbon formation. From the results shown in Figure 6.4, it is clear that the best performance of SOFC-H^+ is still lower than that of SOFC-O^{2-} for the entire range of fuel utilization which confirms that the SOFC-H^+ does not show great promise, at least with the current extremely high resistance in SOFC-H^+.

6.2.4 Development of the SOFC-$H^{\pm}$ Performance

To enhance the performance of SOFC-H^+, it is obvious that the resistance of the cell must be reduced due to the sudden drop in voltage. Figure 6.5 depicts the influence of the total resistance of the SOFC-H^+ cell on the cell performances at 1200 K. It should be noted that the total resistance is defined as the summation of electrolyte resistance and the other resistances.

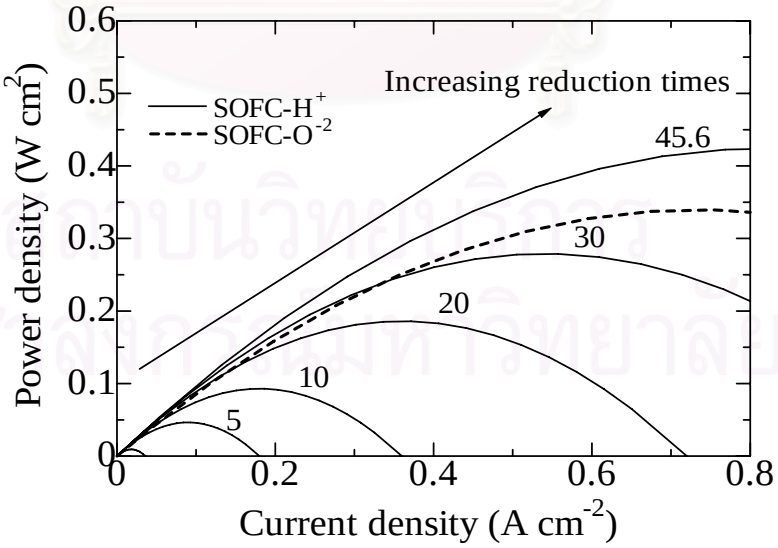

Figure 6.5 Influences of total resistance on the performance of SOFC-H^+ compared with that of SOFC-O^{2-} (T=1200 K, P=101.3 kPa, 400% excess air).

In this section, the reduction time is defined as the ratio by which the total resistance is reduced compared to the current value. The dashed line represents the values of the SOFC-O^{2-}. Obviously, the total resistance is an important factor for improving the performance of SOFC-H^{+}. Higher power density can be obtained when decreasing the total resistance. It was found that when the total resistance of the SOFC-H^{+} is reduced to 1/45.6 of the present value (28.7 Ω cm^2), which would be equal to the total resistance of the current SOFC-O^{2-} (0.628 Ω cm^2), the performance of the SOFC-H^{+} is better than that of the SOFC-O^{2-}. It is clear that due to the superior theoretical performance of the SOFC-H^{+}, it is unnecessary to reduce the total resistance of the SOFC-H^{+} to the level of that of the SOFC-O^{2-}.

The total resistance in the SOFC-H^{+} which yields an equivalent power density as the SOFC-O^{2-} is presented in Figure 6.6 as function of temperature. It can be seen that a reduction by 1/30.7 (0.935 Ω cm^2) is sufficient to offer the same power density as the SOFC-O^{2-} at 0.7 V and 1200 K. When increasing the operating temperature, the required resistance of SOFC-H^{+} has to be further decreased due to a rapid decrease in the total resistance of SOFC-O^{2-}.

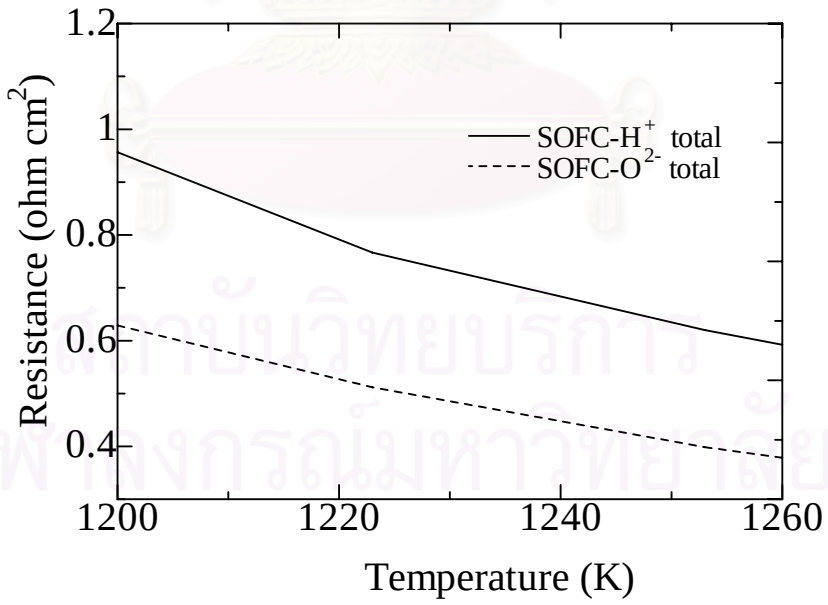

Figure 6.6 Required total resistance of SOFC-H^{+} with the comparable SOFC-O^{2-} performance at various temperatures.

Considering the Pt |SCY| Pt SOFC-H^+ cell in this study, the electrolyte, other and total resistances at 1200 K are 8.5, 20.2 and 28.7 Ω cm^2, respectively. It is seen that the expected value of 0.935 Ω cm^2 cannot be achieved by only reducing the electrolyte resistance. Both the electrolyte and the other resistances need to be improved simultaneously. At T = 1200 K, the electrolyte and the other resistances of the SOFC-H^+ are about 130 and 35 times, respectively, higher than those of the SOFC-O^{2-}. The high value of the other resistances of the SOFC-H^+ is possibly because platinum is not a good ionic conductor although it has high catalytic activity and high electronic conductivity (Handbook of Fuel Cells-Fundamentals, Technology and Applications, vol.1-2, John Wiley & Sons, Ltd., 2003). In addition, since the cermet structure is not applied for the anode, the platinum is more likely to sinter rather than compacted to the electrolyte at high temperature (Garzon et al., 2004). These lead to low interfacial conductivity between the platinum electrodes and the electrolyte. From these comparisons, significant efforts are required to reduce both the electrolyte and the other resistances of the SOFC-H^+ cell.

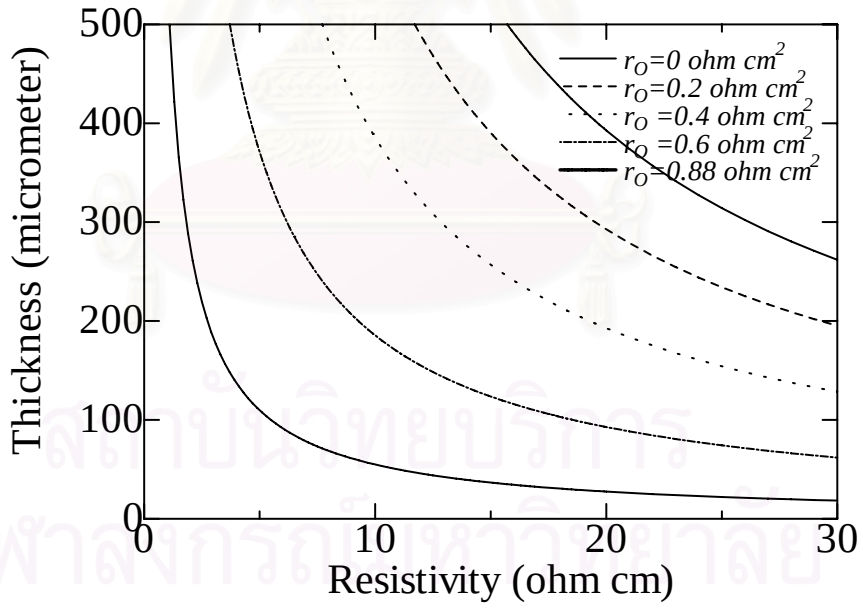

.

Figure 6.7 Resistivity and thickness of proton-conducting electrolyte at various values of the other resistances, r_0. (T=1200 K, P=101.3 kPa, 400% excess air).

Because the electrolyte resistance depends on its thickness and physical properties of material, it is possible to reduce the resistance by reducing the electrolyte thickness and/or using new materials with lower resistivity. Some materials with high proton conductivity have been reported, for example, $BaCe_{0.8}Y_{0.2}O_{3-\alpha}$ (BCY) and $BaCe_{0.9}Nd_{0.1}O_{3-\alpha}$ in which the resistivities at T = 1200 K are 12.5 and 28.6 Ω cm, respectively, compared to 85.0 Ω cm for the SCY used in this study (Iwahara, 1996). Figure 6.7 shows the required electrolyte thickness for different values of material resistivity of the electrolyte and the other resistance. It is clear that for a given value of the other resistance, the higher the material resistivity, the thinner the electrolyte is required. For the currently available high proton conducting material of SCY, when the electrolyte is reduced to a thickness as small as 150 μm which is in the range of an electrode-supported cell for 8YSZ (Handbook of Fuel Cells-Fundamentals, Technology and Applications, vol.1-2, John Wiley & Sons, Ltd., 2003), the other resistance should be reduced to 0.6 Ω cm^2 which is approximately 1/33.7 that of the present value. To achieve the expected value of the other resistance, the electrical conductivities and activity of the cathode and anode must be significantly improved to replace the use of Pt. In addition, the interfacial resistivity between electrolyte/anode and electrolyte/cathode must be suppressed by a careful selection of material and suitable microstructure to enhance the triple-phase boundary. In addition, some other considerations such as mechanical strength, chemical compatibilities and thermal expansion compatibilities among the cell components need to be taken into account in the cell development. However, it is unfortunate that most of these data are currently not available. Therefore, considerable effort in the development of an SOFC-H^+ cell is necessary to eventually commercialize this type of fuel cell.

6.3 Conclusion

Although the theoretical EMF and electrical efficiency of the SOFC-H^+ are superior to those of the SOFC-O^{2-}, its actual voltage and power density are much lower than those of the SOFC-O^{2-} due to large resistance of the cell. It was calculated that in order to achieve an equivalent power density to the SOFC-O^{2-}, the total resistance of the SOFC-H^+ should be reduced to 0.935 Ω cm^2, which is equal to 1/30.7 of the present value (28.7 Ω cm^2), compared to the value of 0.628 Ω cm^2 of the

SOFC-O^{2-} at 1200 K. Due to the superior theoretical performance of the SOFC-H^{+}, it is unnecessary to reduce the total resistance of the SOFC-H^{+} to the same value of the SOFC-O^{2-}. It was found that the reduction of the electrolyte resistance alone is not sufficient to reach the expected value of the total resistance. Both the electrolyte and the other resistances need to be improved simultaneously. The electrolyte resistance can be improved by reducing the electrolyte thickness and/or finding new materials with lower resistivity. When the electrolyte thickness of SCY, the currently available high proton conducting material, is reduced to 150 μm, in the range of an electrode supported cell for 8YSZ, the other resistance should be reduced to 0.6 Ω cm^2 (1/33.7 of the present value). It is clear that the success of the SOFC-H^{+} technology depends on the development of improved cell components.

CHAPTER VII

THERMODYNAMIC ASSESSMENT OF SOLID OXIDE FUEL CELL SYSTEM INTEGRATED WITH BIOETHANOL DISTILLATION COLUMN

In this chapter, the SOFC-O^{2-} was selected to investigate the performance of the SOFC system. An SOFC system integrated with a distillation column (SOFC-DIS) was purposed for improvement of energy consumption in the system. A bioethanol feed stream was purified by distillation and fed to the SOFC system. The exothermic heat released from the system was used for supplying heat to other parts of the system including a distillation column. The effect of operating conditions (i.e., ethanol purity, ethanol recovery, fuel utilization and voltage) on energy involving the SOFC-DIS system was examined. Finally, the possibility to operate the SOFC-DIS system at energy-sufficient conditions was examined. The performance of the SOFC-DIS system and its corresponding operating conditions were presented and discussed.

7.1 Introduction

Among possible fuels for SOFC, ethanol is an attractive green fuel as it can be derived from renewable resources, it is safe and easy to store and handle (Maggio et al., 1998). The group of Tsiakaras has been particularly active in investigating ethanol-fuelled SOFCs (Tsiakaras and Demin, 2001; Douvartzides et al., 2003, 2004). An energy-exergy analysis was also employed to examine the system comprising an external steam reformer, an SOFC stack, an afterburner, two preheaters, a water vaporizer and a mixer (Douvartzides et al., 2003, 2004). However, the studies related to ethanol-fuelled SOFCs usually feed pure ethanol mixed with water in order to obtain a desired ethanol concentration before being fed to the reformer. From an energy point of view, this is not an efficient strategy as unnecessary energy is consumed to purify bioethanol to needlessly high ethanol concentration ethanol which is subsequently diluted by mixing with water and fed to the reformer.

In this chapter, it was proposed to integrate the SOFC with an ethanol purification unit. The ethanol was purified to a desired concentration using a distillation column whose required energy can be directly supplied by the excessive heat from the SOFC system. It was expected that by carefully selecting suitable operating conditions, the integrated system can be operated without a requirement of additional energy sources apart from the bioethanol feed. The influence of operating parameters including ethanol concentration, ethanol recovery, fuel utilization and voltage on electrical performance and net energy of the integrated system (Q_{Net}) were investigated.

7.2 Results and Discussion

7.2.1 Effect of Ethanol Concentration on SOFC Performance and Energy Requirement in the Distillation Column

It is impractical to feed bioethanol directly to an SOFC stack because high water content strongly affect the SOFC performances as presented in Chapter V and VI. Figure 7.1 shows the performance curves of SOFCs fed by different ethanol concentrations. The SOFC operated at a T_{SOFC} of 1200 K with fuel utilization (U_f) of 80%.

(a)

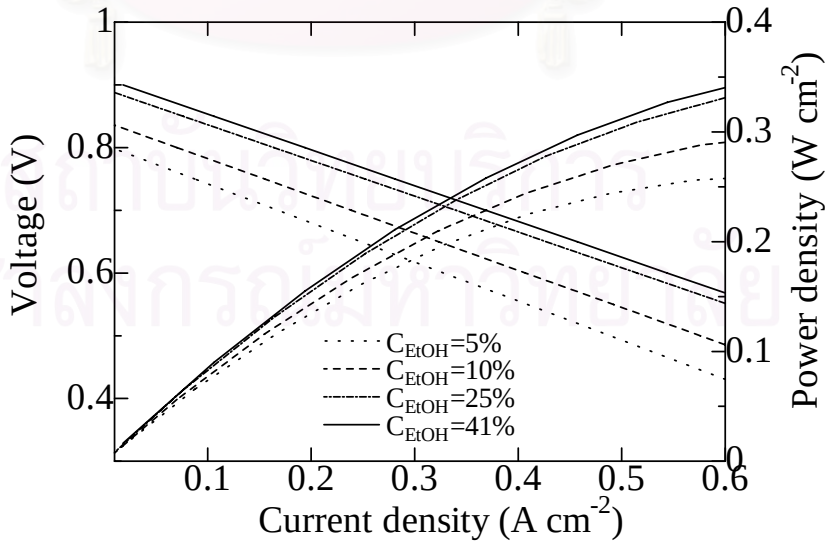

(b)

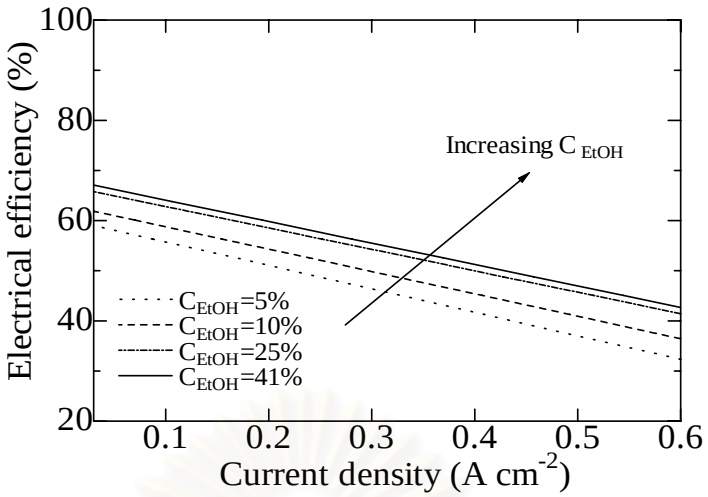

Figure 7.1 Effect of ethanol concentration on SOFC performance: (a) voltage and power density, (b) electrical efficiency (U_f = 80%, P = 101.3 kPa).

From Figure 7.1 it is clear that the power density, cell voltage and electrical efficiency increase with increasing ethanol concentration. This implies that the SOFC stacks perform better when a distillation column is integrated with the SOFC system to purify the bioethanol. However, in practice, the maximum ethanol concentration should be kept below the range of carbon formation to avoid deactivation of the reforming catalyst and anode of the SOFC cell. For example, at T_{RF} = 1023 K, the boundary of carbon formation was at 41 mol% as calculated by Eq. (4.31)-(4.41) with the carbon activity constraint in Eq. (4.52). The results are in good agreement with Assabumrungrat's work (2004). Although it is advantageous to use high ethanol concentrations for the SOFC system, higher energy is required to concentrate the bioethanol.

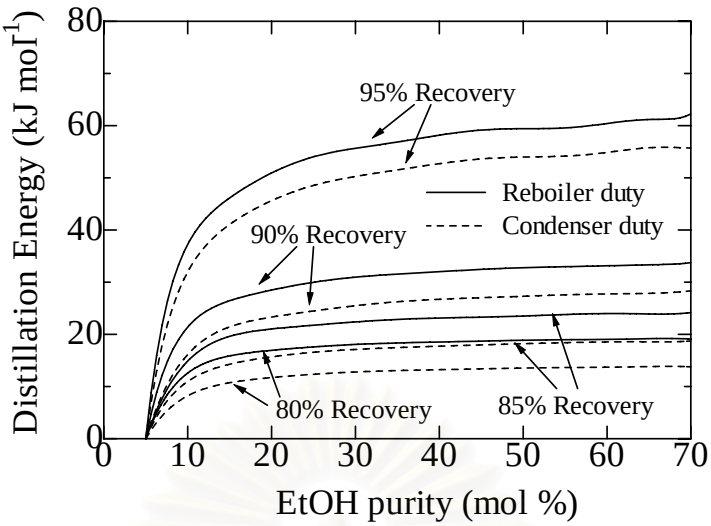

Figure 7.2 Effect of ethanol concentration and ethanol recovery on distillation energy.

Figure 7.2 shows the minimum reboiler and condenser heat duties as a function of ethanol purity and recovery. It is clear that more energy is required when the distillation column is operated to achieve higher ethanol concentration and recovery. The reboiler and condenser heat duties increase dramatically at low ethanol purity and rises steadily at the higher ethanol purity. This is due to a narrow vapour-liquid equilibrium gap for ethanol-water mixture at low ethanol purity and a wider vapour-liquid gap at higher purity.

7.2.2 Performance of the SOFC System Integrated with a Distillation Column (SOFC-DIS) at the Base Condition

Figure 7.3 indicates operating temperature and energy requirement for all important units in the SOFC-DIS system operating at the base conditions; i.e. C_{EtOH} = 25 mol%, EtOH recovery = 80%, cell operating voltage = 0.7 V and U_f = 80%. An electrical power (W_e) of 218.77 kW with an overall electrical efficiency (based on LHV) of 37.72% was achieved. The net useful heat of the SOFC system ($Q_{SOFC,Net}$) and the heat required for the distillation column (Q_D) are 88.36 and 149.11 kW, respectively. In this case, although $Q_{SOFC,Net}$ can be used for supplying heat to the reboiler directly, it is obvious that the value of $Q_{SOFC,Net}$ is not enough for the required Q_D under these base conditions.

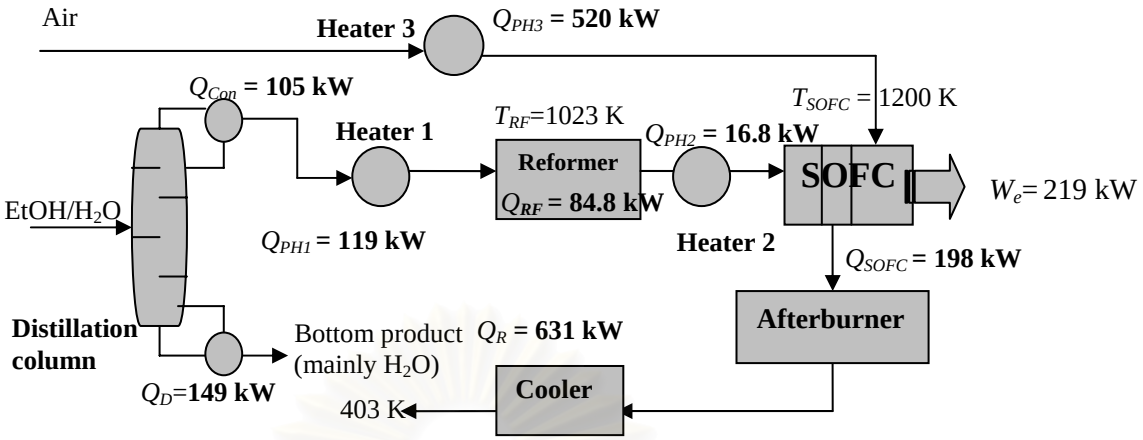

Figure 7.3 Energy and temperature for various units in the SOFC-DIS system (EtOH recovery = 80%, C_{EtOH} = 25 mol %, U_f = 80%, P = 101.3 kPa).

However, by carefully adjusting the operating conditions such as operating voltage, fuel utilization, ethanol concentration and recovery, excess heat from the SOFC system can be increased to satisfy the energy requirements of the reboiler of the distillation column. Proper adjustment of these operating conditions which the system is self energy-sufficient (Q_{Net} = $Q_{SOFC,Net}$ − Q_D = 0) is the subject of the subsequent sections.

7.2.3 Effect of Operating Conditions on Electrical Performances and Thermal Energy involving the SOFC System

7.2.3.1 Effect of SOFC Operating Conditions

Figure 7.4 represents the effect of operating voltage and fuel utilization on the overall efficiency and electrical power (W_e), net useful heat (Q_{Net}) and power density in Fig 7.4(a)-(c), respectively. As mentioned earlier, Q_{Net} is $Q_{SOFC,Net}$ subtracted by Q_D. Therefore, the value of Q_{Net} can be positive, zero or negative. A positive value of Q_{Net} indicates that some extra heat is left over from the overall SOFC-DIS system. For the case where Q_{Net} is negative, $Q_{SOFC,Net}$ is not enough to supply all the required heat to the distillation column; therefore, an external heat source is required. At the point where Q_{Net} is equal to zero, $Q_{SOFC,Net}$ satisfies exactly the reboiler demand. Consequently, this condition offers the maximum electrical power for the SOFC-DIS system without requiring an external heat source.

(a)

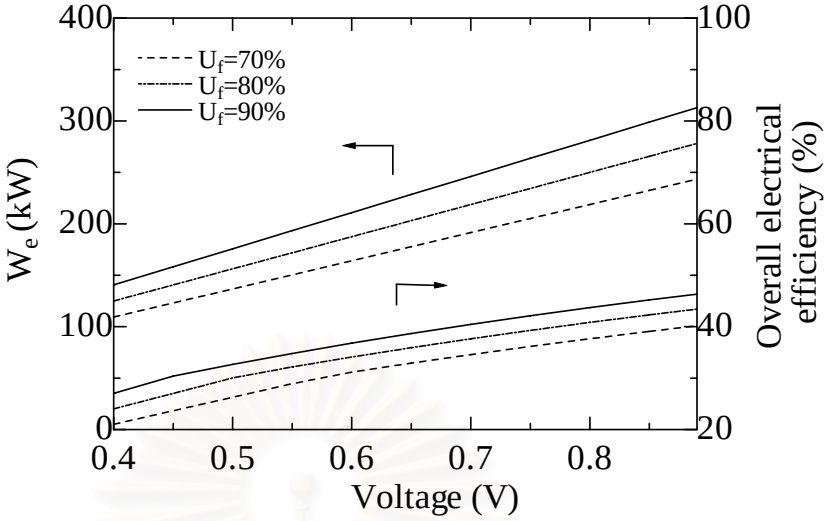

(b)

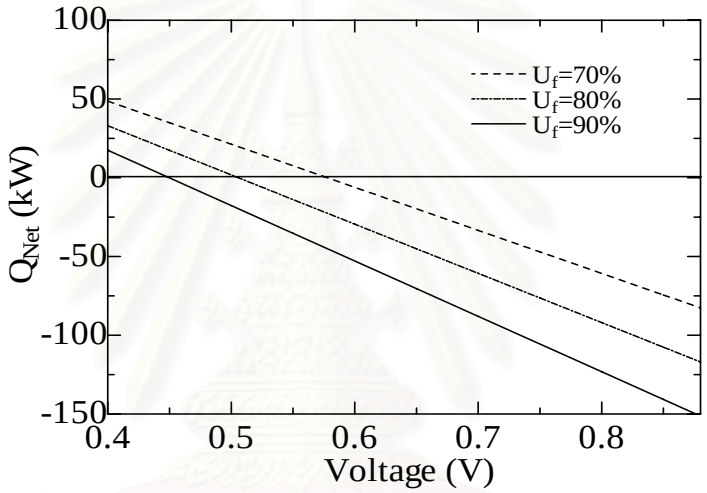

(c)

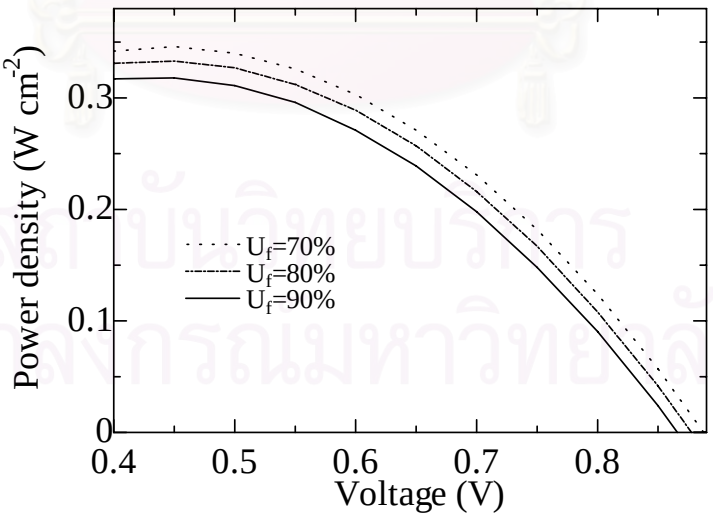

Figure 7.4 Effect of operating voltage and U_f on SOFC-DIS performance: (a) W_e and overall efficiency, (b) Q_{Net}, and (c) power density (EtOH recovery = 80%, C_{EtOH} = 25 mol %, P = 101.3 kPa).

From Figure 7.4 (b) it can be seen that higher Q_{Net} (i.e. the system becomes more energy sufficient) can be obtained when the SOFC-DIS system operates at lower voltage and/or lower fuel utilization. For lower voltage operation, the difference between the theoretical voltage and the actual one is large and results in higher heat losses emitted from the SOFC stack and therefore, Q_{Net} increases. For operation at lower fuel utilizations, more unreacted fuel exiting the SOFC stack is burnt in the afterburner. This leads to higher combustion energy and, as a result, higher Q_{Net}. However, lower electrical power and overall efficiency are obtained at higher Q_{Net}. There is an appropriate voltage for which Q_{Net} = 0 for U_f ranging from 70 to 90% (at C_{EtOH} = 25% and EtOH recovery = 80%). The corresponding voltages are 0.58, 0.51 and 0.45 V, for U_f, = 70, 80 and 90%, respectively. Operation at higher fuel utilization requires lower operating voltage for generating more heat from the stack to compensate for the heat required in the overall system.

Another important SOFC performance indicator which should be of concern is power density. The effects of voltage and fuel utilization on power density are shown in Figure 7.4(c). Operating at low voltage is of no practical value (hence, not shown in Figure 7.4). However, at higher voltage Figure 7.4(c) shows a rapid decrease in power density, resulting in larger stack area and more expensive SOFC stacks. Figures 7.4(c) also indicate that the power densities where Q_{Net} =0 are equal to 0.31, 0.33 and 0.32 $W.cm^{-2}$ for U_f = 70, 80 and 90%, respectively, which also corresponds to an overall electrical efficiency of 30.3% for all fuel utilizations. The fuel utilization factor has thus no notable influence on the overall electrical efficiency and power density when Q_{Net} is kept at zero (at constant ethanol concentration).

In summary, the SOFC-DIS system can be made self energy-sufficient by adjusting the fuel utilization and operating voltage. However, it should be noted that a number of operating parameters must be carefully examined. Operating the SOFC at too low voltage can result in a significant reduction in power density. Moreover, the excessive heat generated in the stack can directly damage the thermophysical property of the SOFC cell components and raises the issue of how to remove this high amount of heat from the stack. It is recommended that adjusting fuel utilization is a better

option to control $Q_{SOFC,Net}$. Also, for practical operation, the electrical power, overall efficiency and power density should be acceptably high.

7.2.3.2 Effect of Ethanol Concentration

From the previous section, it was found that adjusting voltage and fuel utilization can render the system self-sufficient. However, Q_{Net} also depends on the amount of required distillation energy (Q_D) which is strongly influenced by ethanol concentration (C_{EtOH}) and ethanol recovery as shown in Figure 7.2. In this section, the effect of ethanol concentration on electrical performance (W_e, overall efficiency, and corresponding voltage and power density) at conditions for which Q_{Net} = 0 is investigated. The ethanol recovery was kept at 80%. The results are shown in Figure 7.5.

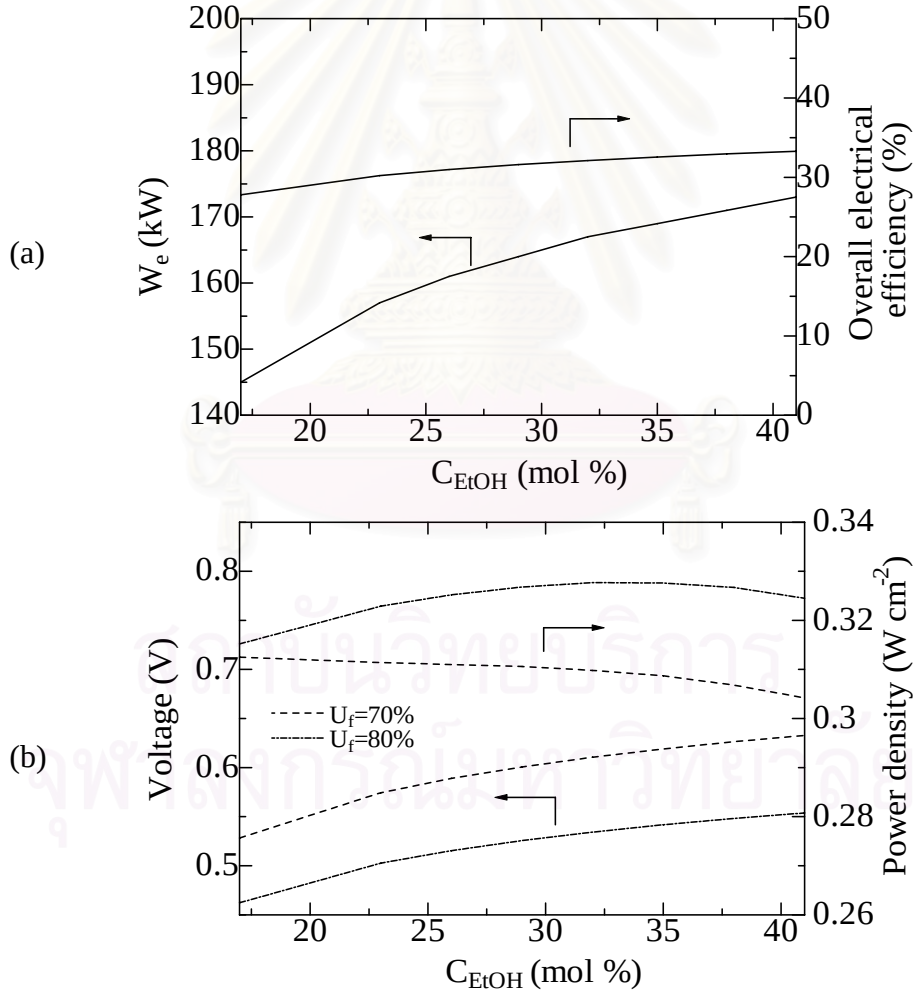

Figure 7.5 Effect of ethanol concentration on SOFC-DIS performance for various U_f when Q_{Net} = 0: (a) W_e and overall efficiency, (b) corresponding voltage and power density (EtOH recovery = 80%, P = 101.3 kPa).

The results shown in Figure 7.5(a) indicate that, for ethanol concentrations between 17 and 41%, $W_{e,}$ and overall efficiency increase with increasing ethanol concentration, independent of the fuel utilization (U_f = 70-80%). It was known that increasing ethanol concentration is beneficial in terms of power produced, but is detrimental in terms of energy demand on the reboiler (see Figure 7.2). Figure 7.5(a) illustrates the fact that the benefit of increasing ethanol concentration is more important than the negative effect of increased reboiler duty. This could be explained by the relatively gentle increase in reboiler duty for ethanol concentrations greater than 17%, as seen in Figure 7.2. The effect of fuel utilization on SOFC performance when Q_{Net} equals zero is also presented in Figure 7.5(b). It can be seen that the SOFC would run at lower voltage for operation at higher fuel utilization. This result is in good agreement with the results described earlier. It can be seen that the operating voltage is around 0.6 and 0.5 V at U_f = 70% and 80%, respectively. Figure 7.5(b) also presents the effect of ethanol concentration on power density. For U_f = 80%, the power density slightly increases when operated at higher C_{EtOH} whereas the opposite is true for U_f = 70%. As expected, the power density is consistently higher at U_f = 80% than at 70%.

In summary, Figure 7.5 indicates that, when keeping Q_{Net} equal to zero, better overall performance (higher overall electrical efficiency, higher power density) is achieved when operating at higher fuel utilization factor (e.g. 80%) and at the highest possible ethanol concentration (i.e. 41%). At these conditions, the overall efficiency reaches 33.3% and the power density 0.32 W cm^{-2} (corresponding to a voltage of 0.55 V and current density of 0.58 A cm^{-2}).

7.2.3.3 Effect of Ethanol Recovery

As mentioned earlier, ethanol recovery is another important parameter affecting Q_D and the overall energy within the system. Figure 7.6(a) presents the effect of ethanol recovery on W_e and overall efficiency at different ethanol concentrations for Q_{Net} = 0. Higher W_e and overall efficiency are obtained when increasing ethanol recovery up to 80%; however, the performance significantly decreases at ethanol recoveries greater than 80%. This is because of the competition between an increase of current and a decrease of operating voltage at that point.

Increasing ethanol recovery also increases current at the same fuel utilization while the operating voltage is also dependent on the required Q_D.

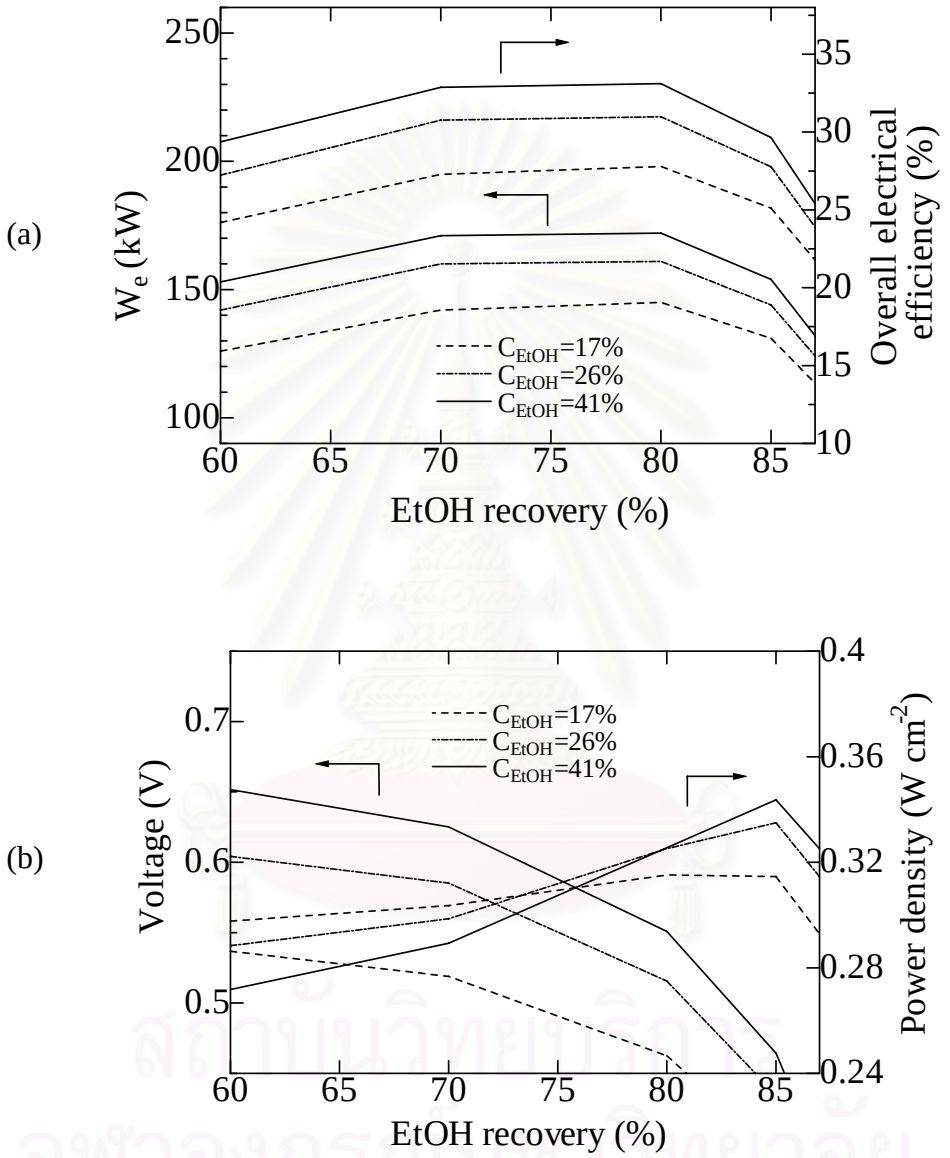

Figure 7.6 Effect of ethanol recovery on SOFC-DIS performance when Q_{Net} = 0 at different C_{EtOH}: (a) W_e and overall efficiency, (b) corresponding voltage and power density (U_f = 80%, P = 101.3 kPa).

It can be seen that at lower ethanol recovery, the required operating voltage is slightly changed due to small change in Q_D. Therefore, the electrical power becomes

higher because of the increase in current. However, at high ethanol recovery, Q_D is dramatically increased and causes a sudden drop in voltage as shown in Figure 7.6(b). This results in a decrease in electrical power. The corresponding voltage and power density at different EtOH recovery is also shown in Figure 7.6(b). It can be seen that increasing ethanol recovery still requires lower voltage. The SOFC-DIS system still needs some energy from the SOFC stack to compensate for the higher demand in Q_D. This is different from the results in Figure 7.5(b) which shows that lower voltage is not required because the SOFC-DIS system gains some benefits from the lower preheating energy for EtOH/H_2O mixture. For the effect of ethanol recovery, more ethanol and water are fed to the SOFC-DIS system when operated at higher ethanol recovery. More energy is, therefore, required for the reformer and EtOH/H_2O preheater. The SOFC stack has to operate at a lower voltage to compensate for the heat which results in a decrease in voltage as shown in Figure 7.6(b). Moreover, it was found that at higher EtOH recovery, a higher power density is obtained.

From the above studies, it is possible to operate the SOFC-DIS system under an energy sufficient condition. The obtained efficiency and power density of SOFC-DIS system are 33.3% and 0.32 Wcm^{-2} at C_{ETOH} = 41%, U_f = 80% and ethanol recovery = 80%. The reboiler heat duty is the limitation for achieving higher performance because the SOFC-DIS has to be operated under inferior conditions in order to provide the required heat to the distillation column. Moreover, a large amount of heat (105 kW) was emitted from the SOFC-DIS at the condenser. The management of this condenser duty could be used to enhance the SOFC-DIS performance and allow the SOFC to operate at more optimal conditions. It is expected that the performance of SOFC-DIS could be further improved.

7.3 Conclusion

An SOFC system integrated with a distillation column (SOFC-DIS) was studied. Bioethanol was used as a feed stream for the SOFC-DIS system. The influence of operating parameters (i.e. EtOH concentration, EtOH recovery, cell operating voltage and fuel utilization) on electrical performance (i.e. electrical power, overall efficiency and power density) and thermal energy involving in the SOFC system (i.e. reboiler heat duty and the net useful heat) was presented. The study

showed that it is possible to operate the SOFC-DIS system in a self energy-sufficient mode by adjusting the operating voltage and/or fuel utilization. The effect of ethanol concentration (17-41 mol %) and ethanol recovery at the energy-sufficient point (Q_{Net} = 0) was presented. It was found that higher ethanol concentration yielded higher electrical power (for C_{EtOH} in the range 17-41%), higher overall electrical efficiency and acceptably high power density. For the effect of ethanol recovery, there is an optimum ethanol recovery at 80% which yielded the optimum electrical power and overall electrical efficiency. Higher power densities can be obtained when operating at higher ethanol recoveries. In brief, this thermodynamic study of the SOFC-DIS system showed the potential of the system when operated without external heat sources. However, the performance of the SOFC-DIS system was quite low (0.32 W cm^{-2}, 173.07 kW_e, 33.3% overall efficiency based on total ethanol flow rate fed to SOFC-DIS system at U_f = 80%, EtOH recovery = 80% and C_{EtOH} = 41%). It was found that the reboiler heat duty was the limitation for the SOFC-DIS system. Moreover, a large amount of heat was lost at the condenser. To improve the performance of the SOFC-DIS system, it is recommended that 1) heat integration of the SOFC-DIS system should be considered e.g., the heat emitted at condenser should be utilized for other purposes and 2) another purifying process (e.g. membranes) which consumes less energy be investigated.

CHAPTER VIII

DESIGN OF A THERMALLY INTEGRATED BIOETHANOL-FUELLED SOLID OXIDE FUEL CELL SYSTEM INTEGRATED WITH A DISTILLATION COLUMN

In this chapter, a design of heat exchanger network for ethanol-fuelled SOFC system integrated with a distillation column (SOFC-DIS) was investigated. The performance enhancement of the SOFC-DIS system by utilizing exothermic heat from a condenser and hot water from the bottom of the distillation column and by implementing cathode recirculation from the cathode outlet was compared. The effect of operating conditions on composite curves and the details of designing of heat exchanger network were also presented in this chapter.

8.1 Introduction

As mentioned earlier, most of the previous studies on the ethanol-fed SOFC system have been carried out by using pure ethanol mixed with water. From an energy point of view, it is not efficient or necessary to purify bio-ethanol to highly pure ethanol as some water is usually required for the steam reforming reaction. Therefore, the SOFC system implemented with a distillation column (SOFC-DIS) has been considered in the previous chapter. Bio-ethanol is purified just to reach a desired ethanol concentration needed for steam reforming. The hot effluent from the afterburner was used for heating all heaters, an external reformer and a boiler of a distillation column. The possibility of operating the SOFC-DIS as a self energy-sufficient system was examined in the previous chapter and the results found that the SOFC-DIS system can operate without an external heat source. Nevertheless, the calculation in the previous chapter was based on the direct subtraction between net supply energy and net energy consumption in the system. No details of heat transfer arrangement were considered. Moreover, other useful heat in the system (i.e. condenser duty and hot water at the bottom of the distillation column) was not utilized. Also, large amount of high temperature air leaving the cathode should be considered as an internal heat source. The main objective of this chapter is to study the

performance of the SOFC-DIS when all heat was considered. Other useful heats e.g. condenser duty and hot water from the bottom of the column and the cathode re-circulation are taken into account to enhance the performance of SOFC-DIS. In addition, the effect of operating conditions on composite curve is examined and the designs of the heat exchanger network for the SOFC-DIS system are lastly investigated.

8.2 Results and Discussion

8.2.1 Base Case SOFC-DIS and Performance Enhancement

The configuration of the base case SOFC-DIS is illustrated by a solid line in Figure 8.1. All the cold process streams were heated using a hot utility to reach the target temperatures and all hot process streams were cooled using a cold utility.

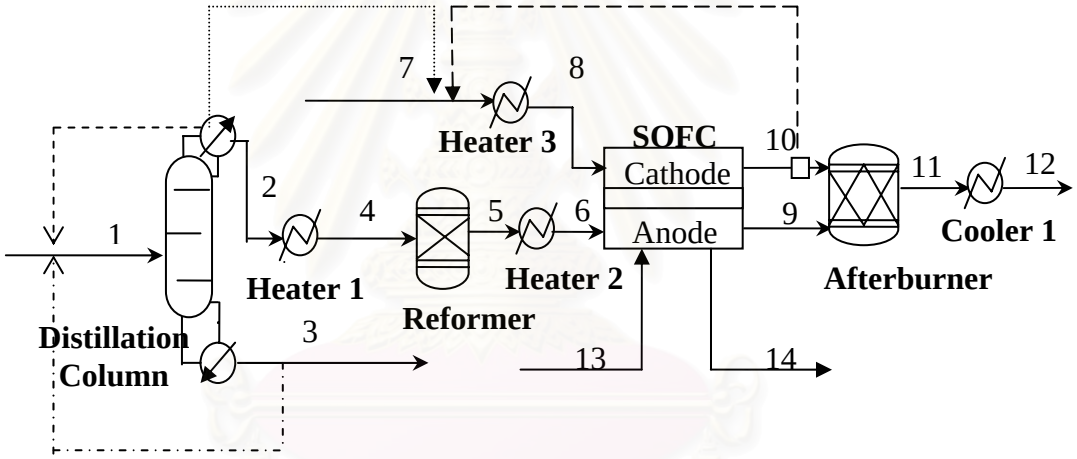

Figure 8.1 Schematic diagram of SOFC-DIS systems.

The operating conditions at the base condition were shown (i.e. C_{EtOH} = 25 mol%, EtOH recovery = 80%, V = 0.7 V, U_f = 80%, T_{RF} = 1023 K and T_{SOFC} = 1200 K). The starting temperature, target temperature, heat load and heat capacity of all hot and cold streams for the base case are presented in Table 8.1. The heat exchanger network of the base case is presented in Figure 8.2. It can be seen that the major energy consumers are Heater2, the air preheater, (580.4 kW or 66.5% of the overall energy consumption) and the reboiler (149.1 kW or 17.1% of the overall energy consumption); the net energy consumption is 873.1 kW which is supplied by the hot utility.

Table 8.1 Information of hot and cold streams at the base case SOFC-DIS (No-HX)

	Stream Label	T_{in} (K)	T_{out} (K)	Load (kW)	MC_p (kW/K)
Hot stream					
Cooler-1	H1	1304.9	403.0	847.3	0.940
Condenser	H2	365.9	365.9	48.8	Large
Hot water	H3	369.3	303.2	45.4	0.687
Cold stream					
Air stream	C1	298.2	1000.0	580.7	0.827
BioEtOH stream	C2	298.2	345.5	47.2	0.998
Anode heater	C3	1023.0	1100.0	7.3	0.095
Distillate stream	C4	365.9	1023.0	50.9	0.078
Reboiler	C5	298.2	369.3	149.1	2.097
Reformer	C6	1023.0	1023.0	85.4	Large

It can be seen that the hot stream from the afterburner is the major energy supplier and contains 847.3 kW of thermal energy which, in this case, corresponds to the cooling energy by the cold utility. Electrical power of 220.5 kW is produced. The overall electrical efficiency, CHP efficiency and corresponding power density of SOFC-DIS are 15.8 %, 76.5% and 0.229 W cm^{-2}, respectively. It can be noticed that the heat content from the condenser (48.8 kW) and from hot water (46.9 kW) have not been utilized. To enhance the system efficiency, the useful heat from the overhead vapour stream going to the condenser and the useful heat from hot water from the bottom of the distillation column are used for providing heat to other parts of the system. As mentioned earlier, the heat from the vapour stream going to the condenser and from hot water are low-temperature heat streams. To utilize this heat, preheating incoming reactants (air or bioethanol) is reasonable. Moreover, a large amount of air is introduced to the system in order to cool down the SOFC stack. However, the amount of air is more than that needed for burning unreacted fuels from the anode. Therefore, an investigation of the performance of SOFC-DIS when the cathode recirculation is implemented into the system will be performed.

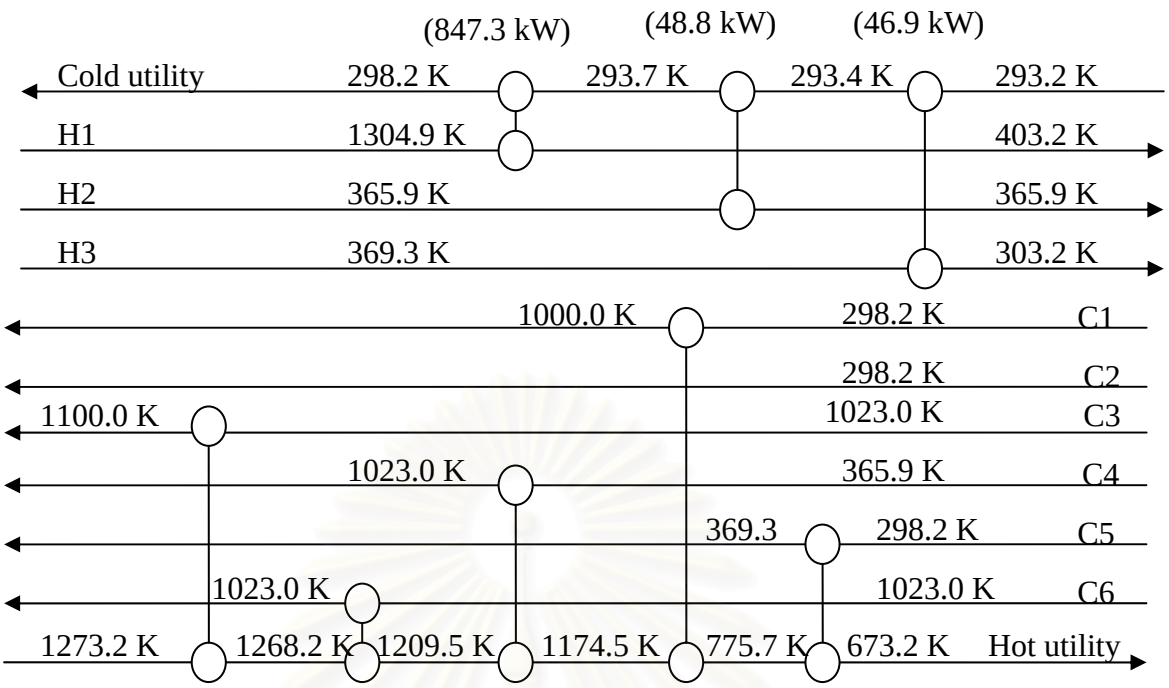

Figure 8.2 Heat exchanger network of base case SOFC-DIS (NO-HX) (C_{EtOH} = 25%, EtOH recovery = 80%, U_f = 80%, V = 0.7 V, T_{SOFC} = 1200 K, $T_{anode,in}$ = 1100 K, $T_{cath,in}$ = 1000 K, T_{RF} = 1023 K and P = 101.3 kPa).

The different configurations of the system are shown in Figure 8.1 with different lines. In this study, the utilization of the heat recovery from the condenser for preheating incoming bioethanol (Cond-Bio) representing by dashed line, the heat recovery from condenser for preheating incoming air (Cond-Air) representing by dotted line, the heat recovery from the hot water from the distillation column for preheating bioethanol (HW-Bio) represented by dash dot line and the implementation of cathode recirculation (CathRec) represented by long dashed line are considered. Heat exchanger networks of different configurations are presented in Figures 8.3-8.6.

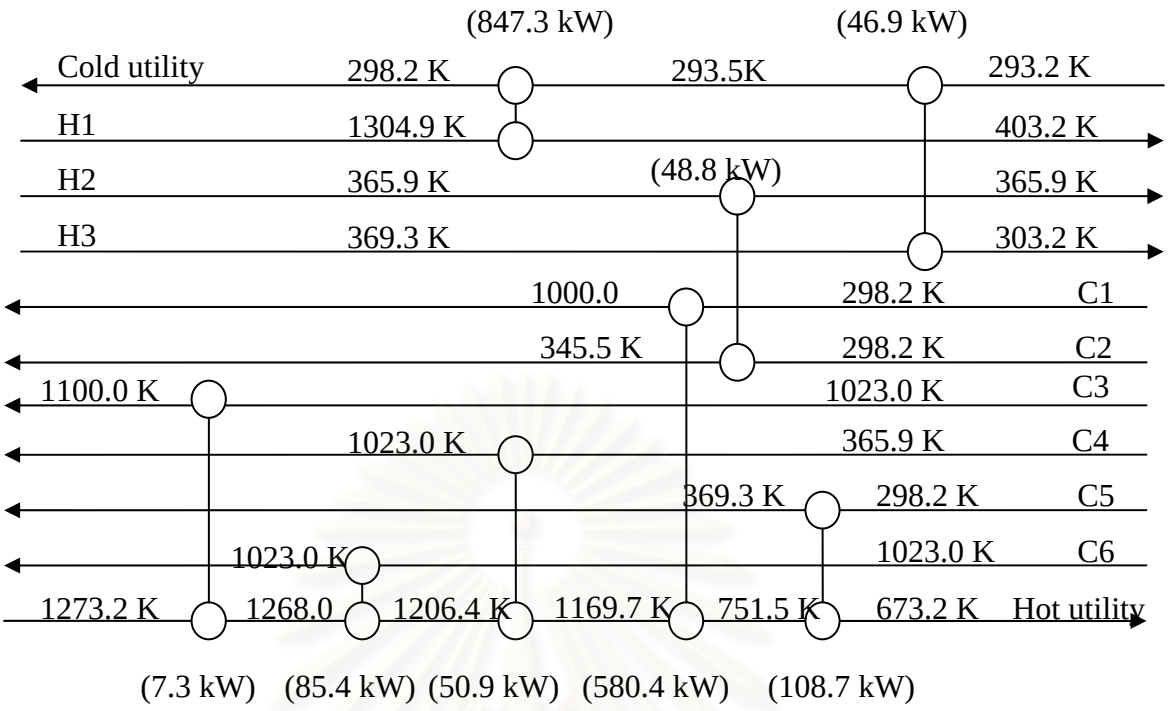

Figure 8.3 Heat exchanger network of SOFC-DIS (CondBio) (C_{EtOH} = 25%, EtOH recovery = 80%, U_f = 80%, V = 0.7 V, T_{SOFC} = 1200 K, $T_{anode,in}$ = 1100 K, $T_{cath,in}$ = 1000 K, T_{RF} = 1023 K and P = 101.3 kPa).

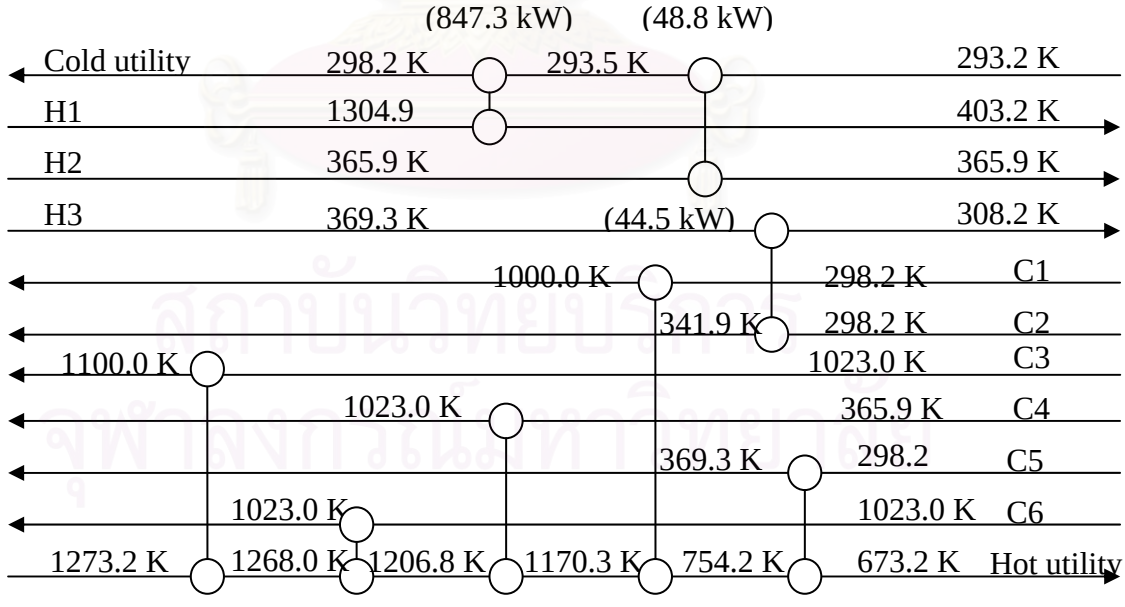

Figure 8.4 Heat exchanger network of SOFC-DIS (HW-Bio) (C_{EtOH} = 25%, EtOH recovery = 80%, U_f = 80%, V = 0.7 V, T_{SOFC} = 1200 K, $T_{anode,in}$ = 1100 K, $T_{cath,in}$ = 1000 K, T_{RF} = 1023 K and P = 101.3 kPa).

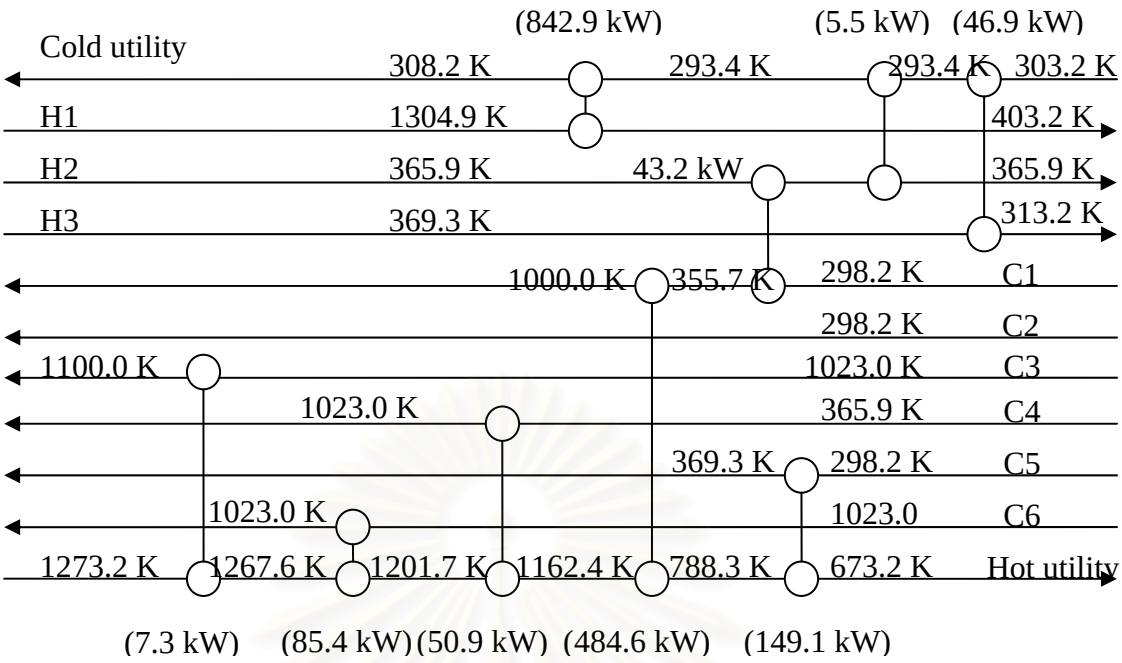

Figure 8.5 Heat exchanger network of SOFC-DIS (Cond-Air) (C_{EtOH} = 25%, EtOH recovery = 80%, U_f = 80%, V = 0.7 V, T_{SOFC} = 1200 K, $T_{anode,in}$ = 1100 K, $T_{cath,in}$ = 1000 K, T_{RF} = 1023 K and P = 101.3 kPa).

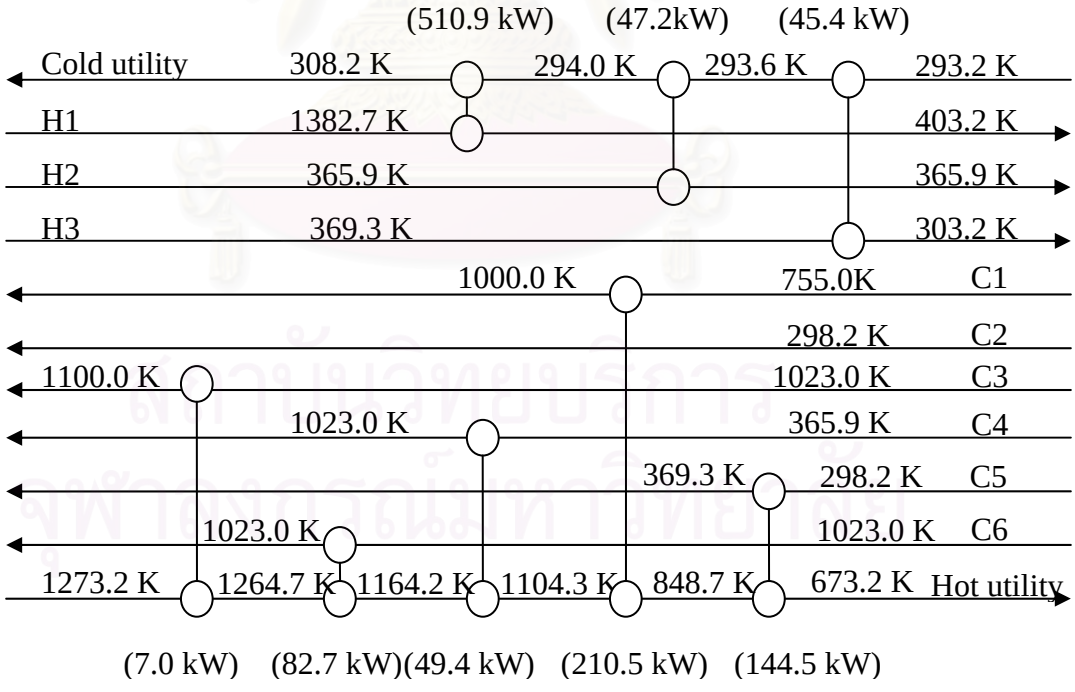

Figure 8.6 Heat exchanger network of SOFC-DIS (CathRec) (C_{EtOH} = 25%, EtOH recovery = 80%, U_f = 80%, V = 0.7 V, T_{SOFC} = 1200 K, $T_{anode,in}$ = 1100 K, $T_{cath,in}$ = 1000 K, T_{RF} = 1023 K and P = 101.3 kPa).

The performances (i.e. overall electrical efficiency, CHP efficiency and total cost index) of all configurations have been summarized in Table 8.2. It should be noted that the total cost index is calculated from the total cost of each configuration divided by the total cost of the base case in which no heat integration is considered. In addition, the total cost is a sum of the operating cost from hot utility and cold utility and capital cost of heat exchangers, heaters and a cooler in the system.

Table 8.2 System performance and total cost index of the SOFC-DIS with different configurations.

	Overall electrical efficiency (%)	CHP efficiency (%)	Total cost index (-)
No HX (base case)	15.79	76.45	1.000
Cond-Bio	16.26	78.73	0.971
HW-Bio	16.21	78.48	0.981
Cond-Air	16.95	81.74	0.946
CathRec	21.67	79.87	0.661
CondBio-CathRec	22.53	74.71	0.643

For preheating bioethanol, both Cond-Bio and HW-Bio are considered. Evidently, it was found that preheating incoming bioethanol can reduce energy consumption at the reboiler. From Table 8.2, the results show that the Cond-Bio yields a slightly higher CHP efficiency and lower total cost index than does the HW-Bio case. Hot water from the bottom of the distillation column yields 46.9 kW for preheating incoming bioethanol in the HW-Bio case. The heat recovery from the condenser (48.8 kW) is fully utilized for preheating bioethanol because the temperature at the condenser remains constant during heat exchange as shown in Figure 8.3. On the other hand, the temperature of the hot water drops while exchanging heat as presented in Figure 8.4. Due to higher overall electrical efficiency, high CHP efficiency and lower total cost index, the Cond-Bio configuration is selected for preheating bioethanol.

To preheat the incoming air, the performance of the Bio-Air and the CathRec configurations were compared. For the CathRec, the SOFC-DIS operates at a split fraction of 0.5 which means that half of the cathode outlet stream is recycled and mixed with fresh air while the rest of cathode stream is fed to the afterburner. It

should be noted that the heat recovery from hot water to preheat incoming air has not been studied because the heat cannot be fully transferred as mentioned earlier in the previous section. From the results, Table 8.2, the CHP efficiency for both the Bio-Air configuration and the CathRec configuration shows similar potential. However, the overall electrical efficiency of the CathRec configuration is 5% higher than that of the Bio-Air. In addition, the total cost index of the CathRec configuration is 28% lower than that of the Bio-Air configuration, therefore, the CathRec configuration is selected to preheat the incoming air. The Bio-Cond and the CathRec configurations are then combined and chosen to be further designed for a process-to-process heat exchanger network. The CHP efficiency and total cost index of Bio-Cond combined with CathRec, the so-called BioCond-CathRec configuration is shown in Table 8.2. The heat exchanger network for the BioCond-CathRec configuration is also presented in Figure 8.7. The design of the process-to-process heat exchanger network of the BioCond-CathRec will be investigated and discussed in the following section.

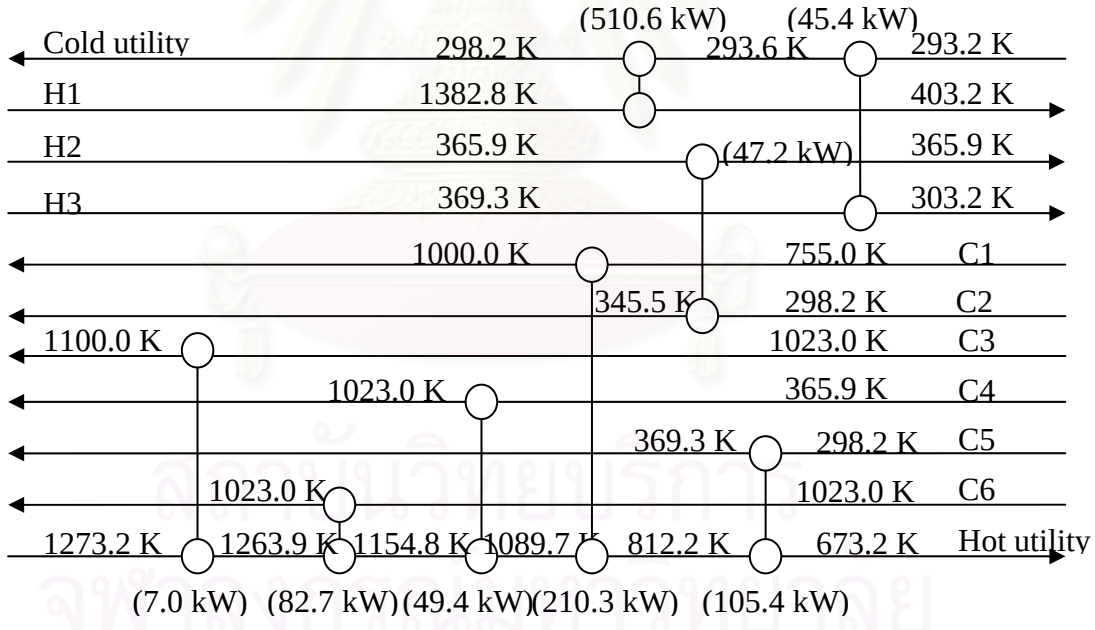

Figure 8.7 Heat exchanger network of SOFC-DIS (CondBio-CathRec) (C_{EtOH} = 25%, EtOH recovery = 80%, U_f = 80%, V = 0.7 V, T_{SOFC} = 1200 K, $T_{anode,in}$ = 1100 K, $T_{cath,in}$ = 1000 K, T_{RF} = 1023 K and P = 101.3 kPa).

8.2.2 Heat Exchanger Network Design

The BioCond-CathRec configuration was chosen as the thermal integration choice for the SOFC-DIS system. The minimum temperature difference for heat exchanging is kept at 10 K and it was assumed that the heat capacity of all streams was constant during heat exchanging process. Cooling water at 293.2 K and fired heat at 1273.2 K were selected as cold and hot utilities respectively.

8.2.2.1 Composite Curves of SOFC-DIS at the Base Condition

The composite curves at the base condition (C_{EtOH} = 25 mol%, EtOH recovery = 80%, U_f = 80%, V = 0.7 V, Sp = 0.5, T_{SOFC} = 1200 K, $T_{cath,in}$ = 1100 K, T_{RF} = 1023 K) is shown in Figure 8.8.

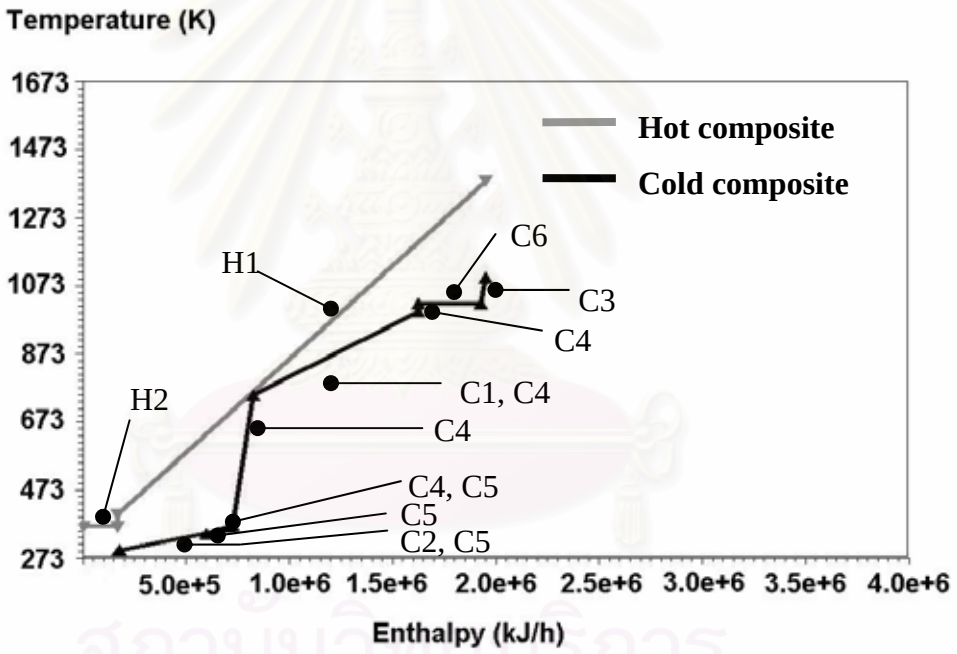

Figure 8.8 Composite curves of SOFC-DIS at base conditions (C_{EtOH} = 25%, EtOH recovery = 80%, U_f = 80%, V = 0.7 V, T_{SOFC} = 1200 K, $T_{anode,in}$ = 1100 K, $T_{cath,in}$ = 1000 K, T_{RF} = 1023 K and P = 101.3 kPa)

No pinch point was detected at this base condition; in other words, the composite curves were adjusted to reduce the hot and cold utilities and the need for a hot utility was eliminated before the curves pinched. The result is that the composite curves at the base condition result in a so-called threshold problem. In this case, no

hot utility is required; the heating and cooling target (Q_{CMin} and Q_{HMin}) are 0 and 55.9 kW, respectively. Figure 8.8 also presents the composite curves with different combinations of hot and cold streams. Obviously, the kink of the composite curves at the base condition occurs on the cold composite curve where the distillate stream (C4) combined with the air stream (C1). The effect of operating conditions on the composite curves and the design of heat exchanger network will be discussed in the following section.

8.2.2.2 Effect of operating conditions on composite curves

The effect of operating conditions (i.e. ethanol recovery, ethanol concentration, fuel utilization, voltage, split fraction, SOFC temperature, cathode inlet temperature) on the composite curves was investigated. The EtOH recovery and C_{EtOH} are in the range of 70-90% and 17-41 mol%, respectively. It should be noted that the maximum ethanol concentration that can be fed to the external reformer without carbon formation is 41 mol% as shown in Chapter VII. In addition, only high ethanol recovery is considered due to high SOFC efficiency. Fuel utilization and voltage were varied from 70-85% and 0.65-0.75 V, respectively and the split fraction was varied from 0.3 to 0.7. The SOFC temperature of 1173 K and the cathode inlet temperature of 1100 K were examined. Figure 8.9 shows the composite curves at these different conditions. Noticeably, it can be seen that the distillation parameters (i.e. ethanol concentration and recovery) does not have significant effect on the composite curves.

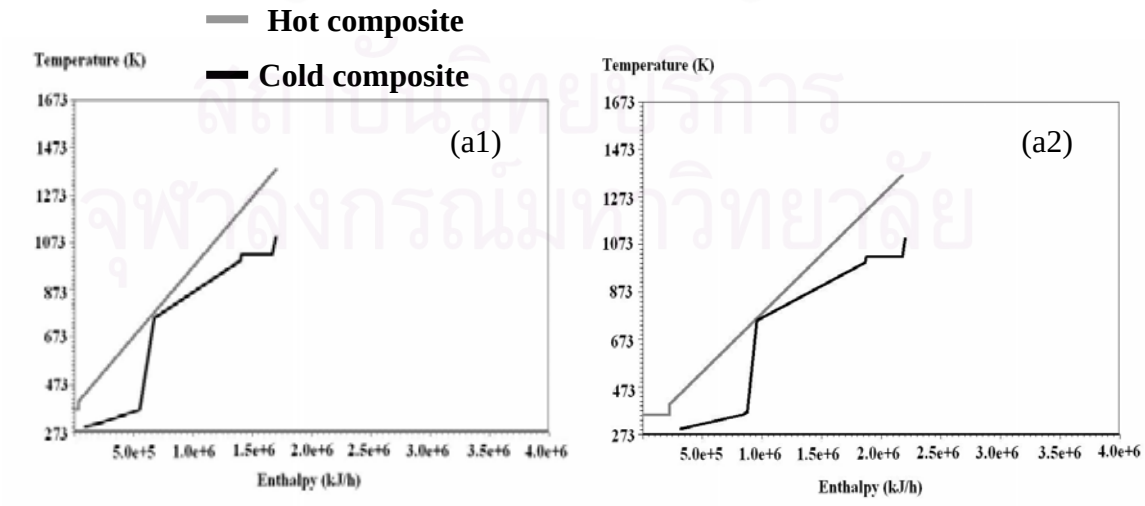

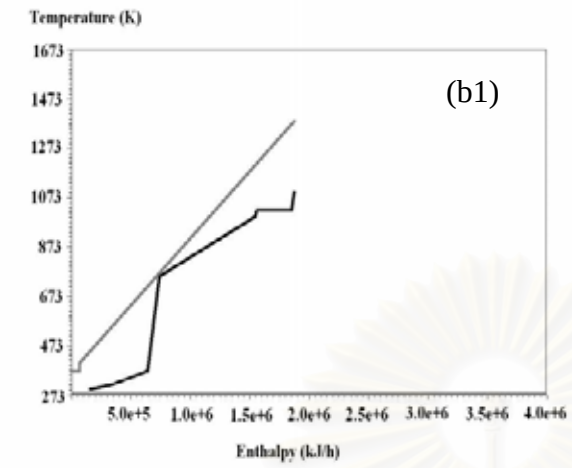
Temperature (K)
1673
1473
1273
1073
873
673
473
273
(b1)
5.0e+5 1.0e+6 1.5e+6 2.0e+6 2.5e+6 3.0e+6 3.5e+6 4.0e+6
Enthalpy (kJ/h)

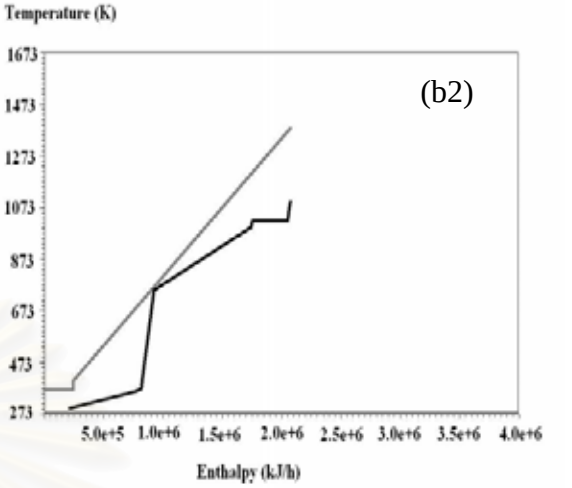
Temperature (K)
1673
1473
1273
1073
873
673
473
273
(b2)
5.0e+5 1.0e+6 1.5e+6 2.0e+6 2.5e+6 3.0e+6 3.5e+6 4.0e+6
Enthalpy (kJ/h)

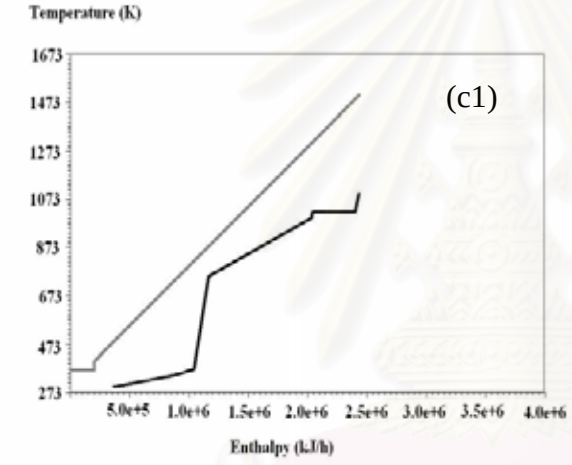
Temperature (K)
1673
1473
1273
1073
873
673
473
273
(c1)
5.0e+5 1.0e+6 1.5e+6 2.0e+6 2.5e+6 3.0e+6 3.5e+6 4.0e+6
Enthalpy (kJ/h)

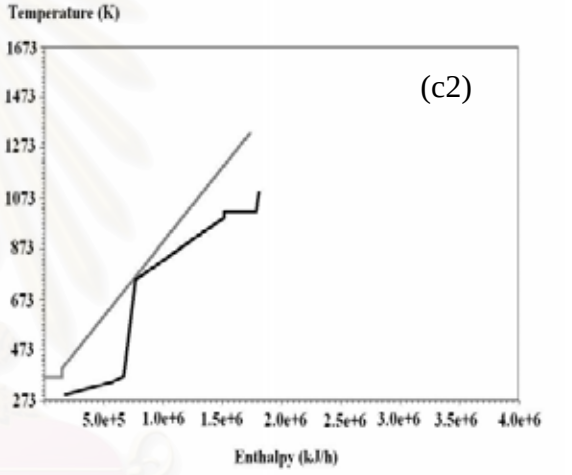
Temperature (K)
1673
1473
1273
1073
873
673
473
273
(c2)
5.0e+5 1.0e+6 1.5e+6 2.0e+6 2.5e+6 3.0e+6 3.5e+6 4.0e+6
Enthalpy (kJ/h)

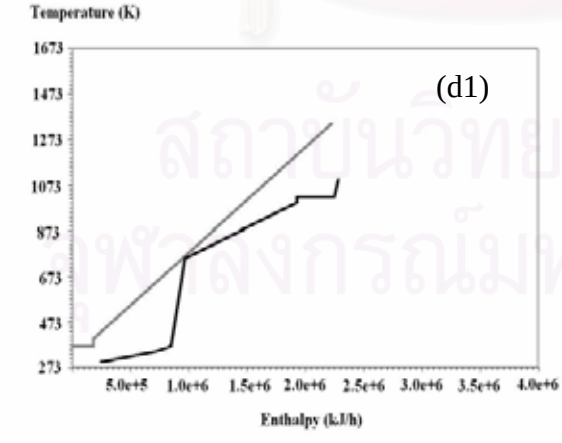
Temperature (K)
1673
1473
1273
1073
873
673
473
273
(d1)
5.0e+5 1.0e+6 1.5e+6 2.0e+6 2.5e+6 3.0e+6 3.5e+6 4.0e+6
Enthalpy (kJ/h)

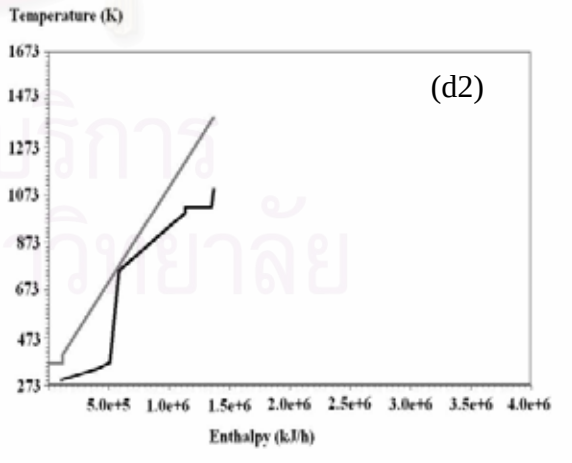
Temperature (K)
1673
1473
1273
1073
873
673
473
273
(d2)
5.0e+5 1.0e+6 1.5e+6 2.0e+6 2.5e+6 3.0e+6 3.5e+6 4.0e+6
Enthalpy (kJ/h)

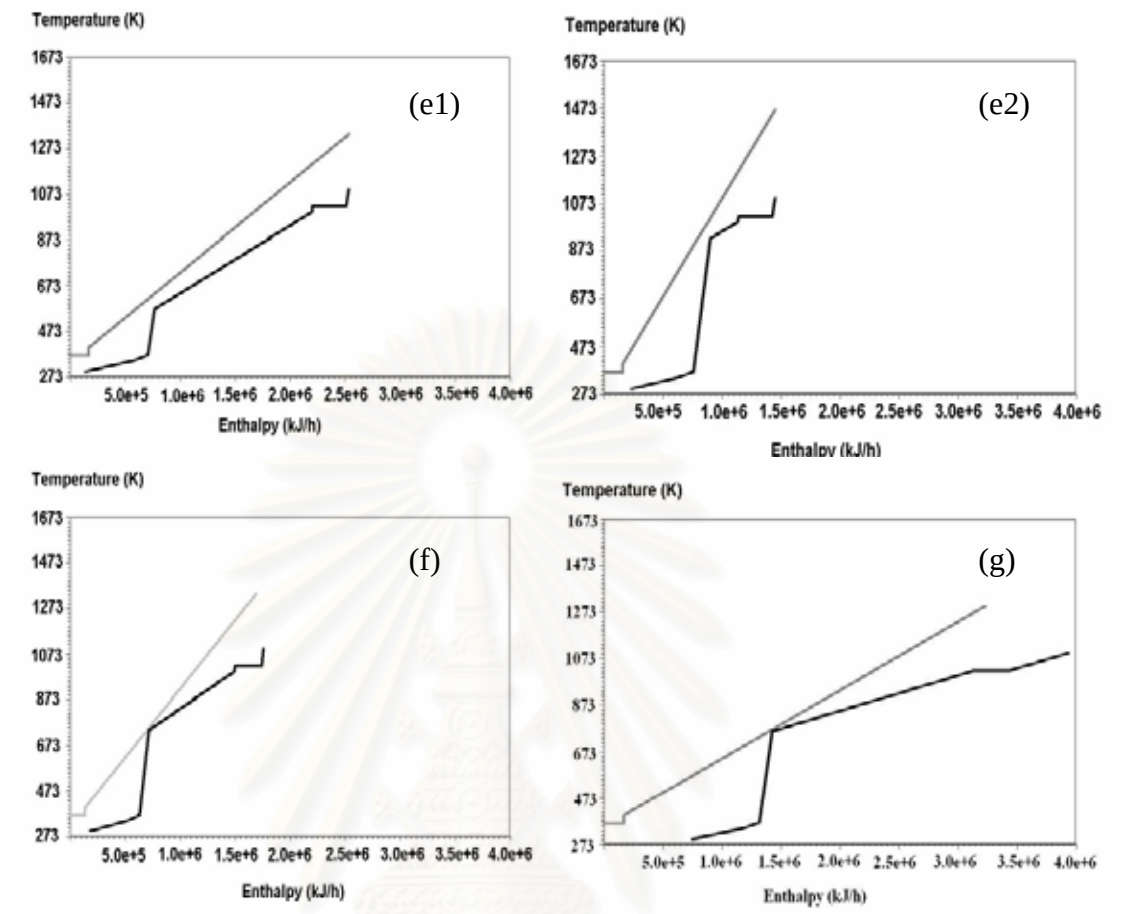

Figure 8.9 Composite curves of SOFC-DIS at different operating conditions: (a1) C_{EtOH}, = 17 mol%, (a2) C_{EtOH}, = 41 mol%, (b1) EtOH recovery = 70%, (b2) EtOH recovery = 90%, (c1) V = 0.65 V, (c2) V = 0.75 V, (d1) U_f = 75%, (d2) U_f = 85%, (e1) Sp = 0.3, (e2) Sp = 0.7, (f) T_{SOFC} = 1173 K, (g) $T_{cath,in}$ = 1100 K.

For SOFC operating conditions, voltage, fuel utilization and split fraction have a strong effect on the composite curves. For the effect of voltage, the higher voltage, the steeper the composite curves. This can be explained that the lower voltage relates to higher amount of heat loss within the SOFC stack. Therefore, to maintain the temperature inside the stack, more air is required, resulting in lower outlet temperature from the afterburner and higher heat capacity of hot stream. It should be noted that the slope of composite curve is inverse with heat capacity of the streams. Hence, the less steep the slope of the hot composite curve is obtained. Moreover, because more air is required for cooling the stack, more heat is needed at the air heater and results in less steep slope of the cold composite curve as illustrated in

Figure 8.9(c1). In addition, for a lower U_f, more unreacted fuel is burnt in the afterburner, resulting in a higher outlet temperature of the hot flue gas and more heat recovered from the afterburner as shown in Figure 8.9(d1). Consequently, the cold composite curve moves horizontally toward the hot composite curve until it reaches the threshold case in which no hot utility is required. For the higher U_f (in this case, U_f = 85%), the lower temperature of the hot flue gas is obtained. The cold composite curve moves horizontally to the hot composite curve and reaches the pinch point before it meets the threshold condition.

The effect of split fraction was investigated. At low split fractions, a lower amount of high temperature air from the cathode is mixed with the fresh air; therefore, lower air inlet temperature and more energy is consumed in the air heater. Consequently, the slope of the cold stream, especially that of the air heater, decreases and the location of the kink on the cold stream changes. Noticeably, the outlet temperature of hot flue gas from the afterburner is lower because more air, heat carrier, is burnt inside the afterburner. The less steep hot stream can be detected due to higher amount of air in the hot flue gas stream. Higher split fractions result in a larger amount of air to be mixed with the fresh air. A higher air inlet temperature and the lower energy consumption at the air heater were observed. However, when the amount of air fed to the afterburner is reduced, the outlet temperature of the hot stream is higher. In addition, lower amount of air in the hot flue gas results in a steeper slope of the hot stream.

From the results, the composite curves can be divided into two groups: 1) the pinch problem and 2) the threshold problem. For the pinch case, the conditions that are found to cause a pinch point in the composite curves are: C_{EtOH} of 41 mol%, operating voltage of 0.65 V, cathode inlet temperature of 1100 K, SOFC temperature of 1173 K and U_f of 85%. Other conditions resulted in the threshold case. The base condition and T_{SOFC} of 1173 K were chosen to be representatives for the threshold case and the pinch case, respectively.

8.2.2.3 Pinch Problem

For the pinch problem, T_{SOFC} of 1173 K was chosen as for designing the heat exchanger network. From Figure 8.9(f), the composite curve shows the pinch point at 743.0 K which is related to the air inlet temperature. It can be noticed that all the pinch problems have the pinch point at the air inlet temperature. To design a MER

(Maximum Energy Recovery) network, it is necessary to design the heat exchanger network above and below the pinch point separately. The following rules for the MER design are required (Linnhoff et al., User Guide on Process Integration for the Efficient Use of Energy, 1982, 1st edition, Institution of Chemical Engineering, UK).

- No use of cold utility above the pinch point
- No use of hot utility below the pinch point.
- No heat transfer across the pinch point.

Since the minimum temperature difference for high temperature processes was selected to be 10 K, the high temperature pinch point was 753.0 K and the lower pinch temperature is 743.0 K. The heat capacity (MC_p) of each stream for an SOFC temperature of 1173 K are presented in Table 8.3. Overally, there are two hot streams (a hot flue gas from the afterburner (H1) and heat recovery from the condenser (H2)) and six cold streams (i.e. a syngas stream (C3), a reformer (C6), a distillate stream (C4), an air stream (C1), a reboiler (C5) and a bioethanol inlet (C2)). However, it should be noted that the heat recovery from the condenser has to be matched with the bioethanol inlet as the CondBio is selected for preheating the incoming bioethanol. For the design above pinch, the MC_p of the hot stream has to be lower than the cold stream near the pinch point in order to avoid the temperature crossover (Linnhoff et al., User Guide on Process Integration for the Efficient Use of Energy, 1982, 1st edition, Institution of Chemical Engineering, UK). The possible cold streams that can be matched with the hot stream near the pinch point are the reformer and the air stream. However, when the reformer is the last unit which is near the pinch point, the hot flue gas cannot supply heat to the reformer due to low inlet temperature for heat exchange. Consequently, the hot flue gas cannot be cooled down to the pinch temperature using process streams. Cold utility is required above the pinch and this violates the rule for MER design. Therefore, the only configuration which ends with the air heat exchanger is considered for the above-pinch design. Below the pinch, one hot stream and two cold streams (i.e. a distillate stream (C4) and a reboiler (C5) are considered. It is known that the MC_p of the hot stream must be higher than that of the cold stream near the low temperature pinch point (Linnhoff et al., User Guide on Process Integration for the Efficient Use of Energy, 1982, 1st edition, Institution of

Chemical Engineering, UK). From Table 8.3, only the MC_p of the distillate is higher than that of the hot flue gas. Therefore, only one match is possible. The hot stream has to exchange heat with the distillate and then with the reboiler.

Table 8.3 Information of each unit operated under pinch problem.

	Stream Label	T_{in} (K)	T_{out} (K)	Load (kW)	MC_p (kW/K)
Hot stream					
Cooler-1	H1	1331.6	403.0	455.5	0.486
Condenser	H2	365.9	365.9	38.6	Large
Cold stream					
Air stream	C1	742.1	1000.0	214.5	0.832
BioEtOH stream	C2	298.2	345.5	48.4	1.023
Syngas stream	C3	1023.0	1100.0	5.7	0.074
Distillate stream	C4	365.9	1023.0	40.3	0.061
Reboiler	C5	298.2	369.4	86.1	1.209
Reformer	C6	1023.0	1023.0	67.6	Large

From these preliminary considerations, there are six possible MER designs, D1 through D6, for the pinch case. The sequences of heat exchanging for MER designs are listed as follows. The first stream label is the first cold stream to be heat exchanged with hot stream and so on.

- D1: C3-C4-C6-C1-C4-C5
- D2: C3-C6-C4-C1-C4-C5
- D3: C4-C3-C6-C1-C4-C5
- D4: C4-C6-C3-C1-C4-C5
- D5: C6-C3-C4-C1-C4-C5
- D6: C6-C4-C3-C1-C4-C5

The total cost index of all six designs is presented in Table 8.4. All six MER designs have the target energy of 21.2 and 62.5 kW for hot utility and cold utility, respectively.

Table 8.4 Total cost index for different designs.

	Total cost index (-)	
Configuration	Pinch case*	Threshold case**
No-HX CondBio-CathRec (base case)	1.0000	1.000
D1 (C3-C4-C6-C1-C4-C5)	0.4033	0.3431
D2 C3-C6-C4-C1-C4-C5)	**0.4030**	**0.3428**
D3 C4-C3-C6-C1-C4-C5)	0.4033	0.3431
D4 (C4-C6-C3-C1-C4-C5)	0.4039	0.3437
D5 (C6-C3-C4-C1-DC4-C5)	0.4033	0.3431
D6 (C6-C4-C3-C1-C4-C5)	0.4036	0.3434

Remark *: Operate at T_{SOFC} = 1173 K and the rest operating parameters are the same as that of base condition.

**: Operate at the base condition (C_{EtOH} = 25%, EtOH recovery = 80%, U_f = 80%, V = 0.7 V, T_{SOFC} = 1200 K, $T_{anode,in}$ = 1100 K, T_{RF} = 1023 K and P = 101.3 kPa).

From the results, it can be seen that the total cost index for all six designs are similar but Design D2: C3-C6-C4-C1-C4-C5, presented in Figure 8.10 shows the lowest total cost index among other designs and is then chosen for a further design. In this case, the total cost index is based on the total cost of No-HX case. It should be noted that although all six MER configurations (D1-D6) yields the lowest energy cost, the configurations are somewhat complex from operability point of view. One should the trade-off between annualised cost and complexity; one maybe able to simplify the design; however, it will no longer be an MER design and will cost more. It can be noticed that there is a loop of heat exchanger network E3-E5-E5-E3 as shown in the dark line in Figure 8.10. Two heat exchanges are present on the distillate stream for heating up to the target temperature, one high temperature heat exchanger (E3) and one low temperature heat exchanger (E5) as shown in Figure 8.10. This increases the complexity of the design and; therefore, results in operability difficulties. In an attempt to simplify the network we removed one of the heat exchangers on the distillate stream; however, it is not obvious which ones of the distillate heat exchangers (E3 or E5) should be eliminated.

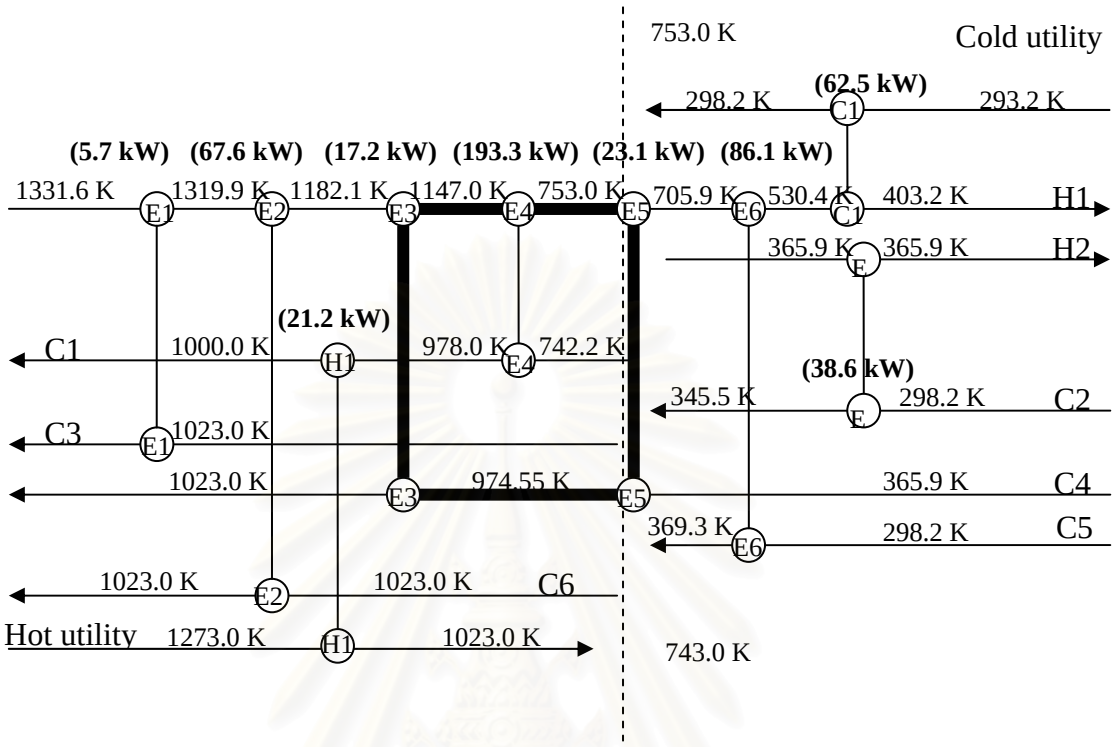

Figure 8.10 MER design of SOFC-DIS (CondBio-CathRec) (C_{EtOH} = 25 mol%, EtOH recovery = 80%, U_f = 80%, V = 0.7 V, T_{SOFC} = 1173 K, $T_{anode,in}$ = 1100 K, $T_{cath,in}$ = 1000 K, T_{RF} = 1023 K and P = 101.3 kPa).

Table 8.5 shows the operating cost index, capital cost index and total cost index for different cases. In this section, the total cost index for pinch cases can be calculated by the ratio of total cost of each design to the total cost of the MER design, in this case, at $T_{SOF\ C}$= 1173K. The total costs index follow the sequence of C3-C6-C1-C4-C5 (1173 K-no E3 case) < C3-C6-C4-C1-C5 (1173 K-no E5 case) < MER case. Generally, eliminating a heat exchanger reduces capital costs but increases operating cost as shown in Table 8.5. The operating cost index of the case 1173 K-no E3 case is much lower than that of the case 1173K-no E5 case because large amount of heating utility is required to heat up air stream to meet the target temperature for the case of 1173K-no E5. However, the 1173-no E3 case requires two heaters to heat up both distillate stream and air stream and results in higher capital cost index but still lower than that of the MER case.

The benefit of eliminating path of utility is also investigated. As shown in Figure 8.11, there is a path connecting the cold and hot utilities via the distillate heater shown by the dark line. The total cost index of the case of no path (1173 K-no E3- no path) and the 1173 K-no E3 are compared and presented in Table 8.5. It was found that the total cost index of the case without path way is 5.6% lower than that of the 1173 K-no E3. However, the operating cost in the case without path is almost twice higher than that of with path; one should consider the effect of increases in the fuel price.

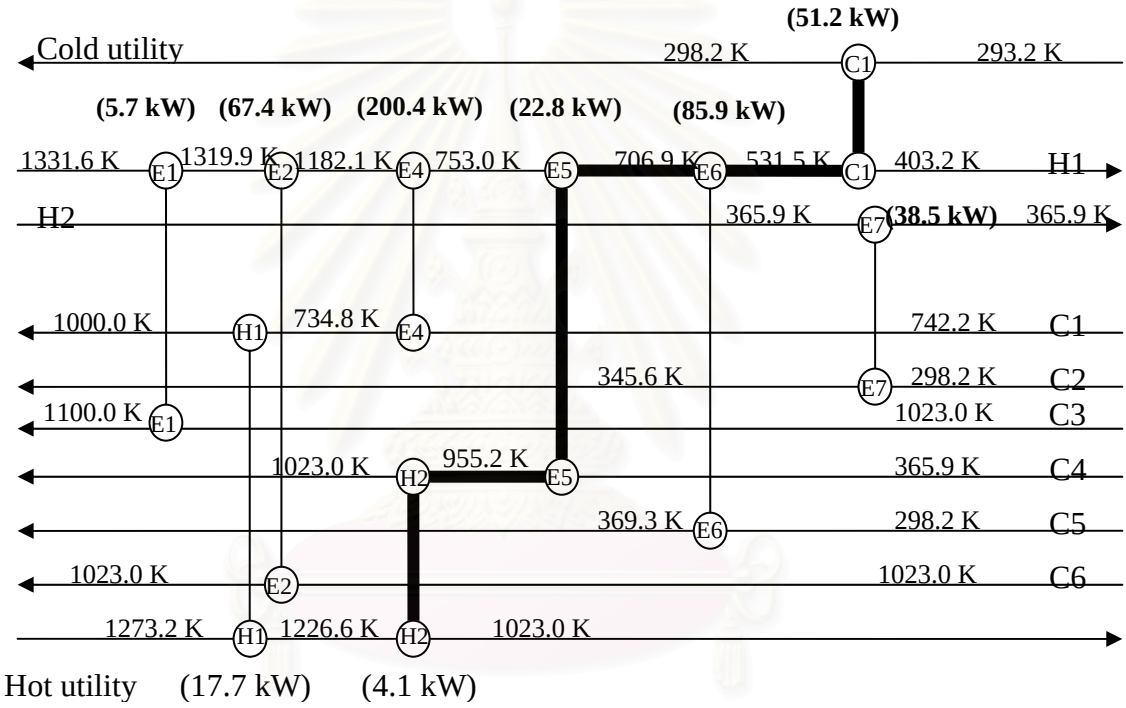

Figure 8.11 The design of SOFC-DIS (CondBio-CathRec) for the 1173K- no E3 case (C_{EtOH} = 25%, EtOH recovery = 80%, U_f = 80%, V = 0.7 V, T_{SOFC} = 1173 K, $T_{anode,in}$ = 1100 K, $T_{cath,in}$ = 1000 K, T_{RF} = 1023 K and P = 101.3 kPa).

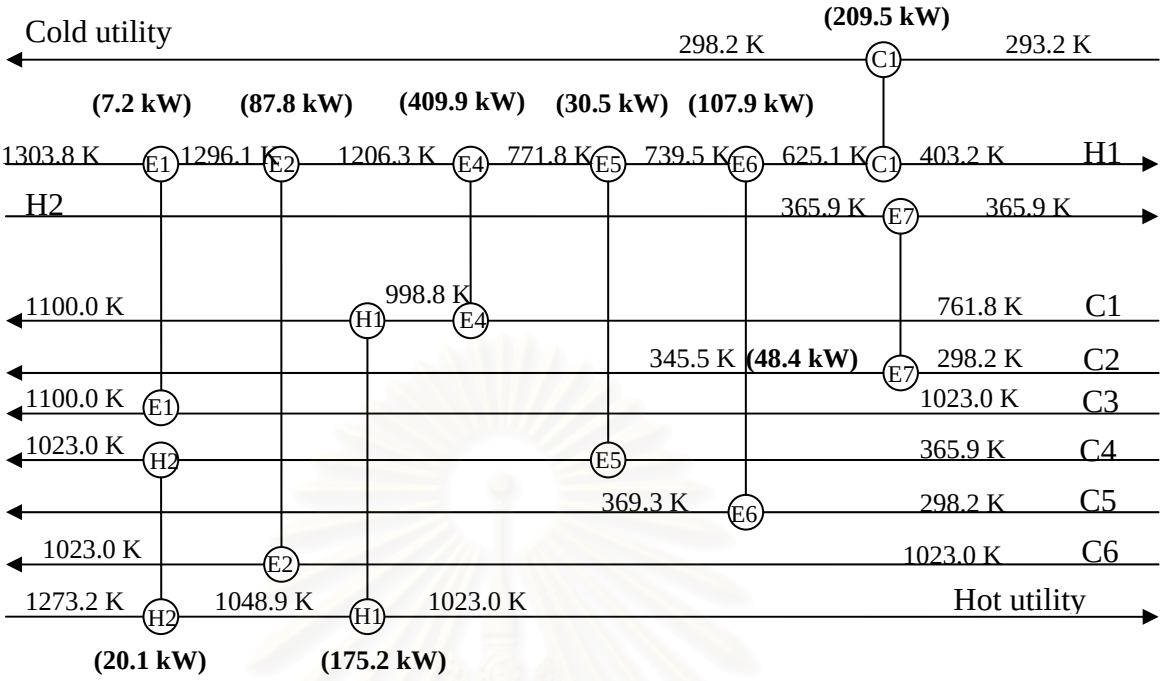

Figure 8.12 The design of SOFC-DIS (CondBio-CathRec) for the $T_{cath,in}$ = 1100 K- no E3 case (C_{EtOH} = 25%, EtOH recovery = 80%, U_f = 80%, V = 0.7 V, T_{SOFC} = 1200 K, $T_{anode,in}$ = 1100 K, T_{RF} = 1023 K and P = 101.3 kPa).

It is recommended that the 1173 K-no E3 is preferable due to lower total cost index; however, two heaters have to be located after the distillate heat exchanger and the air heat exchanger. The corresponding performances of this design are 40.00 %, 51.74 % and 0.181 W cm^{-2} for overall electrical efficiency, CHP efficiency and power density, respectively. The heat exchanger network for $T_{cath,in}$ =1100 K is also presented in Figure 8.12. Similarly, two heaters are required to heat up the air stream and distillate stream to the target temperatures. Implementing two heaters to the heat exchanger network is good for flexibility of operation when operating in wide range of operating conditions.

Table 8.5 Cost estimation of the SOFC-DIS of different scenarios.

	Operating cost index (-)	Capital cost index (-)	Total cost index (-)
Pinch problem			
1173K-MER	1.000	1.000	1.000
1173K-no E3	1.022	0.989	0.992
1173K-no E5	1.997	0.912	0.994
1173K-E3-no path	1.823	0.895	0.966
1100K-MER	1.000	1.000	1.000
1100K-no E3	1.000	0.991	0.994
1100K-no E5	1.155	0.920	1.005
Threshold problem			
Base condition	1.000	1.000	1.000
Base no E3	7.381	0.930	0.996
Base no E5	11.31	1.018	1.124
Base no E3-no path	19.55	0.826	1.020
Avoiding pinch			
1173K-MER	1.000	1.000	1.000
1173K-Uf75	0.240	0.769	0.729
1173K-sp0.3	0.051	0.978	0.907
1173K-sp0.7	0.161	0.758	0.713

8.2.2.4 Threshold Case

The composite curves of the threshold case look similar to those of the pinch case, however, $\Delta T > \Delta T_{min}$. The narrowest gap, ΔT, is the so-called pseudo-pinch and the design is governed by this point. The design of the threshold case follows the same rules as that of the pinch case. Due to the similar composite curves to the pinch case, the same six possible MER designs are available. The cost index of different designs is summarized in Table 8.4. It should be noted that the total cost index for threshold case is based on the total cost of No-HX case. Likewise, the C3-C6-C4-C1-

C4-C5 configuration shown in Figure 8.13 also results in the lowest total cost index compared to other designs.

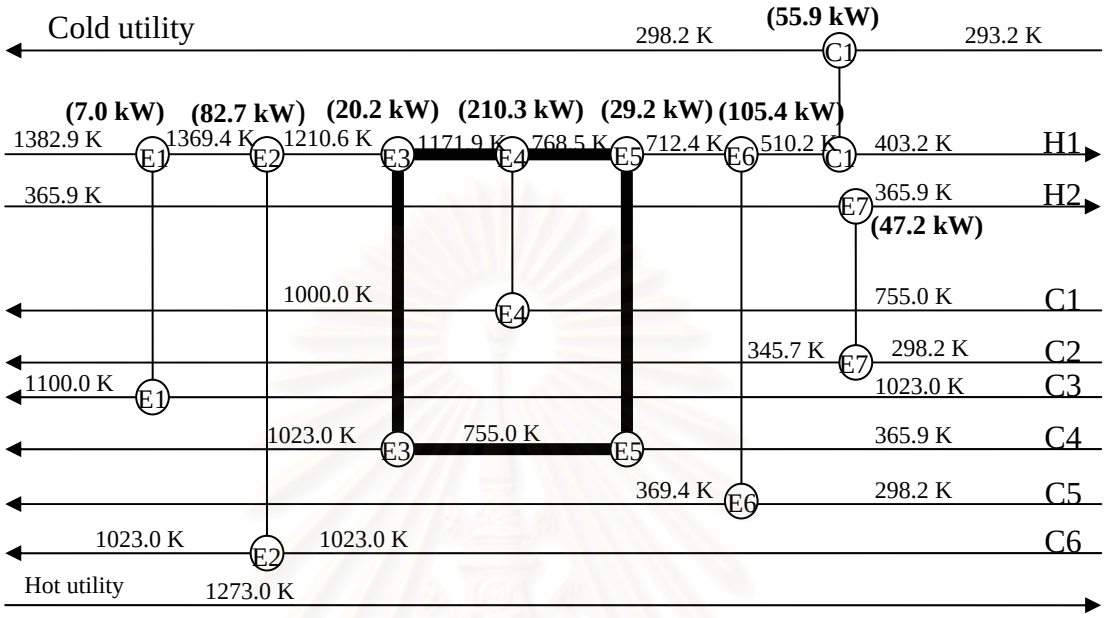

Figure 8.13 The MER design of SOFC-DIS (CondBio-CathRec) at the base condition (C_{EtOH} = 25%, EtOH recovery = 80%, U_f = 80%, V = 0.7 V, T_{SOFC} = 1200 K, $T_{anode,in}$ = 1100 K, T_{RF} = 1023 K and P = 101.3 kPa).

Two distillate heat exchangers are required for the MER design. The pseudo-pinch design and their improvement by eliminating a heat exchanger loop and heat exchanger path way are also considered and their cost indexes are presented in Table 8.5. The C3-C6-C1-C4-C5 yields the lowest cost among other designs. The C3-C6-C1-C4-C5 is, therefore, more preferable. One distillate heater has to be added. The performances of SOFC-DIS with this configuration at the base condition are 40.8 %, 54.3 %, 0.221 W cm^{-2} for overall electrical efficiency, CHP efficiency and power density, respectively.

8.2.2.5 Avoiding a Pinch Point by Operating at Different Conditions

As mentioned earlier, the pinch point was found when operating at C_{EtOH} = 41 mol%, T_{SOFC} = 1173 K or $T_{cath,in}$ = 1100 K, U_f = 85% and V = 0.65 V. It can be noticed

that the pinch point occurs at the air inlet temperature. Therefore, we investigated the effect of the SOFC-DIS operating conditions on the pinch point. As shown in Figure 8.9, the shape of composite curves changes dramatically when U_f, split fraction or voltage change. In this case, only split fraction and fuel utilization are considered. It should be noted that adjusting voltage is not considered in this study because it directly affects the SOFC stack performance. In addition, lower split fraction, higher split fraction and lower fuel utilization are examined. As mentioned in the preceding section, lower split fraction reduces the slope of the cold stream and the kink at the air heater occurs at a lower temperature; this could eliminate the pinch point. For higher split fractions, steeper hot composite curves could also help avoiding the pinch point as shown in the wider gap between the hot and cold composite curves in Figure 8.9(e). Lastly, operating at lower fuel utilization can make the hot composite curve have higher outlet temperature and probably affect the gap between the composite curves.

For T_{SOFC} = 1173 K, the results show that when the SOFC-DIS operates at a higher split ratio (Sp = 0.7) or lower value (Sp = 0.3) or lower U_f = 75%, the pinch point disappears and we have a threshold problem. At U_f = 85%, operating SOFC-DIS at Sp = 0.7 or Sp = 0.3 the pinch point disappears. The total cost index of the pinch case and the threshold case are compared and shown in Table 8.5. In this case, the total cost index is based on the total cost of T_{SOFC}=1173 MER case. When the SOFC-DIS is operated at threshold conditions, lower total cost index is obtained for all cases. The total cost index are in the sequence of 1173 K-Sp=0.7 < 1173 K-U_f = 75% < 1173K-Sp=0.3. However, it should be noted that for $T_{cath,in}$ = 1100 K case, operating at higher or lower split fractions or even lower U_f cannot shift the pinch point.

8.3 Conclusion

The performance of a thermally integrated SOFC system integrated with a distillation column (SOFC-DIS) was presented in this chapter. The implementation of cathode recirculation and the utilization of other useful heat in the SOFC-DIS system (i.e. condenser duty and hot water from the bottom of the column) to preheat the incoming air/bioethanol were considered to enhance the performance of the SOFC-DIS system. It was found that a utilization of condenser duty to preheat an incoming bioethanol and a cathode recirculation significantly helped reducing an energy demand for the reboiler and the air heater, respectively. The SOFC-DIS with an implementation of a cathode recirculation and a utilization of condenser duty for

heating bioethanol was selected for designing a heat exchanger network. The hot effluent from the afterburner was designed to provide heat to other equipments in the system (i.e. an anode preheater, a distillate downstream heater, an external reformer, an air heater and a reboiler of the distillation column). The sequence of heat exchanging for five-unit operations (i.e. an anode preheater, a distillate downstream heater, an air heater, an external reformer and a reboiler) in the SOFC-DIS was examined. The results were found that no pinch point occurs except for C_{EtOH} = 41 mol% or the cathode inlet temperature of 1100 K or T_{SOFC} = 1173 K or U_f = 85%. The designs for the threshold case and the pinch problems were also discussed. It was found that the composite curves for the threshold case were similar to the pinch case. The kink or the narrowest space occurred at the air inlet temperature, and the similar configuration was obtained. Six possible MER designs are possible for SOFC-DIS. Among these, C3-C6-C4-C1-C4-C5 showed the lowest total cost index for both pinch and threshold case. Moreover, it was found that the high temperature distillate heat exchanger before heat exchanging with the air heat exchanger should be eliminated so that the complexity of MER design is avoided. Therefore, the C3-C6-C1-C4-C5 configuration was recommended for both pinch and threshold cases. One distillate heater and one air heater have to be implemented to the network for T_{SOFC} = 1173K whereas one distillate heater is enough for the base condition. The corresponding performances of the pinch case at 1173 K were 40.00 %, 51.74 % and 0.181 W cm^{-2} for overall electrical efficiency, CHP efficiency and power density, respectively while 40.8 %, 54.3 %, 0.221 W cm^{-2} were obtained for overall electrical efficiency, CHP efficiency and power density in the threshold case (at the base condition). Lastly, the performance of the SOFC-DIS at pinch conditions was compared with the SOFC-DIS at threshold conditions (no pinch). The results showed that operating at lower/ higher split fraction or lower fuel utilization can shift the pinch point and result in a threshold problem except at $T_{cath,in}$ = 1100 K. The performance of the SOFC-DIS at threshold conditions resulted in lower total costs index compared to the pinch cases. This information will be useful in choosing the heat exchanger network for the SOFC-DIS. With its flexibility, it was recommended that C3-C6-C1-C4-C5 with one air heater and one distillate heater should be chosen for further studies.

CHAPTER IX

CONCLUSIONS AND RECOMMENDATIONS

9.1 Conclusions

Simulation of solid oxide fuel cell (SOFC) system fuelled by ethanol was studied in this research. The study begins with the theoretical performance of direct internal reforming SOFC (SOFC-DIR) with different types of electrolyte (i.e. proton-conducting electrolyte, SOFC-H^+, and oxygen ion- conducting electrolyte, SOFC-O^{2-}). The effect of feeding pattern (i.e. co- and counter-current) and mode of operation (i.e. well-mixed and plug flow) was also examined. The performance of different types of electrolyte was compared at their best conditions. In the case of SOFC-O^{2-}, their best performance was found at the boundary of carbon formation where the inlet steam was least required to prevent carbon formation. In contrast, SOFC-H^+ was highest at the optimal inlet steam to ethanol ratio. The effect of mode of operation on their best performances was also investigated. Because different mode of operation affected the composition inside the SOFC stack, average EMF and their best performances were influenced. However, different feeding pattern (i.e. co- and counter-current) does not have a strong effect on their best performance although the distribution is different. The performance at their best conditions can be ordered in the sequence: SOFC-H^+(PF-Co) ≈ SOFC-H^+(PF-CC) > SOFC-O^{2-}(PF-Co) ≈ SOFC-O^{2-}(PF-CC) > SOFC-H^+(WM) > SOFC-O^{2-}(WM). Conclusively, operating SOFC under plug flow mode yielded the higher efficiency. Moreover, at the same mode of operation, SOFC-H^+ is theoretically superior to SOFC-O^{2-}.

The actual performance of SOFC with different types of electrolyte was studied. Losses (i.e. activation loss and ohmic loss) were included in performance calculation. Unlike theoretical performance, the actual performance of SOFC-H^+ is much lower although the inlet steam to ethanol ratio at their best performance is considered. This is because the total resistance of proton conductor is 45.6 times that of oxygen ion conductor. To yield the competitive performance as SOFC-O^{2-}, both ohmic and other resistance (activation and contact loss) should be simultaneously reduced. The match between resistivity and thickness of electrolyte for each value of other resistance was determined.

The SOFC-O^{2-} was chosen to further investigate SOFC system. The integration of a distillation column to the SOFC system fuelled by bioethanol (SOFC-DIS) was proposed in order to save distillation energy in the conventional ethanol-fed SOFC system which fed pure ethanol and then mixed with water. The SOFC-DIS system consists of an SOFC stack, an external reformer, heaters and a distillation column. The exothermic heat from SOFC system provided heat to other parts of the system, i.e., heaters, a reformer and a reboiler of the distillation column. It was found that the SOFC-DIS can operate without supplying heat from an external heat source when operating at suitable fuel utilization and operating voltage.

The system configuration and the design of heat exchanger network of SOFC-DIS system were finally examined. Some alternatives for developing system configuration were compared. The utilization of heat from condenser duty to preheat incoming bioethanol and the implementation of cathode recirculation were found to be the most efficient and yield the lowest total cost index. It was found that a pinch point was found in some operating conditions, i.e., 41 mol% C_{EtOH} or V = 0.65V or $T_{cath,in}$ = 1100 K or T_{SOFC} = 1173 K. The composite curve of all studied operating conditions can be divided into two groups: pinch case and threshold case. The design of these two different cases obtained the same heat exchanger network due to its similarity shape. It was recommended that the hot effluent gas from the afterburner should be heat exchanged with an anode heat exchanger first, then a reformer, an air heat exchanger, a distillate heat exchanger and a reboiler, respectively. Some heaters (i.e. an air heater and a distillate heater) were needed in the system.

9.2 Recommendations for Future Work

a) In this study, the ethanol reforming was assumed to be at its thermodynamic equilibrium. The calculation will be more accurate if kinetic expressions are obtained.

b) A distillation unit was integrated to the SOFC system in order to purify bioethanol before feeding to the system. Another ethanol purification alternative with moderate energy consumption such as pervaporation is recommended for future study. Although implementing a membrane to the system can save more energy, the additional electrical power is required for pumping bioethanol to permeate through the membrane. The performance of SOFC system integrated with membrane

purification unit should be further concerned.

c) From this study, the obtained heat exchanger network yielded the lowest total cost index in the sense of least complexity. However, another alternative to achieve higher performance or lower cost is to optimize process conditions. Economics aspects for the bioethanol-fuelled SOFC system should be further investigated in order to yield higher performance and lower cost of electricity.

REFERENCES

Achenbach E., Three-dimensional and time-dependent simulation of a planar solid oxide fuel cell stack. J. Power Sources 49 (1994): 333-348.

Aguiar P., Adjiman C.S. & Brandon N.P., Anode-supported intermediate temperature direct internal reforming solid oxide fuel cell. I: model-based steady-state performance. J. Power Sources 138 (2004): 120-136.

Aguiar P., Adjiman C.S. & Brandon N.P., Anode-supported intermediate-temperature direct internal reforming solid oxide fuel cell: II. Model-based dynamic performance and control. J. Power Sources 147 (2005): 136-147.

Aguiar P., Chadwick D. & Kershenbaum L., Modelling of an indirect internal reforming solid oxide fuel cell. Chem. Eng. Sci. 57 (2002): 1665-1677.

Assabumrungrat S., Laosiripojana N., Pavarajarn V., Sangtongkitcharoen W., A. Tangjitmatee & P. Praserthdam, Thermodynamic analysis of carbon formation in a solid oxide fuel cell with a direct internal reformer fuelled by methanol. J. Power Sources 139 (2005): 55.

Assabumrungrat S., Pavarajarn V., Charojrochkul S., & Laosiripojana N., Thermodynamic analysis for solid oxide fuel cell with direct internal reforming fueled by ethanol. Chem. Eng. Sci. 59 (2004): 6015-6020.

Assabumrungrat S., Sangtongkitcharoen W., Laosiripojana N., Arpornwichanop A., Charojrochkul S. & Praserthdam P., Effect of electrolyte type and flow pattern on performance of methanol-fuelled solid oxide fuel cells. J. Power Sources (2005): 18-23.

Alzate C. A. C.& Toro O. J. S., Energy consumption analysis of integrated flowsheets for production of fuel ethanol from lignocellulosic biomass. Energy 31 (2006): 2447-2459.

Badwal S.P.S & Foger K., Solid Oxide Electrolyte Fuel Cell Review, Ceram. int. 22 (1996): 257-265.

Bedringas K.W., Ertesvag I.S., Byggstoyle S. & Magnussen B. F., Energy analysis of solid-oxide fuel cell (SOFC) systems. Energy 22 (1997): 403-412.

Bove R., Lunghi P. & Sammes N. M., SOFC mathematic model for systems simulations. Part one: from a micro-detailed to macro-black-box model. Int. J. Hydrogen Energy 30 (2005): 181-187.

Bove R., Lunghi P. & Sammes N. M., SOFC mathematic model for systems simulations—Part 2: definition of an analytical model. Int. J. Hydrogen Energy 30 (2005): 189-200.

Braun R.J., Klein S.A., Reindl D.T., Evaluation of system configurations for solid oxide fuel cell-based micro-combined heat and power generators in residential applications. J. Power Sources 158 (2006): 1290-1305.

Buchholz S. E., Dooley M. M.& Eveleigh D. E., Zymomonas — an alcoholic enigma. Trends in Biotechnology 5 (1987): 199-204.

Chan S.H., Low C.F.& Ding O.L., Simulation of a solid oxide fuel cell power system fed by methane. Int. J. Hydrogen Energy 30 (2005): 167-179.

Colpana C. O., Dincerb I.& Hamdullahpura F., Thermodynamic modeling of direct internal reforming solid oxide fuel cells operating with syngas. Int. J. Hydrogen Energy 32 (2007): 787 – 795

Costamagna P., Selimovic A., Borghi M.D. & Agnew G., Electrochemical model of the integrated planar solid oxide fuel cell (IP-SOFC). Chem. Eng. Journal 102 (2004): 61-69.

Dicks A. L.& Martin P. A., A fuel cell balance of plant test facility. J. Power Sources 71 (1998): 321-327.

Demin A. & Tsiakaras P., Thermodynamic analysis of a hydrogen fed solid oxide fuel cell based on a proton conductor. Int. J. Hydrogen Energy 26 (2001): 1103-1108.

Demin A. K., Tsiakaras P. E., Sobyanin V. A. & Hramova S. Y., Thermodynamic analysis of a methane fed SOFC system based on a protonic conductor. Solid State Ionics 152-153 (2002): 555-560.

Demin A., Tsiakaras P., Gorbova E. and Hramova S., A SOFC based on a co-ionic electrolyte. J. Power Sources 131(2004): 231-236.

Douvartzides S.L, Coutelieris F.A., Demin A.K., & Tsiakaras P.E., Fuel options for solid oxide fuel cell: a Thermodynamic analysis. AIChE J. 49 (2003): 248-257.

Douvartzides S. L., Coutelieris F. A. & Tsiakaras P. E., On the systematic optimization of ethanol fed SOFC-based electricity generating systems in terms of energy and exergy. J. Power Sources 114 (2003): 203-212.

Douvartzides S., Coutelieris F. & Tsiakaras P., Exergy analysis of a solid oxide fuel cell power plant fed by either ethanol or methane. J. Power Sources 131 (2004): 224-230.

EG&G Service Parsons, Inc. Science Applications International Corporation, Fuel Cell Handbook, 5th ed., Morgantown, West Virginia, 2000, pp. 234.

Fontell E., Kivisaari T., Christiansen N., Hansen J. B. & Pålsson J., Conceptual study of a 250 kW planar SOFC system for CHP application. J. Power Sources 131 (2004): 49-56.

Franlin's SOFC hits good power density on ethanol, Navy funding, Fuel Cells Bulletin 8 (2005): 8.

Freni S., Maggio G. & Cavallaro S., Ethanol steam reforming in a molten carbonate fuel cell: a thermodynamic approach. J. Power Sources 62 (1996): 67-73.

Garcia E.Y. & Laborde M.A., Hydrogen production by the steam reforming of ethanol: Thermodynamic analysis. Int. J. Hydrogen Energy 16 (1991): 307-312.

Garzon F. H., Mukundan R., Lujan R.& Brosha E. L., Solid state ionic devices for combustion gas sensing . Solid State Ionics 175 (2004): 487.

Hagiwara, A., Michibata, H., Kimura, A., Jaszcar, M.P., Tomlins, G.W. & Veyo, S.E., Proceedings of the Third International Fuel Cell Conference (1999) D2-4: 369.

Handbook of Fuel Cells-Fundamentals, Technology and Applications, vol.1-2, John Wiley & Sons, Ltd. (2003).

Herle J. V., Maréchal F., Leuenberger S. & Favrat D., Energy balance model of a SOFC cogenerator operated with biogas. J. Power Sources 118 (2003): 375-383.

Hernandez-Pacheco E., Singh D., Hutton P. N., Patel N. & Mann M. D., A macro-level model for determining the performance characteristics of solid oxide fuel cells. J. Power Sources 138 (2004): 174.

Hernández-Pacheco E., Mann M.D., Hutton P. N., Singh D. & Martin K.E., A cell-level model for a solid oxide fuel cell operated with syngas from a gasification process. Int. J. Hydrogen Energy 30 (2005): 1221-1233.

Inui Y., Matsumae T., Koga H., Nishiura K., High performance SOFC/GT combined power generation system with CO_2 recovery by oxygen

combustion method. Energy Conversion and Management 46 (2005): 1837–1847.

Iwahara H., Proton conducting ceramics and their applications. Solid State Ionics 86-88 (1996): 9.

Larrain D., Herle J. V., Maréchal F. & Favrat D., Generalized model of planar SOFC repeat element for design optimization. J. Power Sources 131 (2004): 304-312.

Leah R.T., Brandon N.P. & Aguiar P., Modelling of cells, stacks and systems based around metal-supported planar IT-SOFC cells with CGO electrolytes operating at 500–600 °C. J. Power Sources 145 (2005): 336-352.

Linnhoff B., Townsend D.W., Boland D., Hewitt G.F., Thomas B. E. A., Guy A. R., Marsland R. H., User Guide on Process Integration for the Efficient Use of Energy 1982, 1st edition, Institution of Chemical Engineering, UK.

Maggio G., Freni S. & Cavallaro S., Light alcohols/methane fuelled molten carbonate fuel cells: a comparative study. J. Power Sources 74 (1998): 17-23.

Matelli J. A. & Bazzo E., A methodology for thermodynamic simulation of high temperature internal reforming fuel cell systems. J. Power Sources 142 (2005): 160-168.

Möller B.F., Arriagada J., Assadi M. & Potts I., Optimisation of an SOFC/GT system with CO_2-capture. J. Power Sources 131 (2004): 320–326.

Nagata S., Momma A., Kato T. & Kasuga Y., Numerical analysis of output characteristics of tubular SOFC with internal reformer. J. Power Sources 101 (2001): 60-71.

Omosun A. O., Bauen A., Brandon N. P., Adjiman C. S. & Hart D., Modelling system efficiencies and costs of two biomass-fuelled SOFC systems. J. Power Sources 131 (2004): 96-106.

Palsson J., Selimovic A. & Sjunnesson L., Combined solid oxide fuel cell and gas turbine systems for efficient power and heat generation. J. Power Sources 86 (2000): 442–448.

Riensche E., Meusinger J., Stimming U. & Unverzagt G., Optimization of a 200 kW SOFC cogeneration power plant. Part II: variation of the flowsheet. J. Power Source 71 (1998): 306-314.

Riensche E., Stimming U. & Unverzagt G., Optimization of a 200 kW SOFC cogeneration power plant: Part I: Variation of process parameters. J. Power Sources 73 (1998): 251-256.

Riensche E. , Meusinger J., Stimming U. & Unverzagt G., Optimization of 200 kWS SOFC cogeneration power plant. PartII: Variation of the flowsheet. J. Power Source 71 (1998): 306-314.

Roger P. L., Lee K. J., Tribe D. E., Process Biochemistry August/September, (1980) 7-11.

Salar R., Taherparvar H., Metcalfe I.S. & Sahibzada M., in Proceedings of 2001 Joint International Meeting - the 200th Meeting of The Electrochemical Society, Inc. and the 52nd Annual Meeting of the International Society of Electrochemistry, San Francisco, California, 2001.

Sangtongkitcharoen W., Assabumrungrat S., Pavarajarn V., Laosiripojana N. & Praserthdam P., Comparison of carbon formation boundary in different modes of solid oxide fuel cells fueled by methane. J. Power Sources 142 (2005): 75-80.

Schneller T. & Schober T., Chemical solution deposition prepared dense proton conducting Y-doped $BaZrO_3$ thin films for SOFC and sensor devices. Solid State Ionics 164 (2003): 131.

Schober T., Krug F. & Schilling W., Criteria for the application of high temperature proton conductors in SOFCs. Solid State Ionics 97 (1997): 369.

Shell D. J., Riley C. J., Dowe N., Farmer J., Ibson K. N., Ruth M. F., Toon S. T. & Lumpkin R. E., A bioethanol process development unit: initial operating experiences and results with a corn fiber feedstock. Bioresource Technol. 91 (2004): 179-188.

Shimada T., Wen C., Taniguchi N., Otomo J. & Takahashi H., The high temperature proton conductor $BaZr_{0.4}Ce_{0.4}In_{0.2}O_{3-\alpha}$, J. Power Sources 131 (2004): 289-292.

Smith R., Chemical Process Design, 1995, McGRAW-HILL International Editions, Chemical Engineering Series.

Suwanwarangkul R., Ph.D. Thesis, University of Waterloo, (2005) pp.264.

Tsiakaras T. & Demin A., Thermodynamic analysis of solid oxide fuel cell system fueled by ethanol. Chem. Eng. Sci. 102 (2001): 210-217.

Vasudeva K., Mitra N., Umasankar P. & Dhinggra S.C., Steam reforming of ethanol for hydrogen production: Thermodynamic analysis. Int. J. Hydrogen Energy 21 (1996): 13-18.

Zhang W., Croiset E., Douglas P. L., Fowler M. W. & Entchev E., Simulation of a tubular solid oxide fuel cell stack using AspenPlus^{TM} unit operation models. Energy Conversion and Management 46 (2005): 181-196.

APPENDICES

APPENDIX A

THERMODYNAMIC DATA OF SELECTED COMPONENT

Table A1 Heat capacities of selected component (C_p)

Components	$C_p = a + bT + c\,T^2 + d\,T^3 + e\,T^4$ [J/mol K]				
	a	$b\times10^3$	$c\times10^5$	$d\times10^8$	$e\times10^{13}$
Ethanol	27.091	110.55	10.957	-15.046	461.01
Methane	34.942	-39.957	19.184	35.103	393.21
Carbon monoxide	29.556	-6.5807	2.0130	-1.2227	22.617
Carbon dioxide	27.437	42.315	-1.9555	0.3997	-2.9872
Water	33.933	-8.4186	2.9906	-1.7825	36.934
Hydrogen	25.399	20.178	-3.8549	3.1880	-87.585

Table A2 Heat of formation(H_f) and entropy (S^0) of selected component

Components	$H_f = a + bT + cT^2$ [kJ/mol]			S^O[J/mol.K]
	a	$b\times10^3$	$c\times10^5$	
Ethanol	-216.961	-69.572	3.1744	282.59
Methane	-63.425	-43.355	1.7220	186.27
Carbon monoxide	-112.19	8.1182	-8.0425	197.54
Carbon dioxide	-393.42	0.1591	-0.1395	213.69
Water	-241.80	0	0	188.72
Hydrogen	0	0	0	130.57

APPENDIX B

DETERMINING GIBBS ENERGY

B1. Determining Gibbs energy (G) at any temperatures by equations below:

$$G = H - TS \quad \text{(B1)}$$

$$dG = dH - d(TS) \quad \text{(B2)}$$

Take integration to the equation above:

$$\int dG = \int dH - \int d(TS) \quad \text{(B3)}$$

$$G_T - G_{STD} = \int_{298}^{T} dH - \int_{298}^{T} d(TS) \quad \text{(B4)}$$

Where

$$H = H(T) = a + bT + cT^2 \quad \text{(B5)}$$

$$S = S(T) = S^{o} + \int_{298}^{T} C_P dT \quad \text{(B6)}$$

Where T = The temperature range of 500 - 1,500 K

S^O= The entropy at standard state (298 K, 1 atm)

B2. Determining the equilibrium constant (K)

$$G_T = -RT \ln K \quad \text{(B7)}$$

Rearrange the above equation;

$$K = exp\left(-\frac{G_T}{RT}\right) \quad \text{(B8)}$$

APPENDIX C

NEWTON'S METHOD

Newton's method is used to solve a zero of function. The method is faster than other methods (e.g. secant or bisection method) because the convergence is quadratic rather linear. In this section, system of nonlinear equations is presented. Let us assume the system equations:

$$f_i\,(x_1, x_2, \ldots\ldots, x_n) = 0 \qquad \text{(C1)}$$

which can be simply represented as

$$F(X) = 0 \qquad \text{(C2)}$$

where $X=(x_1, x_2,\ldots,x_n)^T$ (C3)

and $F=(f_1,f_2,\ldots,f_n)^T$. (C4)

Let r_i be the root of equation i and R is the set of r_i

$$0 = F(R) = F(X + H) \approx F(X) + F'(X)H + o(H^2) \qquad \text{(C5)}$$

where $H=R-X$. If X is small close to the target tolerance, in other words X is close to R, $o(H^2)$ can be ignored. After eliminating $o(H^2)$, H can be calculated by the following equation.

$$H = \frac{-F(X)}{F'(X)} \qquad \text{(C6)}$$

It should be noted that $F'(X)$ is $n \times n$ Jacobian matrix as presented in Eq. (C7).

$$J(x) = \begin{bmatrix} \frac{\partial f_1(x)}{\partial x_1} & \cdots & \frac{\partial f_1(x)}{\partial x_n} \\ \vdots & \vdots & \vdots \\ \frac{\partial f_n(x)}{\partial x_1} & \cdots & \frac{\partial f_n(x)}{\partial x_n} \end{bmatrix} \quad \text{(C7)}$$

The next guess value of X can be calculated by the following equation.

$$X^{(k+1)} = X^{(k)} + H^{(k)} \quad \text{(C8)}$$

The procedure of the calculation:

1. Set the initial value of x_i
2. Fine $f(x)$ and $J(x)$
3. Solve the equation: $J(x)\,H = -F(x)$ to get H
4. Set $X = X + H$
5. If $|H| < \varepsilon_H$ or $|F(X)| < \varepsilon_X$, the calculation ends (Remark: ε_H and ε_X are the tolerance of H and X, respectively).

APPENDIX D

LIST OF PUBLICATIONS

International Publications

1) W. Jamsak, S. Assabumrungrat, P. L. Douglas, N. Laosiripojana, and S. Charojrochkul, Theoretical performance analysis of ethanol-fuelled solid oxide fuel cells with different electrolytes, Chem. Eng. J., 119, 11-18 (2006).
2) W. Jamsak, S. Assabumrungrat, P. L. Douglas, E. Croiset, N. Laosiripojana, R. Suwanwarangkul, S.Charojrochkul, Performance of ethanol-fuelled solid oxide fuel cells: Proton and oxygen ion conductors, Chem. Eng. J., 133, 187-194 (2007).
3) W. Jamsak, S. Assabumrungrat, P. L. Douglas, E. Croiset, N. Laosiripojana, R. Suwanwarangkul, S.Charojrochkul, Thermodynamic assessment of solid oxide fuel cell system integrated with bioethanol purification unit, J. Power Sources, 174, 191-198 (2007).

International Conferences

1) W. Jamsak, S. Assabumrungrat, P. L. Douglas, N. Laosiripojana, and S. Charojrochkul, Performance Analysis of Ethanol-Fuelled Solid Oxide Fuel Cells with Different Type of Electrolyte, Regional Symposium on Chemical Engineering (RSCE 2004), Bangkok, Thailand, December 1-3, 2004 (oral presentation).
2) W. Jamsak, S. Assabumrungrat, P. L. Douglas, E. Croiset, N. Laosiripojana, R. Suwanwarangkul, S.Charojrochkul, Performance Assessment of Bioethanol-Fed Solid Oxide Fuel Cell System Integrated with Distillation Column, 10th International Symposium on Solid Oxide Fuel Cells (SOFC-X), Nara, Japan (2007) (Oral presentation).

National Conferences

1) W. Jamsak, S. Assabumrungrat, P. L. Douglas, N. Laosiripojana, and S. Charojrochkul, Performance Analysis of Ethanol-Fuelled Solid Oxide Fuel Cells with Different Type of Electrolyte, RGJ–Ph.D. Congress VI supported by Thailand Research Fund (TRF), Pattaya, Chonburi, Thailand, April 28-30, 2005 (Poster presentation).
2) W. Jamsak, S. Assabumrungrat, P. L. Douglas, E. Croiset, N. Laosiripojana, R. Suwanwarangkul, S. Charojrochkul, Performance Assessment of Bioethanol-Fed Solid Oxide Fuel Cell System Integrated with a Distillation Column**,** RGJ seminar series 56th 2007, Chulalongkorn University, Bangkok, Thailand, September 28, 2007 (Poster presentation).

VITAE

Miss. Wasana Jamsak was born in May 8, 1982 in Bangkok, Thailand. She finished high school from Bodin Decha (Sing Singha Seni) school, Bangkok in 1999. She received her Bachelor's Degree in Chemical Engineering, from the Department of Chemical Engineering, Chulalongkorn University in 2003. Afterward, she continued studying Doctoral degree of Chemical Engineering, Chulalongkorn University since June 2003 and received Royal Golden Jubilee Scholarship from Thailand Research Fund. During her Doctoral degree, she collaborated with Professor Peter L. Douglas and did some parts of her research in Department of Chemical Engineering, University of Waterloo, Canada for one year and four months.